Adjoint Sensitivity Analysis of the Intercontinental Impacts of Aviation Emissions on Air Quality and Health

by

Jamin Koo

B.S., University of Illinois at Urbana-Champaign (2009)

Submitted to the School of Engineering
in partial fulfillment of the requirements for the degree of

Master of Science in Computation for Design and Optimization

at the

MASSACHUSETTS INSTITUTE OF TECHNOLOGY

September 2011

Author .....
School of Engineering
August 4, 2011

Certified by .....
Qiqi Wang
Assistant Professor of Aeronautics and Astronautics
Thesis Supervisor

Accepted by .....
Nicolas Hadjiconstantinou
Associate Professor of Mechanical Engineering
Director, Computation for Design and Optimization Program

Adjoint Sensitivity Analysis of the Intercontinental Impacts of Aviation Emissions on Air Quality and Health

by

Jamin Koo

Submitted to the School of Engineering
on August 4, 2011, in partial fulfillment of the
requirements for the degree of
Master of Science in Computation for Design and Optimization

Abstract

Over 10,000 premature mortalities per year globally are attributed to the exposure to particulate matter caused by aircraft emissions. Unlike previous studies that focus on the regional impacts from the aircraft emissions below 3,000 feet, this thesis studies the impact from emissions at all altitudes and across continents on increasing particulates in a receptor region, thereby increasing exposure. In addition to these intercontinental impacts, the thesis analyzes the temporal variations of sensitivities of the air quality and health, the proportion of the impacts attributable to different emission species, and the background emissions' influence on the impact of aircraft emissions.

To quantify the impacts of aircraft emissions at various locations and times, this study uses the adjoint model of GEOS-Chem, a chemical transport model. The adjoint method efficiently computes sensitivities of a few objective functions, such as aggregated PM concentration and human exposure to PM concentration, with respect to many input parameters, i.e. emissions at different locations and times.

Whereas emissions below 3,000 feet have mostly local impacts, cruise emissions from North America impair the air quality in Europe and Asia, and European cruise emissions affect Asia. Due to emissions entering Asia, the premature mortalities in Asia were approximately two to three times larger than the global mortalities caused by the Asian emissions. In contrast, North America observed only about one-ninth of the global premature mortalities caused by North American emissions because emissions get carried out of the region. This thesis calculates that most of the premature mortalities occured in Europe and Asia in 2006.

Sensitivities to emissions also have seasonal and diurnal cycles. For example, ground level NO_X emissions in the evening contribute to 50% more surface PM formation than the same emissions in the morning, and cruise level NO_X emissions in early winter cause six times more PM concentration increase than the same emissions in spring. Aircraft NO_X emissions cause 78% of PM from aviation emissions, and given the population exposure to PM concentration increase, NO_X contributes 90% of the total impact. By showing the second-order sensitivities, this study finds

that increases in background emissions of ammonia increase the impact of aircraft emissions on the air quality and increases in background NO_X emissions decrease the impact.

These results show the effectiveness of the adjoint model for analyzing the long-term sensitivities. Some of the analyses presented are practically only possible with the adjoint method. By regulating emissions at high sensitivities in time and region, calculated by the adjoint model, governments can design effective pollutant reduction policies.

Thesis Supervisor: Qiqi Wang
Title: Assistant Professor of Aeronautics and Astronautics

Acknowledgments

First I would like to thank my advisor, Professor Qiqi Wang, for his great support. I am very lucky to become the first student of Professor Wang, who is patient and understanding, while providing a great research guidance with enthusiasm. Professor Steven Barrett deserves sincere appreciation for his great explaination of atmospheric science and thorough comments throughout the course of this research. I cannot think of anyone else who is willing to and is capable of examining my writing in such detail. I am also priviledged to work under the supervision of Professor Ian A. Waitz, the dean of engineering at MIT. Knowing his support on this project and having conversations with him fostered inspirations and confidences; in one sentence, he is an extraordinary advisor. I also thank Chris Sequeira for his support; he has been very attentive to my research and its progress, providing valuable feedbacks in a timely manner. Professor Daven Henze of the University of Colorado at Boulder is definitely at the top of my list to appreciate. There were about four hundered e-mails sent back and forth between Daven and me, while he helped me tremendously with running GEOS-Chem Adjoint and I bugged him with various bug reports. I am also thankful to Laura Koller, an academic administrator for Computation for Design and Optimization, for making my educational experience trouble-free.

Next round of my acknowledgement goes to researchers and students in PARTNER. I thank Akshay Ashok, who is the most deterministic person I have ever met, for sitting next to me and answering my never-ending questions related to this research with 0% uncertainty and Rhea Liem, who is a complement of Akshay in a probabilistic sense(Rhea=Akshay^c), for bringing exciting and fonding moments to the lab at a random sequence. I also thank Philip Wolfe and Alex Nakahara for bearing with my constant noisy chat with Akshay, while educating me with obscure facts that can only be learned through extensive reading or participating in trivias. I also thank Steve Yim, Christoph Wollersheim, Hossam El-Asrag, Alex Mozdzanowska, Jim Hileman, Mina Jun, Fabio Caiazzo, Chris Gilmore, Kevin Lee, Gideon Lee, Sergio Amaral and everyone else in the lab for making PARTNER a great, lively, loving place. It would

also be unwise of me to forget thanking the unknown hacker who hacked our linux clusters from Netherlands, giving me frustration, anxiety, and more work in addition to having me delay my graduation date.

My final and sincere acknowledgement goes to the three greatest teachers of Maum Meditation, who have continuously provided me with care and love in addition to helping me become who I am now and providing me a lifetime guidance.

Without the help of everyone around me, not limited to the people I mentioned above, my experience at MIT and growth as a researcher would have not been fun, fruitful, and rewarding to this extent.

Contents

THIS PAGE INTENTIONALLY LEFT BLANK

List of Figures

List of Tables

Chapter 1

Introduction

Intercontinental transport of air pollution has been studied by various researches both using observations and numerical simulations. It is estimated that 380,000 premature mortalities per year are caused by aerosols produced and transported from other regions, among which 90,000 mortalities are caused by exposure to non-dust aerosols [4]. Besides aerosols, the precursors of aerosols and ozone are also transported across continents, causing negative health impacts. Mortalities caused by ozone in a receptor continent can be reduced by about 20 to 50% when ozone precursor emissions are removed completely in other continents [5]. These researches, along with other studies on intercontinental transport of pollutants, suggest the importance of a hemispheric treaty on regulating emissions [6]. The impact from long range transport of pollutants is especially important considering emissions from aircraft. Aircraft emissions are unique in that they are emitted at higher altitudes, remaining in the atmosphere longer and being transported to a farther distance due to stronger winds aloft. Because of the long-range transport, studying the cruise emissions' impact on the air quality requires the intercontinental transport of pollutants.

1.1 Aviation Activities and Policies

The aviation sector is projected to grow at an annual rate of 4.8 - 5 % and will double the current aircraft activities by 2020 to 2025 [7, 8, 9]. Aviation activities are highly

correlated with economic trends and GDP. High growth rates in Asia, notably China and India, are driving the demand of the aviation industry [7]. Although current research shows that the contribution of aviation emissions to environmental damage is small, about 0.1% of anthropogenic pollution, compared to 1% of highway pollution in the U.S., it is important to control the emissions of this sector because of the rapid growth of air transportation [10].

The International Civil Aviation Organization (ICAO), an organization of the United Nation, created the Committee for Aviation Environmental Protection (CAEP) to analyze environmental policies for aviation and further establish standards for noise and emissions. Three environmental goals of ICAO [7]. are

- "to limit or reduce the number of people affected by significant aircraft noise";
- "to limit or reduce the adverse impact of aviation emissions on local air quality";
- "and to limit or reduce the impact of aviation greenhouse gas emissions on the global climate."

Aircraft noise is the first regulated because it is readily perceived in the vicinity of airports, first regulated by ICAO's noise certification at an international level in 1971. In 1981, ICAO set the NO_x emissions standard, which became effective in 1986, to improve the air quality of the near-by regions of airports [7]. In addition to the local air quality, its focus expanded to the global climate impact. In addition, emissions standards have become more stringent as listed in the latest updated standards in ICAO *Annex 16 - Environmental Protection, Volume II - Aircraft Engine Emissions to the Convention on International Civil Aviation* [9].

Member states of ICAO, currently 183 countries, are recommended to implement ICAO Standards and Recommended Practices (SARPs). The U.S., as a member state, adopted several regulations based on updates of ICAO's SARPs. Moreover, in the U.S. the Partnership for AiR Transportation Noise and Emissions Reduction (PARTNER), an FAA Center of Excellence, was formed to assess the impact of aviation emissions on climate change, air quality, and noise. To study the costs and benefits

of different policies for environment, the Aviation environmental Portfolio Management Tool (APMT) was developed by Federal Aviation Administration (FAA) and PARTNER and is currently being used [11, 12]. The work of this thesis will aid the tool suite development on the aspect of assessing the air quality impacts of aviation. Specifically, it will provide the spatial and temporal sensitivity matrices of air quality with respect to aviation emissions. The sensitivities quantify how emissions in different regions damage air quality to different extents, which can assist policymakers in implementing effective emission reduction strategies.

1.2 Air Pollution and Health Impacts

The aviation policies of the US and other member nations of ICAO are in accordance with other regulations concerning air quality. The Clean Air Act of 1970 and 1977 in the U.S. authorized the Environmental Protection Agency (EPA) to regulate the national air quality using National Ambient Air Quality Standards; the EPA updated these standards on several occasions, with the last air quality standards for $PM_{2.5}$ set at the annual mean of 15.0 $\mu g/m^3$ and 35 $\mu g/m^3$ for 24-hour average [13, 14]. These standards also set ozone level at 0.075 ppm for 8-hour and 0.12 ppm for 1-hour averages, as well as setting different annual means limits for nitrogen oxides, sulfur dioxides, lead, and carbon monoxide [15].

These standards were established based on research on health impacts caused by these pollutants. Many of these studies found a high correlation between long-term exposure to $PM_{2.5}$ and lung cancer and cardiopulmonary disease [2, 16]. Particulate matter is a mixture of liquid droplets and particles that can be inhaled. Among various categories of PM, $PM_{2.5}$, or particulate matter with diameter less than $2.5\mu m$, is found to be more damaging when exposed for a long term period. The Environmental Protection Agency (EPA) lists the health consequences: cardiovascular symptoms, cardiac arrhythmias, heart attacks, respiratory symptoms, asthma attacks, and bronchitis that could result in increased hospital admissions, emergency room visits, absences from school or work, and restricted activity days [14].

Most of the air quality impacts caused by aviation emissions come from the formation of $PM_{2.5}$, which can be categorized into primary PM and secondary PM [10]. Primary particulate matter is PM that is directly emitted from an engine or formed immediately after exiting an engine; this category includes non-volatile PM - assumed to be black carbon (BC), or soot - and volatile PM from sulfur and organics, or organic carbon (OC). OC is formed about 30 meters behind the engine when volatile organic compounds (VOCs) are photo-oxidized and condensate to form organic carbon [17, 18]. Secondary PM is formed through chemical reaction of its precursors with other chemical species in the atmosphere. The precursors are nitrogen oxides (NO_x), sulfur dioxide (SO_2), and volatile organic compounds. When NO_x and SO_2 are emitted, they are oxidized, becoming HNO_3 and H_2SO_4. The oxidization process can be achieved with OH, ozone, and H_2O_2, and the availability of the oxidants determines the amount of PM formation [19]. As a neutralization process, sulfuric acid and ammonia form ammonium sulfate, $(NH_4)_2SO_4$, and the remaining ammonia reacts with nitrate to form ammonium nitrate, NH_4NO_3 [20]. Ammonium sulfate and ammonium nitrate are the most important secondary PM species. Volatile organic compounds, or hydrocarbons, can also form secondary particulates. Both primary and secondary particulate matter introduced by aircraft emissions are $PM_{2.5}$ [21].

In addition to the formation of particulates, aviation emissions cause the formation of ozone. The ozone production pathway due to aviation emissions is 1) volatile organic compounds and carbon monoxide emitted from aircraft are oxidized, and then 2) the resulting species react with NO_x to form ozone [20]. It is understood that exposure to ozone causes asthma, bronchitis, breathing difficulties, coughing, irritation, and permanent lung damage [15]. The health impact caused by aircraft emissions induced ozone is estimated to be about 4% to 8% of the impact from aviation induced $PM_{2.5}$ [10, 22] although this proportion on the health impact does not include the effect of cruise emissions. This study focuses on the impacts on $PM_{2.5}$.

1.3 Motivation for Adjoint Sensitivity Analysis

Most studies on aviation's air quality impacts in the last few decades focus on aircraft's landing and take-off (LTO) emissions, or emissions below 3,000 feet. However, a recent study by Barrett et al. [1] shows that aerosols created from aircraft emissions above 3,000 feet have global health impact of about 8,000 premature mortalities per year. Understanding that the health impact from emissions above 3,000 feet is two to four times larger than the impact from LTO emissions, this thesis focuses on how emissions in various regions, at both low and high altitudes, impact the ground level air quality, thereby causing premature mortalities.

Furthermore, emissions at different geographical locations have different influences on air quality. A study by Sequeira [23] indicates that the regional variability on the health effects of aviation emissions are large. The aviation LTO emission induced PM related mortalities in Los Angeles county are 18% of that of the US as a whole, and 43% of PM mortalities in the US occurs in ten counties with the highest PM-related mortality incidences [24]. Moreover, using ultra low sulfur fuel in LA county alone could reduce aviation LTO related mortalities by 10% [23]. It is valuable to quantify this spatial variability.

Unlike other studies on intercontinental transport of aerosols and ozone that were performed with forward model simulations, this thesis addresses it using the adjoint model approach. Forward model analysis is source oriented, suited for a simulation with more model responses than input parameters. Performing a forward simulation tracks the changes in all model responses due to a single hypothetical perturbation in an aircraft emission, as shown in the left side of Fig. 1-1. In contrast, an adjoint simulation traces changes in a model response back to changes in all inputs, as shown in the right side of Fig. 1-1. Adjoint model is receptor oriented, suited for a simulation with more input parameters than responses.

In order to quantify the impact caused by aircraft emissions at various regions using the forward sensitivity analysis, separate simulations must be run for each of the regions. Each of the simulations perturbs the aviation emissions at one particular

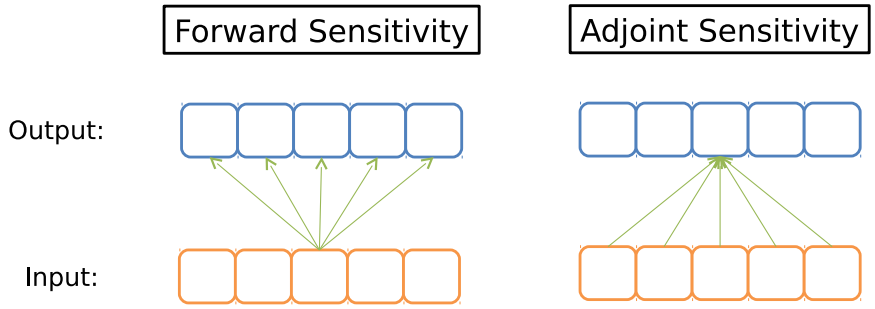

Figure 1-1: Forward and adjoint analyses

location, showing how emissions in the particular regions influence air quality at all locations. In contrast, a single adjoint simulation can show how emissions at each of the locations impact one output: the concentration change in a particular grid box or a weighted sum of concentration changes in all grid boxes. For examples, a forward simulation gives the outcomes associated with proposed emissions changes, and an adjoint simulation shows what emissions reductions are needed to achieve an air quality objective. Thus, when finding the sensitivities of few outputs to many inputs, it is more efficient to run adjoint simulations, rather than forward simulations. In order to get sensitivities with respect to emissions at all locations, only one adjoint simulation is required whereas the forward model requires $N + 1$ number of simulations, where N is the number of grid boxes. Chapter 2 will further demonstrate the effectiveness of running an adjoint simulation for studying how air quality in a region of interest is changed by aircraft emissions in various regions.

1.4 Thesis Organization

The rest of this thesis is organized into three chapters.

Chapter 2 discusses the adjoint method and its usage in GEOS-Chem, a chemical transport model (CTM) used to model the atmospheric chemistry and physics for this thesis. A major contribution of this thesis is incorporating the component of aircraft emissions in the forward and the adjoint models of the CTM, thereby deriving the sensitivities of various metrics of air quality with respect to aviation emissions.

Chapter 3 discusses the sensitivity results of adjoint simulations, showing the sensitivities of air quality with respect to emissions. Increases in concentration of pollutants and in population exposure to pollutants in receptor regions are traced back to the source, aircraft emissions at all locations and altitudes. By providing source-receptor matrices of aviation emissions to the air quality and health impacts, Chapter 3 demonstrates the varying degree of impact caused by emissions from different longitudes, latitudes, and altitudes. In addition to the spatial variation of sensitivities, a temporal variation, including diurnal and seasonal cycles, in sensitivities is discussed.

Chapter 4 concludes this thesis and discusses what can be improved for future studies. Potential future studies include 1) performing a principal component analysis to find the meteorological influence on first-order sensitivities, 2) studying aviation's impact on aerosol optical properties, and 3) finding the sensitivities of climate impact due to emissions. The chapter further discusses the policy implications of the sensitivity data, explaining how adjoint sensitivities can assist in the design of pollutant reduction policies.

THIS PAGE INTENTIONALLY LEFT BLANK

Chapter 2

The Adjoint Method

The word "adjoint" in mathematics means conjugate transpose. For a matrix with real entries, its corresponding adjoint matrix is its transpose. Applying this nomenclature to a linear system is an intuitive example that shows why solving an adjoint equation provides an efficient way of calculating the gradient with respect to input parameters. For a linear system, $Ax = y$, relating the input x to the output y, the adjoint equation is $A^T\hat{y} = \hat{x}$, where $\hat{x} = \frac{dJ}{dx}$ notation refers to the gradient of the objective function, J, with respect to the input variable, x. And $\hat{y} = \frac{dJ}{dy}$ denotes the gradient of J with respect to y, the output. The objective function must be written in terms of the output variable, or $\frac{dJ}{dy}$ should exist, to calculate the gradient of J with respect to x.

How sensitive the output, y, is to perturbations in input, x, can be easily calculated by carrying out the multiplication: $A\delta x = \delta y$. Given the relationship between the output and the objective function, $J = \hat{y}^T\delta y$, the change in an objective with respect to changes in input parameters, x, can be found by

$$\begin{aligned} \delta J &= \hat{y}^T\delta y \\ &= \hat{y}^T A\delta x \\ &= \hat{x}^T\delta x \end{aligned} \tag{2.1}$$

where the adjoint equation is $\hat{x} = A^T\hat{y}$. Having $\hat{x}$ has an advantage when calculating

multiple responses of applying different perturbations to x. Without it a full simulation is required to see the change in the objective function for each perturbation in x, but with the gradient information a simple multiplication of the gradient and the perturbation gives the first-order approximation to the change in the objective function.

For a system of partial differential equations (PDEs), there are two ways of deriving adjoint equations: 1) using a continuous adjoint approach and 2) using a discrete adjoint approach. In the continuous adjoint approach, typically a nonlinear partial differential equation is linearized, and then the linearized adjoint of the PDE is found, which then gets discretized into an adjoint equation. In the discrete adjoint approach, the nonlinear PDE is first discretized and then linearized, followed by derivation of the adjoint equation. In Fig 2-1, the green arrows represent the continuous adjoint approach, and the black arrows show the discrete adjoint path.

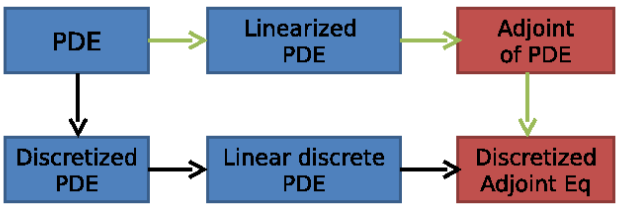

Figure 2-1: Discrete and continuous adjoint

Since the discrete adjoint approach uses the same discretization that the forward model uses, the discrete adjoint matrix will be a conjugate transpose of its primal matrix: A in Eq. 2.1. Unlike its discrete counterpart, the continuous adjoint scheme computes the adjoint equation and discretizes the equation, causing the continuous adjoint matrix to be different from the conjugate transpose of its primal matrix. The continuous adjoint and discrete adjoint are consistent when the discretization is sufficiently fine.

It is often easier to implement the continuous adjoint approach although boundary conditions can complicate the process, and the continuous adjoint variable can be easily interpreted since it has a physical significance. On the other hand, the discrete

adjoint variable represents the exact gradient of a discrete objective function, having an easier verification process. However, the discrete approach causes the code to be long and inefficient and is often cumbersome to derive. There are more advantages and disadvantages to these two approaches [25], but discussing them is beyond the scope of this thesis. As it will be explained later, the continuous and discrete adjoint methods can be used together.

2.1 Advantages of Adjoint Analysis

Solving for an adjoint equation entails changing the order of matrix-matrix and matrix-vector operations, as shown in Fig. 2-2. This figure depicts a simulation with N time steps, and each time step involves a multiplication with a matrix A. The quantity of interest, J, is a direct function of $\vec{x}^N$, and its sensitivity derivative to $\vec{x}^1$ needs to be calculated.

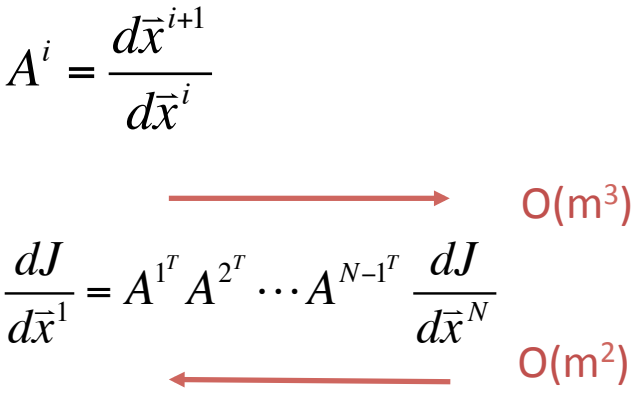

Figure 2-2: Order of operations for forward method versus adjoint method

Let A be $m \times m$ matrix, x be vector of m entries, and J be a scalar. Multiplying from the left to right needs $N-2$ matrix-matrix multiplications and 1 matrix-vector multiplication, which requires $O(m^3)$ operations. However, multiplying from right to left needs $N-1$ matrix-vector multiplications, or $O(m^2)$ operations. Thus, running an adjoint simulation, or multiplying from the right, is computationally more efficient.

Traditional forward model analysis is source oriented, comparing two simulations with and without an input, or aviation emissions in this case. A benefit of this approach is being able to see how model outputs in all regions are impacted due to a perturbation in an input. However, if there are more inputs than outputs, it becomes increasingly difficult to run using the forward analysis. This thesis focuses on the output, or the objective function, of PM concentration change in different continents and the entire world. In order to study how emissions from different location impact the air quality, emissions at each of the locations have to be a separate set of inputs, thus requiring many numbers of runs. The adjoint analysis traces backward from the change in PM concentrations to emissions and allows us to see the sensitivity of PM concentrations to emissions at all locations and times in an efficient manner.

2.2 GEOS-Chem, a Chemical Transport Model

In atmospheric science, the adjoint analysis is widely used, but primarily for data assimilation and not for sensitivity studies. There has been no prior work focusing on a long-term global scale sensitivity analysis. This is because most emission studies show their relationship with the local air quality. Most of emissions are at the surface, not having large impacts outside their emitted regions. For aviation emissions, however, about 90% of total emissions are emitted above 3,000 feet and are likely to cause intercontinental air quality impacts. Therefore, it is important to see the intercontinental effects by running simulations that span long period.

Global atmospheric simulations was perforemd with GEOS-Chem, a global tropospheric chemical transport model. It uses the assimilated meteorology data from the Goddard Earth Observing System of the NASA Global Modeling and Assimilation Office. For this chemical transport model, the adjoint model implementation is widely used [26, 27]. Using the adjoint code of GEOS-Chem, studies have been conducted on data assimilation and also on sensitivities of atmospheric composition to emissions. As mentioned earlier, these sensitivity studies were based on local air quality and local emissions for few week period. Unlike previous studies, this thesis extends the length

of simulations for the adjoint studies to capture the intercontinental transporting mechanisms.

2.2.1 GEOS-Chem and GEOS-Chem Adjoint

GEOS-Chem and its adjoint model with the standard NO_X-O_X-hydrocarbon-aerosol simulation were used for this research. This tropospheric chemistry mechanism includes the gas-phase chemistry of about 90 chemical species and other aerosol chemistries. The gas-phase chemistry is solved by Kinetic PreProcessor (KPP) [28], and sulfate-nitrate-ammonium thermodynamic equation is calculated by MARS-A, an inorganic aerosol thermodynamic equilibrium module [29, 30, 31]. The 90 chemical species are lumped together as tracers that are listed in Table D.1 to expedite the simulation for non-chemistry modules that do not require separate treatment for individual species.

The results from NO_X-O_X-hydrocarbon-aerosol simulation of GEOS-Chem have been validated with networks of observations from different sites [32, 33, 34]. Many studies used the results based on the model's simulation of aerosol and ozone chemistry, some of which incorporate intercontinental transport [35, 36].

Unlike its use of a comprehensive chemistry module in troposphere, GEOS-Chem implements a simplified stratospheric chemistry used to model the boundary condition of the upper troposphere. The stratospheric chemistry is modeled by a linearized ozone (LINOZ) scheme, which implements the first order Taylor expansion of the relationship between ozone mixing ratio, temperature, and overhead ozone column [37]. Using only one tracer, LINOZ models the cross-tropopause flux and ozone gradient near tropopause. Because a significant portion of aviation emissions is emitted in the lower stratosphere, having a more complex stratospheric chemistry model may improve the result of the analysis in this thesis.

The adjoint model exists for GEOS-Chem using combination of discrete and continuous adjoint, developed in the last decade. Its sensitivity results were validated with the comparison with forward model's finite difference for each of the modules separately and all modules together [27, 26]. Using adjoint of GEOS-Chem, the source

of inorganic $PM_{2.5}$ and ozone precursor emissions in the US and other regions have been mapped by the inverse modeling using the adjoint of GEOS-Chem [38, 39, 40].

As shown in Fig. 2-2, the adjoint simulation changes the order of operations. Thus, it runs backward in time from the last time step to the first time step. Fig. 2-3 shows the modules of GEOS-Chem in each of the time steps. First, it runs forward in time while saving checkpoints, and then it runs backward in time using the adjoint modules shown on the right side of Fig. 2-3.

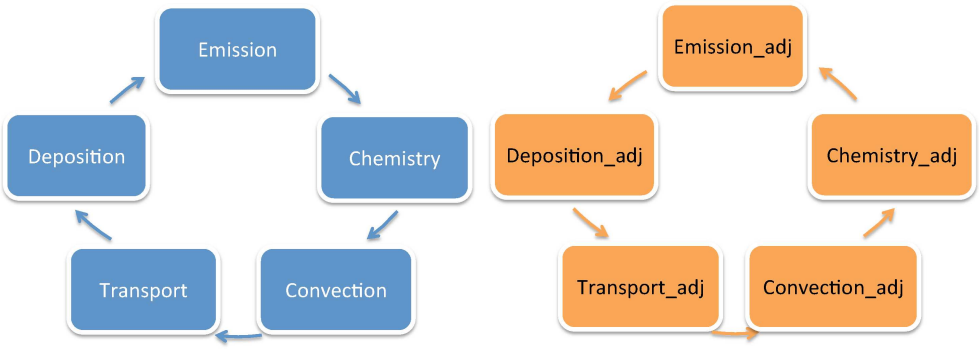

Figure 2-3: GEOS-Chem forward and adjoint modules

There exists a difficulty stabilizing the adjoint code because the adjoint code was not built in parallel with the forward code. Running GEOS-Chem, the chemistry and transport module frequently brings the mass of chemical species to be slightly negative because of the approximations in the numerical schemes. When the mass becomes negative, the forward model sets the value zero, preventing the mass from being numerically unstable. This is a reasonable treatment because the mass of a chemical specie is always positive. The adjoint sensitivity values, nevertheless, can be negative, meaning that an increase in emissions of some species in certain regions could decrease the PM concentration. For this reason, adjoint solutions cannot be stabilized by setting negative values to zero. Our way of preventing divergence of the adjoint solution was running with more stringent tolerance limits and smaller time steps in the KPP chemistry solver.

2.2.2 Aircraft Emissions Inventory

The inventory for aviation emissions used in this thesis was created by the US Department of Transportation John A. Volpe National Transportation Systems Center using Aviation Environmental Design Tool(AEDT)[41, 42] This inventory estimates the total amount of global fuel burn (FB) in 2006 to be 1.88×10^{11} kg. The detailed breakdown of emissions is given in Table 2.2. The receptor regions, where the objective functions of pollutants and population exposure are considered, are defined using the grid boxes of GEOS-Chem and are shown in Fig. 2-4. The coordinates of the regions are listed in Table 2.1

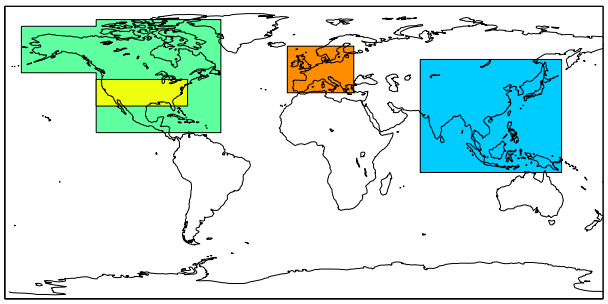

Figure 2-4: Regions considered in this thesis

Table 2.1: Coordinates of regions used in this thesis

	US	NA	EU	ASIA
Lon	(-127.5, -72.5)	(-127.5, -52.5) + (-172.5, -127.5)	(-12.5, 64)	(67.5, 152.5)
Lat	(28, 44)	(12, 80) + (48, 76)	(36, 63)	(-12, 56)

Table 2.2: Yearly full flight emissions in various regions

	Fuel Burn ($\times 10^{10}$ kg)	NO_X ($\times 10^{8}$ kg)	SO_X ($\times 10^{7}$ kg)	HC ($\times 10^{7}$ kg)	CO ($\times 10^{8}$ kg)	BC ($\times 10^{6}$ kg)	OC ($\times 10^{6}$ kg)
US	4.28	5.42	5.20	3.30	2.30	1.57	0.88
NA	6.51	8.52	7.89	4.51	3.07	2.37	1.33
EU	3.34	4.64	4.05	1.74	1.35	1.20	1.33
ASIA	3.94	6.06	4.78	1.59	1.13	1.41	0.91
World	18.8	26.6	22.8	9.78	6.79	6.81	4.50

Compared to the global aviation fuel burn, 73.4% of global emissions are emitted

in Europe, Asia, and North America. This thesis will focus on emissions in those regions.

To clarify the terms being used in this thesis, emissions are attributed by location of emission. For example, North American emissions refer to emissions in the air above the geographical region of North America. It should not be interpreted as emissions by North American carriers, emissions by planes departing from or arriving at North America, or emissions in the airspace of the region. The same applies to other emissions of different continents or countries.

In Table 2.3 the percentage of landing and take-off emissions in the world are shown, as a fraction to total emissions. As mentioned earlier, about 90% of fuel is burnt at above 3,000 feet, and similar proportions of NO_X, SO_X and BC are emitted at above 3,000 feet. But for HC, CO, and OC, about 40% is emitted in the LTO phase because these emissions are associated with low thrust operations such as taxing.

Table 2.3: Percentage of LTO emissions over total aircraft emissions in the world

Fuel Burn	NO_X	SO_X	HC	CO	BC	OC
11.5%	9.9%	11.5%	44.7%	40.4%	14.4%	40.6%

2.2.3 Improvement to GEOS-Chem Adjoint

Prior to this thesis work, adjoint simulations using GEOS-Chem spanned for a few days to a few weeks. Because the work in this thesis requires extending the simulation time to seventeen months as will be shown, extensive modification and testing of the code was necessary. Several errors, including a mathematical one and simple coding errors, were discovered and fixed during the testing. Although the errors did not surface during shorter simulations of others, they caused numerical instabilities in longer simulations, causing sensitivities to diverge to infinity. These bugs were reported, and the corrections were made together with the developers.

For example, a mathematical correction to the code is applying the appropriate conversion between the continuous and discrete adjoint variables. Continuing the earlier discussion of the continuous and discrete adjoint method in the beginning of

this chapter, it is possible to mix the two in computations. This must be done carefully when converting from one to another. The discrete and continuous adjoint variables may not represent the same physical quantity, thus may have different values and units. Converting from one to another requires a multiplication or division by a grid-dependent factor, as explained in more detail in Appendix A. This topic is rarely discussed in literatures, perhaps due to the rare exploitation of mixing two types of adjoint methods. GEOS-Chem Adjoint uses continuous adjoint for its transport module and discrete for the rest of the modules. Without the use of appropriate conversion between the discrete and continuous adjoint variables, the code erroneously produced high sensitivities in the polar regions, where the grid size is smaller.

Running an adjoint simulation of GEOS-Chem takes about 2.5 times longer than what it takes to run its forward counterpart [27]. This is because it involves running the forward model and the adjoint model, where checkpoints are saved and read, respectively. The adjoint model requires the values of variables of the forward model at every timestep, thus the forward model must write the variables to checkpoints and the adjoint model must read from them. One year of simulation requires about 3TB of storage for checkpoints and 1TB of storage for adjoint sensitivities. This input and output intensive task required large transfer between computing nodes and data storage nodes, which is the bottleneck in the analyses. One improvement made by this work was decoupling the forward and the adjoint simulations. The forward model was only run once to produce checkpoints, and all of adjoint simulations read in the same checkpoint files. Decoupling reduced the time of simulation to one-half, having a running time comparable to the forward model.

Another addition to the code is flexible specification of the objective function. The adjoint code was written to use the sum of tracers as an objective function. As explained earlier, the adjoint solutions give sensitivities of a scalar objective. Because of the lack of grid specific information, sensitivities cannot be post-processed into sensitivities of another objective function. For example, sensitivity of the sum of PM concentration cannot be post-processed to sensitivity of the sum of population exposure to PM. Thus, in order to calculate how much people are exposed to PM

due to aircraft emissions, the model must pre-multiply population information to the objective function. The modified code reads in a weight file that can be pre-multiplied to the objective function, and as a result, changing the objective function is an easy task.

2.2.4 Verification of the Adjoint Model in GEOS-Chem

Although detailed verification can be found in Henze et al. [27] and Singh et al. [26], additional verifications of the model specific to sensitivities of PM with respect to aviation emissions are performed. To verify the adjoint sensitivities completely, the number of simulations required to run equals the number of grid boxes multiplied by the number of emissions species. As performed in pervious papers [27, 26], finite difference sensitivities and adjoint sensitivities are compared without turning on the horizontal transport module. By isolating each vertical stack of grids, the required number of simulations is reduced to the number of emissions multiplied by the number of PM species. This provides an efficient verification process of modules other than the horizontal transport, testing chemistry, convection, deposition, and emissions. And the horizontal transport was verified independently by running additional simulations without the use of other modules.

Verification of Non-horizontal Transport Modules

Fig. 2-5 and 2-6 show finite difference sensitivities versus adjoint sensitivities. There are a total of 5 aerosol components (NH_4^+, SO_4^{2-}, NO_3^-, BC, OC) and 6 emission sources (NO_X, SO_X, CO, HC, BC, OC), totaling 30 sensitivity comparison plots. The comparisons of sensitivities shown here were done with one-week simulations, not with 17 months. However, noting that changing in length of the run from one day, one week, one month to three months did not change how accurate the adjoint simulation is measuring the sensitivities, sensitivity comparisons for the 17-months simulation are expected to be similar.

Linear regression was done on the plots in Fig. 2-5 and 2-6, and its slope and r^2

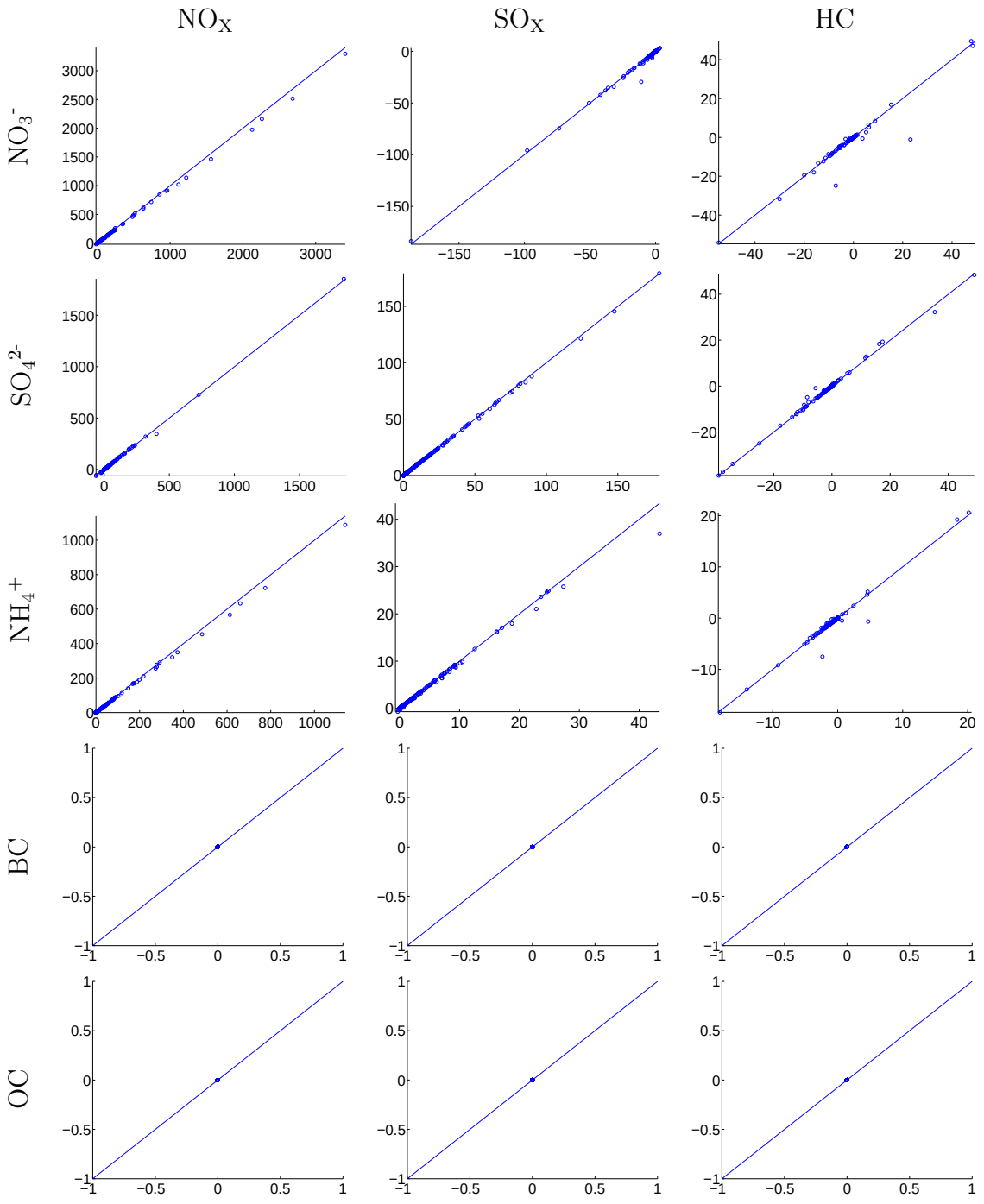

Figure 2-5: Adjoint vs finite difference results for kg·hr of aerosol produced due to aircraft NO_X, SO_X, and HC emissions

values are listed in the following Table 2.4 and 2.5. It is shown that adjoint sensitivity values are very close to finite difference values, with exceptions of aerosols created by primary PM species (BC and OC). In this case, the forward model shows that addi-

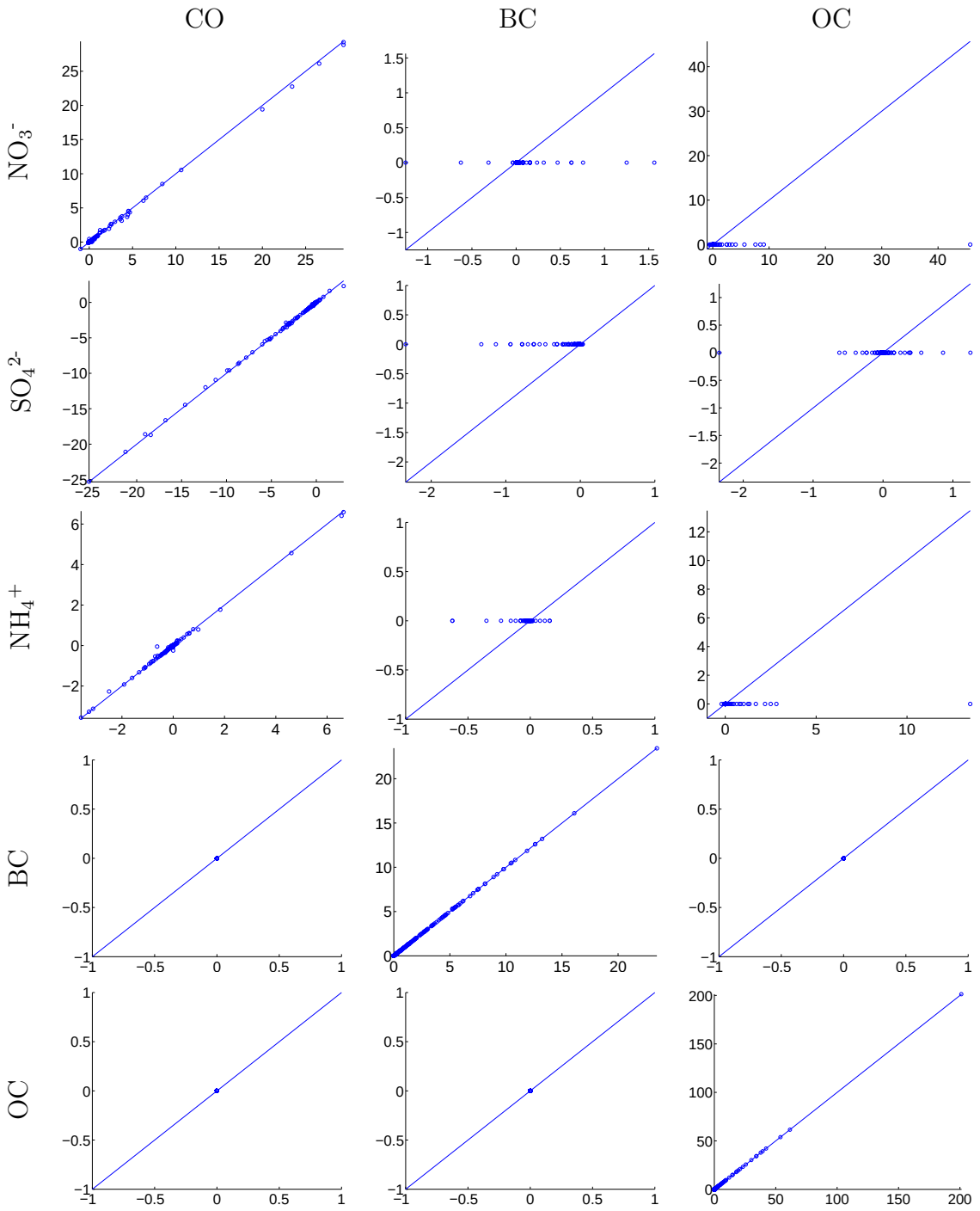

Figure 2-6: Adjoint vs finite difference results for kg·hr of aerosol produced due to aircraft CO, BC, and OC emissions

tion of primary PM would changes secondary particulates whereas the adjoint model calculates no change in secondary PM due to primary PM emissions. This discrepancy occurs because of the absence of aerosol optical module in the adjoint model.

As mentioned previously, the adjoint model was developed as particular modules are needed, so GEOS-Chem Adjoint does not include all modules found in the forward model. Nevertheless, the changes in secondary PM caused by primary PM are about two orders of magnitude smaller than ones caused by NO_X and SO_X emissions.

Table 2.4: Slope of linear regression line for forward difference sensitivities versus adjoint sensitivities

	NO_X	SO_X	HC	CO	BC	OC
NO_3^-	0.951	0.993	0.959	0.982	-	-
SO_4^{2-}	1.002	0.990	0.987	0.990	-	-
NH_4^+	0.949	0.948	1.001	0.981	-	-
BC	-	-	-	-	1.000	-
OC	-	-	-	-	-	1.001

Table 2.5: r^2 of linear regression line for forward difference sensitivities versus adjoint sensitivities

	NO_X	SO_X	HC	CO	BC	OC
NO_3^-	1.00	0.99	0.92	1.00	-	-
SO_4^{2-}	1.00	1.00	0.99	1.00	-	-
NH_4^+	1.00	1.00	0.97	1.00	-	-
BC	-	-	-	-	1.00	-
OC	-	-	-	-	-	1.00

Verification of the Horizontal Transport Module

The transport module was tested using one-month simulations. The testing on an one-month simulation is expected to be similar to a testing on a longer period because most of the aerosols will be deposited in one month, thus does not accumulate impacts for longer period. Black carbon was considered for this testing since black carbon does not chemically react with other species in GEOS-Chem's chemistry module. Two forward runs were performed: one reference run and another run with extra 100 kg/hr of black carbon emissions in the regions noted in the first column of Table 2.6. Then the change in black carbon in the US surface level is compared to adjoint results. In order to reduce the effect of discrete addition, addition of black carbon emissions was based on a three dimensional Gaussian distribution.

Having a Gaussian perturbation gave a better result than adding a constant amount of black carbon to several grid boxes. This suggests that when the grid is refined and when the perturbation is in a continuous fashion, the results from finite difference and adjoint simulations will match with better accuracy.

This is one of the reasons why the north pole's finite difference and adjoint sensitivities have such a large discrepancy in Table 2.6. This difference can be reduced by using a finer resolution. The next finer grid resolution in GEOS-Chem is $2^\circ \times 2.5^\circ$, and running on this resolution requires 4 times the computational resources. Noting that winds are predominantly westerly in the latitudes of interest and we consider intercontinental impacts of emissions, a $4^\circ \times 5^\circ$ grid gives an adequate approximation.

Table 2.6: Comparison of forward difference and adjoint sensitivities for the transport module

Region of emissions	Forward Difference ($kg \cdot hr$)	Adjoint ($kg \cdot hr$)	Difference (%)
LTO emissions in Europe	1.24×10^1	1.45×10^1	15.61
Cruise emissions in Europe	1.83×10^3	1.68×10^3	8.55
LTO emissions in North Pole	1.03×10^3	1.57×10^3	41.54
Cruise emissions in North Pole	2.37×10^3	2.32×10^3	2.13
Cruise emissions in Asia	1.71×10^3	1.63×10^3	4.79
LTO emissions in South of Alaska	2.04×10^3	1.92×10^3	6.06
LTO emissions in the US	4.26×10^5	4.40×10^5	3.23

Chapter 3

Sensitivity Results

In this chapter, sensitivities of surface PM concentration and population exposure to PM to aircraft emissions are discussed. All simulations are run from April 1, 2006 to March 31, 2007 on a 4° of latitude by 5° of longitude horizontal grid resolution with GEOS5 vertical resolution. The first section discusses the definition of sensitivities, the second section shows the spin-up period that is required to capture the full impact of aircraft emissions, the third section discusses the methods for premature mortality calculations, and the rest of the chapter discusses the simulation results.

3.1 Definition of Sensitivities

Before discussing the sensitivity results, this section describes what sensitivities represent and how to compute the air quality or health impacts. There are two parts in each sensitivity metric: the cost function that is sensitivity of (or the numerator in the sensitivity) and the source that is sensitivity to (or the denominator in the sensitivity). For example, in the sensitivity of PM concentration to aviation emissions, the cost function is PM concentration and the source is aviation emissions.

The cost function in this thesis is averaged over time and space as shown in the following equation:

$$J = \frac{1}{V_r T_r} \iint pm(s,t) dv dt \tag{3.1}$$

where pm is the concentration of PM at spatial location, s, and time, t. V is the total volume of the domain of the objective function, and T is the length of the simulation. The subscript r in Eq. 3.1 and 3.2 represents the time and region of the receptor, or the objective function, and the subscript s in Eq. 3.3 represents the region and time of the source. In this case, the objective function is the PM concentration averaged over a one-year period.

The change in the cost function can be written as:

$$\delta J = \frac{1}{V_r T_r} \iint \delta pm(s,t) dv dt \tag{3.2}$$

$$= \frac{1}{V_s T_s} \iint \sum_{k=1}^{K} \frac{\partial J}{\partial c_k(s,t)} \delta c_k(s,t) dv dt \tag{3.3}$$

where $\frac{\partial J}{\partial c_k(s,t)}$ is the sensitivity of the objective function to the emission of chemical species k, calculated by the adjoint simulation, and $c_k(s,t)$ represents the emission density of specie k at location s and time t. The integrals in Eq. 3.2 are integrations over space and time where the cost function is considered, and the integrals in Eq. 3.3 are integrations over volume and time where emissions are considered.

Changing the above continuous notations to discrete notations, the sensitivities are given as three-dimensional spatial matrices or as four-dimensional spatial and temporal matrices. As indicated in Eq. 3.4, the inner product of a sensitivity matrix, shown in Fig. 3-1a, and an emission matrix, shown in Fig. 3-1b, calculates the change in the cost function caused by the emissions.

$$< \frac{\partial J}{\partial C}, \delta C >= \delta J \tag{3.4}$$

where $\frac{\partial J}{\partial C}$ is sensitivities of the objective function to 1kg of chemical species and δC is the emissions in kg in this discrete equation.

3.1.1 Interpreting Sensitivity Plots in this Thesis

Sensitivities, $\frac{dJ}{dc(s,t)}$, represent the amount of PM created averaged over the receptor space and time due to 1 kg of emissions at the location and time of emissions. All

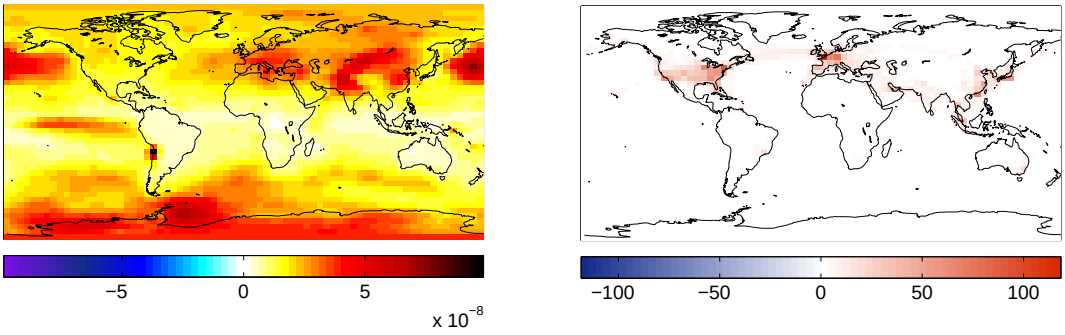

(a) Sensitivities (in $\mu g\,m^{-3}/kg\,hr^{-1}$) (b) Emissions (in kg/hr)

Figure 3-1: Sensitivities of global surface PM concentration to NO_X emissions (in $\mu g\,m^{-3}/kg\,hr^{-1}$) and global aircraft NO_X emission rate (in $kg\,hr^{-1}$) averaged over all altitudes: Inner product of two matrices gives the change in PM concentration (in $\mu g/m^3$) due to aircraft NO_X emissions

spatial sensitivity plots in this thesis are averaged over time of emissions, representing the annual average of PM concentration at the surface of a receptor location due to 1 kg/hr of emissions at the emitted location. For example, in Fig. 3-1a emitting 1 kg/hr of NO_X for one year spread over the vertical space of Santiago, Chile, increases the annual average of global PM concentration by $9 \times 10^{-8} \mu g/m^3$. To show the three dimensional sensitivities, many of plots, including ones in Appendix B, average sensitivities in altitudes, latitudes, or longitudes. As an example, sensitivities in Fig. 3-1a are averaged over all altitudes.

3.2 Spin-Up Period

The spin-up period is a time frame introduced to capture the complete impact of emissions on air quality. There is a time lag between when an aircraft emits primary PM and PM precursors, formation of PM in the ground layer of the receptor region, and removal of PM from the atmosphere. This time lag is shown in Fig. 3-2. Without the spin-up period, the impact of emissions emitted towards the end of a simulation will not be fully counted into the sensitivity. For example, if particulates last one week in a certain situation, sensitivity of primary PM emitted one day before the ending time will represent roughly one-seventh of its sensitivity. In this case, the

objective function, or sum of particulate matter, is summed only for one day rather than seven days.

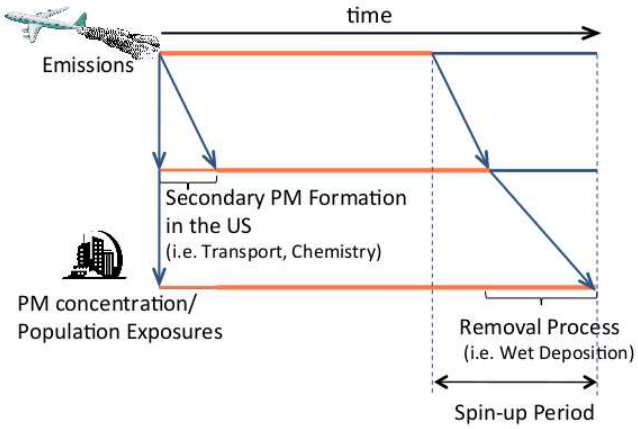

Figure 3-2: Explanation of spin-up period

To avoid this underestimation, we need to run a spin-up period at the end for the adjoint simulation, or in the beginning of the simulation for the forward model. To determine how long it takes from emission to formation and removal of PM, seven simulations were run. These simulations all start from the same time, January 1, 2006, and end at different times, having the simulation time from one month to seven months at one-month intervals. The simulations were run with full flight global aviation emissions.

Fig. 3-3 shows the sensitivities of surface PM concentration in the US with respect to global aircraft emissions for the different lengths of the run. For a one-month run, sensitivities to emissions are smaller than longer runs even in the same interval because PM lasts longer than simulation time of one month. To compare the values of the different lengths, sensitivities of surface PM concentration in the US in the first month were compared.

If we consider the time after one month as a spin-up period, a one-month simulation has no spin-up period, a two-month simulation has a one-month spin-up period, and likewise, a seven-month simulation has a six-month spin-up period. Considering that the sensitivities of six month spin-up period as reference sensitivities (six months period is a long enough time for the formation and removal of PM), sensitivities of

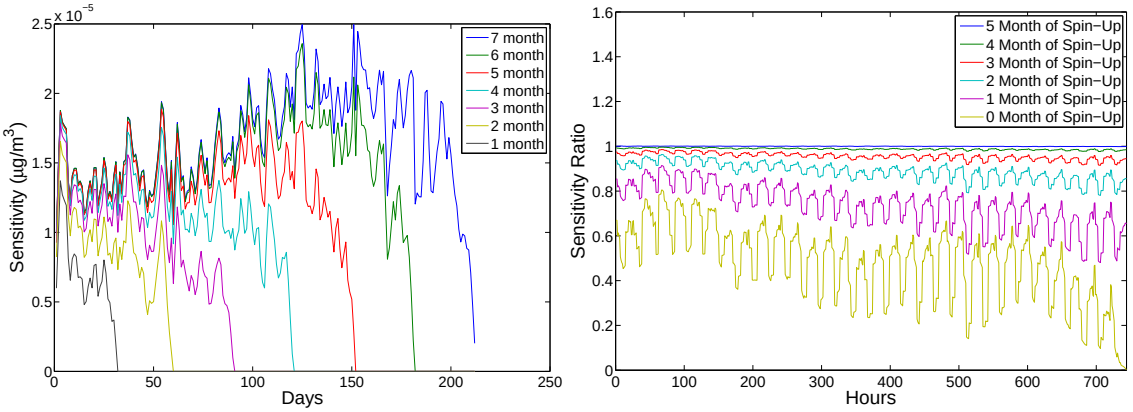

(a) Sensitivities to 1kg of emission

(b) Ratio of sensitivities using various spin-up periods to sensitivities with a six-month spin-up period

Figure 3-3: Comparison of different spin-up periods of the sensitivities of surface PM concentration in the US to global aircraft emissions

each simulation are divided by the reference sensitivities. These ratios are shown in Fig. 3-3.

It is shown that sensitivities without a spin-up period are about one-half of the reference sensitivities. Also, a five-month spin-up period creates sensitivities within 0.1 percent deviation from the reference sensitivities. This means that 99.9% of particulates are scavenged within six months after when the precursors or primary particulates are emitted in GEOS-Chem simulations. Also we can see that about 95% of PM will be removed from atmosphere within four months of its emission. The average of the ratios for each month is plotted in Fig. 3-4. The ratios calculated in Fig. 3-4 are the impacts on the last month before the spin-up period. However, since these undervalued sensitivities only occur at the end of simulation, the underestimation for the annual impact is much smaller. For example, with a twelve-month simulation without spin-up period, the last, the second to the last, the third to the last months calculates, 48%, 74%, and 89% of total impact, respectively. On average, having no spin-up period computes 92% of the annual impact. For the calculation of sensitivities in time, having 48% of the impact calculated in the last month and the full impact in the first several months brings challenge. Therefore, all simulations in this thesis use seventeen months: twelve-month simulation period and five-month

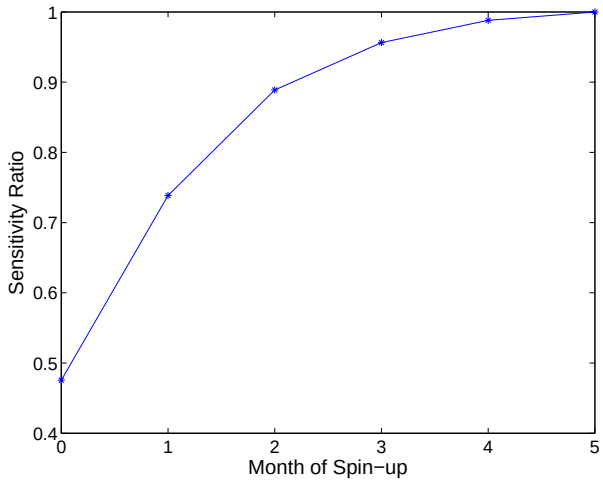

Figure 3-4: Ratio of impacts in the last month captured from simulations with different spin-up periods compared to a simulation with a six-month spin-up period

spin-up period.

3.3 Premature Mortality Calculation

For PM related mortalities, the following concentration-response function (CRF) is used. This is the work of Barrett et al. 2011, which is a forthcoming paper to be published as *"Public health, climate, and economic impacts of desulfurizing jet fuel"*, but not yet submitted.

$$\begin{aligned} \triangle Mort = & \sum_{i,j} [\beta^{CP} \, f_{k,30+} \, P_{i,j} \, \triangle \chi_{i,j} \, B_k^{CP} + \beta^{LC} \, f_{k,30+} \, P_{i,j} \, \triangle \chi_{i,j} \, B_k^{LC}] \\ & - \sum_{i,j} [(\beta^{CP} \, B_k^{CP} + \beta^{LC} \, B_k^{LC}) \, f_{k,30+} \, P_{i,j} \, \triangle \chi_{i,j}] \end{aligned} \tag{3.5}$$

In the equation, $k = k(i,j)$, which is the function of i and j, is the country of interest, $f_{k,30+}$ is the fraction of population over the age of 30, and β is the risk coefficients that shows the fractional increase in mortality given one μg/m^3 increase in PM. $\triangle \chi_{i,j}$ is the change in $PM_{2.5}$ concentration in μg/m^3, B_k is the baseline incidence rate of mortality in the country k, and $P_{i,j}$ is the number of population exposed to PM. The superscripts CP and LC denote cardiopulmonary disease and long cancer, respectively. Table 3.1 summarizes the baseline incidence rates and fraction of population over the age of 30

in various regions used in this study.

Table 3.1: Baseline incidence rates and fraction of population over the age of 30

	US	NA	EU	Asia	World
B^{CP} ($\times 10^{-3}$)	2.48	2.48	3.48	2.31	2.47
B^{LC} ($\times 10^{-3}$)	0.55	0.55	0.42	0.19	0.21
$f_{k,30+}$	0.59	0.59	0.59	0.47	0.46
Pop (billion)	0.27	0.50	0.55	3.60	6.44

Numerous studies, including Harvard Six Cities Study and American Cancer Society (ACS) studies, draw an association between long-term exposure to $PM_{2.5}$ and mortalities. These studies determine the risk coefficients for all cause mortalities ranging from 0.1% to 3.2% per $1\mu g/m^3$ [16]. A linear relationship is assumed for mortalities and long-term exposure.

Table 3.2: Risk coefficients in the US from Pope et al. 2002 [2] and Laden et al. 2006 [3]

	Pope2002	Laden2006
All-cause	0.6	1.6
Cardiopulmonary	0.9	2.8
Lung cancer	1.4	2.7

The risk coefficient for all-cause mortalities are less likely to be uniform in the world than the risk coefficients for cardiopulmonary disease and lung cancer. Instead of using the all-cause mortality risk coefficient, this thesis uses risk coefficients for cardiopulmonary disease and lung cancer. The coefficients for cardiopulmonary and long cancer have not been clearly defined with its uncertainties. Thus, cardiopulmonary and lung cancer risk coefficients are calculated from the risk coefficients for all-cause mortality, which is assumed to have the shape of the Weibull distribution with mean value of 1.06%.

It is assumed that the total premature mortalities from pollutants equals the sum of the premature mortalities from lung cancer and cardiopulmonary disease caused by exposure the pollutants, which leads to the equation:

$$\beta^{AC}_{US}\, B^{AC}_{kUS} = \beta^{CP}\, B^{CP}_{kUS} + \beta^{LC}\, B^{LC}_{kUS}. \tag{3.6}$$

In order to calculate the risk coefficients for lung cancer and cardiopulmonary disease, this thesis uses the ratio between the two, $\gamma = \frac{U(1.4,2.7)}{U(0.9,2.8)}$, calculated by applying the uniform distributions to values in Table 3.2. Using the ratio, $\gamma = \frac{\beta^{LC}}{\beta^{CP}}$, risk coefficients $\beta^{CP} = \frac{\beta^{AC} B_{US}^{AC}}{B_{US}^{CP} + \gamma B_{US}^{LC}}$ and $\beta^{LC} = \gamma \beta^{CP}$ are calculated and applied to Eq. 3.5. With the distributions and parameters mentioned above, this thesis performs Monte Carlo analysis of mortality calculation for the uncertainty quantification.

3.4 Regional PM Exposure due to Intercontinental Effects

This section presents the intercontinental effects of aircraft emissions on the changes in PM concentration and population exposure to PM. The impacts of LTO emissions are first discussed, followed by the impacts of full flight emissions. These impacts on air quality and the health of the exposed population show the importance of studying the long-range transport of aerosols and their precursors emitted from aircraft.

3.4.1 Landing and Take-off Emissions

Various studies demonstrate the impact of landing and take-off emissions [43, 24, 10, 23, 44, 7, 8]. By giving comparisons, this part of the thesis discusses the impacts of LTO emissions on air quality and health of several regions.

Direct and Indirect Effect of Emissions

How aircraft emissions impact the air quality can be seen by looking at the sensitivities, shown in Fig. 3-5. The sensitivities to primary PM emissions in Fig. 3-5 are only visible immediately around Europe, indicating that primary PM of LTO emissions has a direct impact on their emitted regions but not beyond it. In contrast, sensitivities to CO are non-zero in the north hemisphere. This is because CO emissions have an indirect, hemispheric effect to PM formation by increasing the ozone concentration in the hemisphere. Increasing ozone concentration increases the concentration of

hydroxyl radical, thereby increasing oxidation of NO_X and SO_X. However, because CO competes with NO_X and SO_X for oxidizants, the direct, short-term influence on their emitted location is decreasing PM concentrations. For NO_X and SO_X emissions, sensitivities spread out to a larger domain around Europe, but not to an hemispheric extent. One difference is sensitivities to NO_X follow the upsteam wind direction and sensitivities to SO_X is more evenly spread around Europe.

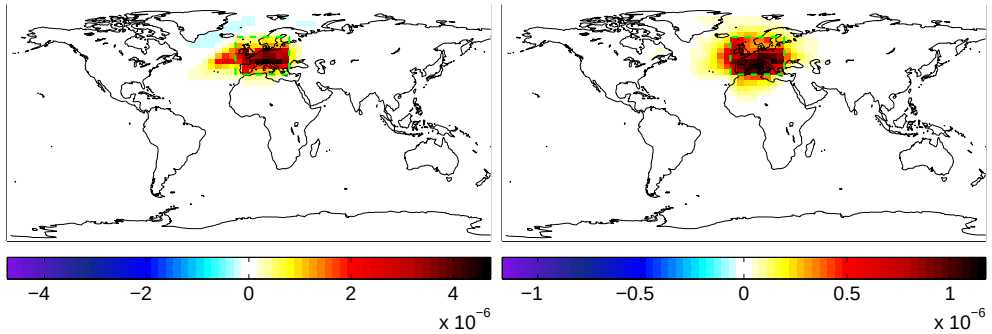

(a) Sensitivities to NO_X (b) Sensitivities to SO_X

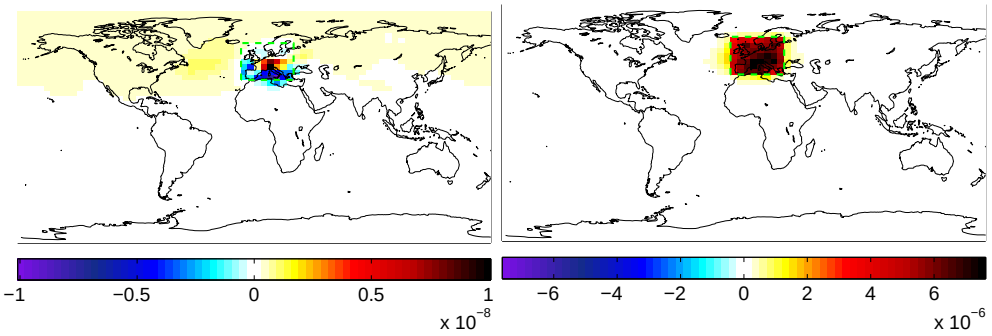

(c) Sensitivities to CO (d) Sensitivities to primary PM

Figure 3-5: Sensitivities of surface PM concentration (in $\mu g/m^3$) in Europe with respect to 1 kg/hr of various ground level emissions (in $\mu g\,m^{-3}/kg\,hr^{-1}$)

How emissions impact air quality in Europe can be extended to other regions. For example, Fig. 3-6 shows how the ground level NO_X emissions impact air quality in different regions. It is shown that NO_X emissions impact the PM concentration in the vicinity of their emitted region following the downstream wind direction.

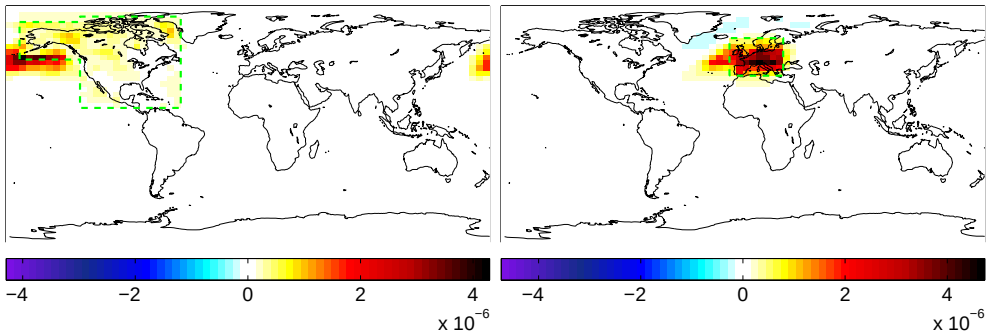

(a) Sensitivities of PM in North America (b) Sensitivities of PM in Europe

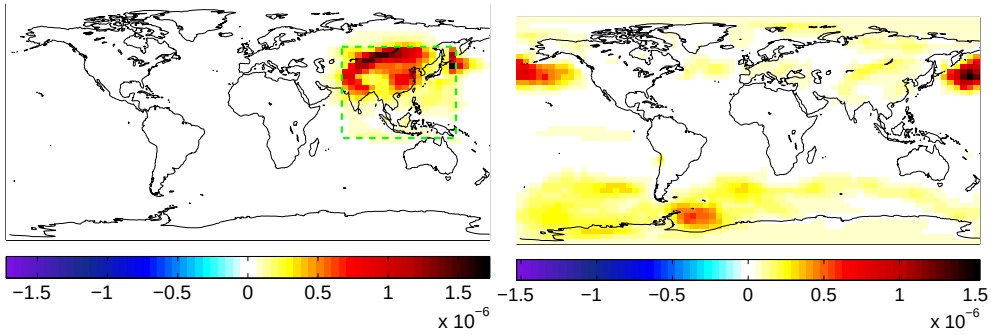

(c) Sensitivities of PM in Asia (d) Sensitivities of PM in the world

Figure 3-6: Sensitivities of surface PM concentration in various regions with respect to ground level NO_X emissions (in $\mu g\,m^{-3}/kg\,hr^{-1}$)

Intercontinentnal Source-Receptor Matrices for LTO emissions

Using the sensitivities calculated from GEOS-Chem Adjoint, the impacts of LTO emissions in source regions to receptor regions are found. Table 3.3 shows that about 91% to 98% of the PM concentration increase is caused by the emissions in its own receptor region. With these values of concentration increase, population exposure to PM cannot be quantified because population distributions of the regions are not constant. To see the health impact, the source-receptor matrix for population exposure to PM concentration increase is separately calculated and is shown in Table 3.4. Brunelle-Yeung mentions that her study of the impact of aviation emissions on the US air quality can be improved by including the emissions from Canada and Mexico [43]. The population exposure to PM concentration increase in Table 3.4 shows that 94.3% of LTO emissions' impact on the US comes from the US and 4.8% comes from other parts of North America.

Table 3.3: Impact of LTO emissions in source regions on surface PM concentrations in receptor regions (in $\times 10^{-3}\,\mu g/m^3$)

From \ To	US	NA	EU	Asia	World
US	4.50	1.07	0.22	0.04	0.12
NA	4.84	1.53	0.29	0.06	0.17
EU	0.02	0.02	18.92	0.07	0.41
Asia	0.02	0.01	0.06	2.02	0.26
World	4.89	1.56	19.54	2.21	0.95

Table 3.4: Impact of LTO emissions in source regions on population exposures to PM in receptor regions (in $\times 10^{6}\,\text{people} \cdot \mu g/m^3$)

From \ To	US	NA	EU	Asia	World
US	2.33	2.49	0.24	0.66	3.47
NA	2.45	3.34	0.33	0.93	4.71
EU	0.01	0.01	21.59	0.70	23.42
Asia	0.01	0.01	0.07	31.13	31.33
World	2.47	3.37	22.10	33.66	62.21

Looking at Table 3.5, there approximately 2,000 premature mortalities in the world due to aircraft LTO emissions in one-year. Most of the mortalities are concentrated in Europe and Asia, including 1,360 and 1,030 premature mortalities, respectively. The number of premature mortalities in the world is calculated to be lower than the combined number of mortalities in Europe and Asia. This is because the global premature mortalities are calculated by applying globally averaged values for the fraction of population over the age of 30, $f_{k,30+}$, and for the baseline incidence rates, B, whereas each of the regions uses its own regions' specific values. The coefficients used in this thesis are presented in Table 3.1. It is possible to use country specific coefficients for CRF using the adjoint simulation, but it must be done prior to running a simulation. As mentioned in Chapter 2, an objective function of the adjoint method is a scalar. So it is not possible to post-process the grid specific information. Thus, the adjoint simulation must find sensitivities of an objective function (coefficients pre-multiplied population exposure) for the accurate mortality calculation.

Total mortalities in the US are computed to be 210 by Masek [44] whereas adjoint

Table 3.5: Impact of LTO emissions in source regions on premature mortalities in receptor regions with the 95% confidence interval (in people)

From \ To	US	NA	EU	Asia	World
US	110	120	20	20	110
	(40, 200)	(50, 220)	(10, 30)	(10, 40)	(40, 210)
NA	120	160	20	30	150
	(50, 220)	(60, 290)	(10, 40)	(10, 50)	(60, 280)
EU	0	0	1320	20	750
	(0, 0)	(0, 0)	(510, 2430)	(10, 40)	(29, 1390)
Asia	0	0	0	960	1010
	(0, 0)	(0, 0)	(0, 10)	(370, 1770)	(390, 1870)
World	120	160	1360	1030	2000
	(50, 220)	(60, 300)	(530, 2500)	(400, 1910)	(780, 3700)

simulation gives 110. The RSM and GEOS-Chem Adjoint models have many differences: 1) chemical transport models (CTM), 2) concentration-response functions 2) background emissions, 3) aviation emissions inventories, and 4) grid sizes.

The work of this thesis found less change in the PM concentration while predicting larger number of mortalities. A factor might be the use of different CRFs. Smaller mortalities could also be attributed to due to the coarse sizing of the grid. Having a larger grid gives smoothed-out peak of people exposed to pollution in large cities, which in turn causes smaller mortalities.

3.4.2 Cruise Emissions

Whereas LTO emissions only have local air quality impacts, emissions above 3,000 feet increase PM concentrations both in their emitted regions and in regions away from their emissions. Emissions at cruise altitudes get transported following the downstream wind direction, causing the long-range transport of particulate matter and PM precursors. Fig. 3-7 plots sensitivities of PM concentration in various regions to cruise emissions. It can be seen that sensitivities vary from region to region but the variation is comparatively smaller than the one of LTO emissions. Sensitivities to cruise emissions are more evenly distributed, keeping the same order of magnitude within the hemispheres.

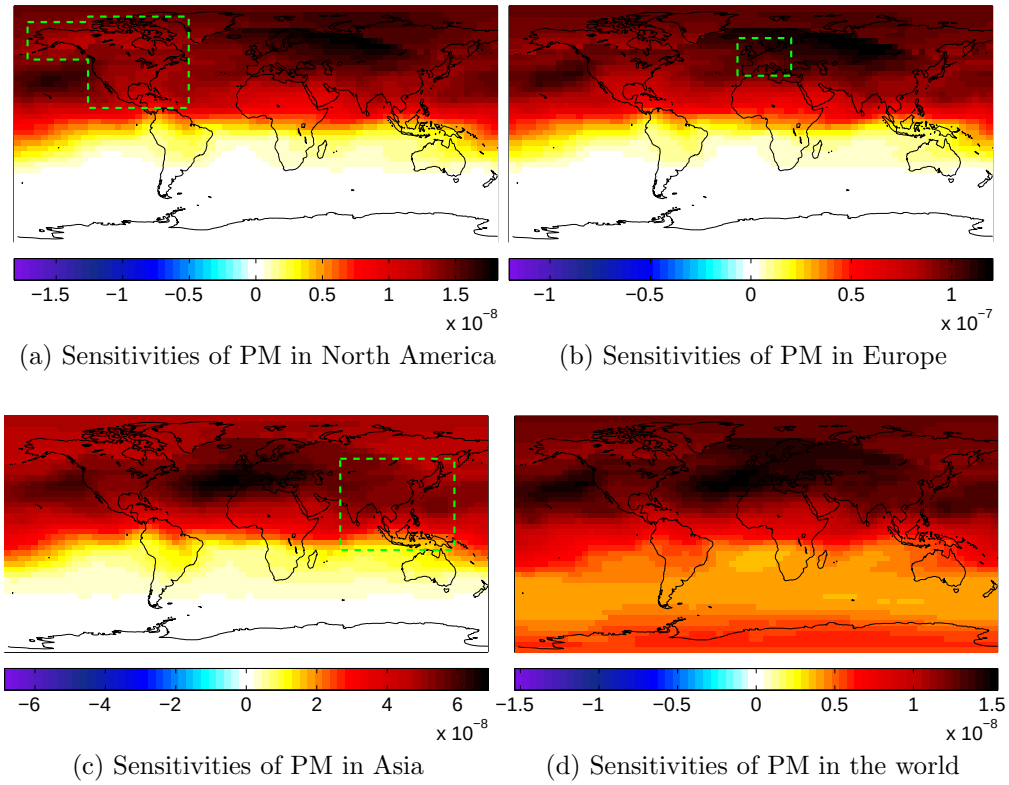

(a) Sensitivities of PM in North America

(b) Sensitivities of PM in Europe

(c) Sensitivities of PM in Asia

(d) Sensitivities of PM in the world

Figure 3-7: Sensitivities of surface PM concentration in various regions with respect to cruise level NO_X emissions (in $\mu g\,m^{-3}/kg\,hr^{-1}$)

Streamline of Wind Transporting the Pollutants

Fig. 3-8 plots sensitivities of the US PM concentration to NO_X emissions and shows the plume of sensitivity rising to north west of the US. A sensitivity plot shows how much emissions in various regions affect PM concentration in a receptor location, and Fig. 3-8 shows emissions in north west increases PM concentration in the US more than emissions in other regions. As discussed earlier, because of the westerly wind in the mid latitudes, emissions west of the receptor region influences the US.

Furthermore, sensitivities north of the receptor region is larger because of the meridional circulation, which is explained in Fig. 3-9 [1]. The meridional circulation in the mid-latitudes carries the aircraft emissions south, thus increasing PM concentration south of emitted locations. The figure shows the distribution of aircraft fuel burn and black carbon at the surface level.

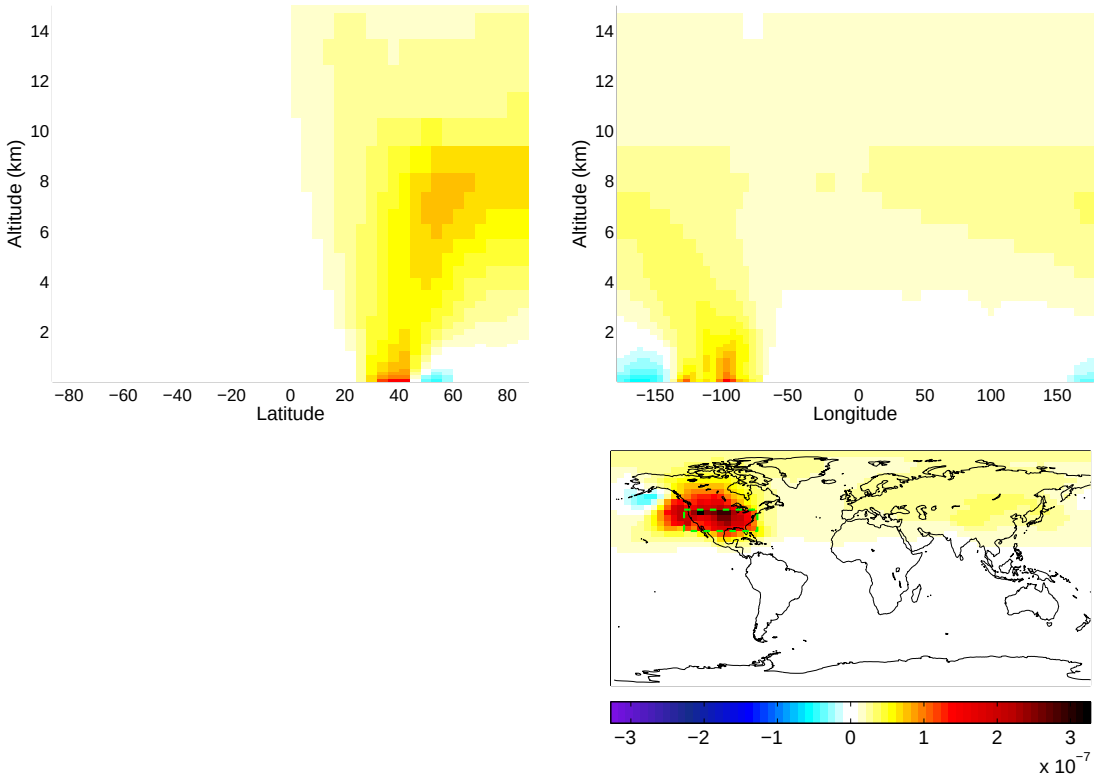

Figure 3-8: Sensitivities of surface PM concentration in the US due to 1kg/hr of NO_X emissions (in $\mu g\,m^{-3}/kg\,hr^{-1}$)

Intercontinentnal Source-Receptor Matrix for Full Flight Emissions

As what is analyzed for LTO emissions, the impact from full flight emissions are analyzed. Table 3.6 gives the PM concentration change due to total aircraft emissions, and Table 3.7 gives population exposure to PM concentration changes. The comparison of this adjoint simulation for global full flight emissions is done with Barrett et al. [1].

Table 3.6: Impact of full flight emissions in source regions on surface PM concentrations in receptor regions (in $\times 10^{-3}\,\mu g/m^3$)

From \ To	US	NA	EU	ASIA	World
US	8.32	2.80	6.74	3.56	1.20
NA	10.24	4.16	10.37	5.51	1.85
EU	2.02	1.03	28.91	3.78	1.55
ASIA	2.00	1.06	5.18	6.12	1.26
World	16.68	7.54	50.89	19.68	6.08

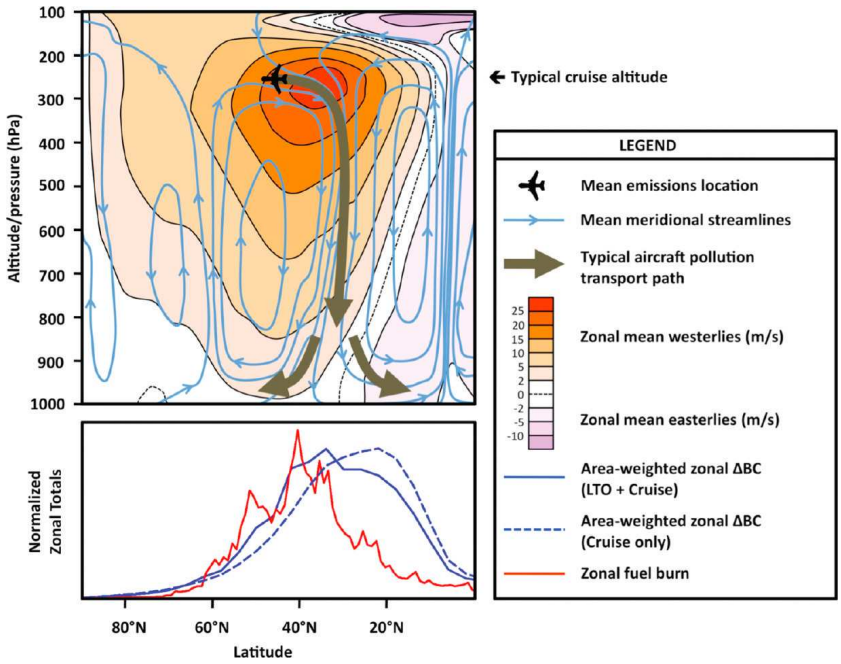

Figure 3-9: Streamline of wind and the transport of PM from aircraft emissions [1]

Table 3.7: Impact of full flight emissions in source regions on population exposures to PM in receptor regions (in $\times 10^6$ people $\cdot\, \mu g/m^3$)

From \ To	US	NA	EU	ASIA	World
US	3.76	4.56	7.91	52.39	69.23
NA	4.44	6.44	12.13	80.16	105.50
EU	0.74	1.09	32.64	52.86	93.32
Asia	0.71	1.21	6.23	91.30	102.00
World	6.75	10.15	58.43	283.90	376.60

The global mortalities are computed to be 12,600 with the 95% confidence interval of (6000, 19900) in Barrett et al. and 12,150 with the 95% confidence interval of (4820,22370) in this study [1]. These values are consistent with less than 20% difference. Albeit many differences in the model, such as 1) the use of different CRFs, 2) applying averaged population over the age of 30 and baseline incidence rate for global objective function, 3) different year of simulation, consistency in the number of mortalities is excellent.

The number of mortalities in each of the regions are also consistent. The mortalities in the US in this study are about 30% smaller and mortalities in other regions

Table 3.8: Impact of full flight emissions in source regions on premature mortalities in receptor regions with the 95% confidence interval (in people)

From \ To	US	NA	EU	Asia	World
US	180	220	490	1620	2240
	(70, 330)	(90, 400)	(190, 900)	(630, 2990)	(880, 4130)
NA	210	310	750	2470	3400
	(80, 390)	(120, 560)	(300, 1370)	(980, 4530)	(1340, 6230)
EU	20	50	2010	1630	3010
	(10, 40)	(20, 100)	(790, 3700)	(640, 3010)	(1170, 5550)
Asia	30	60	380	2830	3300
	(10, 60)	(20, 110)	(100, 710)	(1100, 5210)	(1280, 6090)
World	320	490	3600	8760	12150
	(130, 590)	(190, 890)	(1430, 6610)	(3470, 16130)	(4820, 22370)

are higher than ones from Barrett et al. These discrepancies may come from using different concentration response functions and different coefficients because there are uncertainties associated with CRFs and the coefficients.

In Table 3.8, it is shown that more than a half of the premature mortalities caused by aircraft emissions in North America and Europe are caused by emissions in their own regions. However, in Asia less than a third of the mortalities is caused by its own emissions. The last column of Table 3.8 shows the premature mortalities that the region causes and the last row gives aviation induced mortalities occurred in each of the regions. Compared to the number of mortalities North American emissions cause, the premature mortalities in North America due to global aircraft emissions are about an order of magnitude smaller. The number of mortalities in Europe is similar to what the emissions in the region cause; however, Asian mortalities are two to three times larger than total mortalities caused by Asian aircraft emissions.

Using the term from Barrett et al. [1], North America is a net exporter of pollution and Asia is a net importer of pollution. This is because of the mean winds in the regions, explained in the earlier section. In the mid-latitudes, westerly winds carry North American emitted pollutants to Europe over the Atlantic Ocean and European emissions to Asia. However, emissions in Asia do not reach North America because PM and its precursors are washed out in inter-tropical convergence zone. In

lower latitudes, the prevailing wind direction is from east to west. Therefore, the Asian emissions in low latitudes get carried to west, increasing the European PM concentration, but not as large as the impcat of European emissions on Asian air quality.

3.4.3 Comparisons between LTO and Cruise Emissions

This thesis shows LTO emissions' impact is about 10 to 40% of total aircraft emissions impact depending on the regions, and this value is consistent with 20 to 30% as shown in Barrett et al. [1]. In addition, a report to the European Commission, comparing the European LTO and non-LTO emissions, indicates that the contribution from LTO and non-LTO emissions on PM concentration change at the surface of Europe is about 50% [45]. This is consistent with the result from this thesis, estimating non-LTO emissions' impact in Europe to be approximately 60% of the impact of total aircraft emissions.

3.5 Effect of Seasons and Times of Day

Sensitivities of PM at the surface to aircraft emissions also vary temporally, both at different times of day and at different seasons of year. For this, sensitivities of PM concentrations in the world with respect to 1kg of the world emissions at each hour are plotted. Because sensitivities have a diurnal cycle, sensitivities at local times of day averaged over one year period are also plotted. In order to see the impact of aircraft emissions, the sensitivities are spatially weighted by aircraft emissions.

3.5.1 Diurnal Cycle

The amplitude of the diurnal variation of sensitivities grows as we focus on the ground level emissions as shown in Fig. 3-10. Each figure shows sensitivities averaged over 365 days binned hourly by local time of day. Fig. 3-10 show that the amount of pollution created depends largely on the time at which ground level emissions occur. For cruise

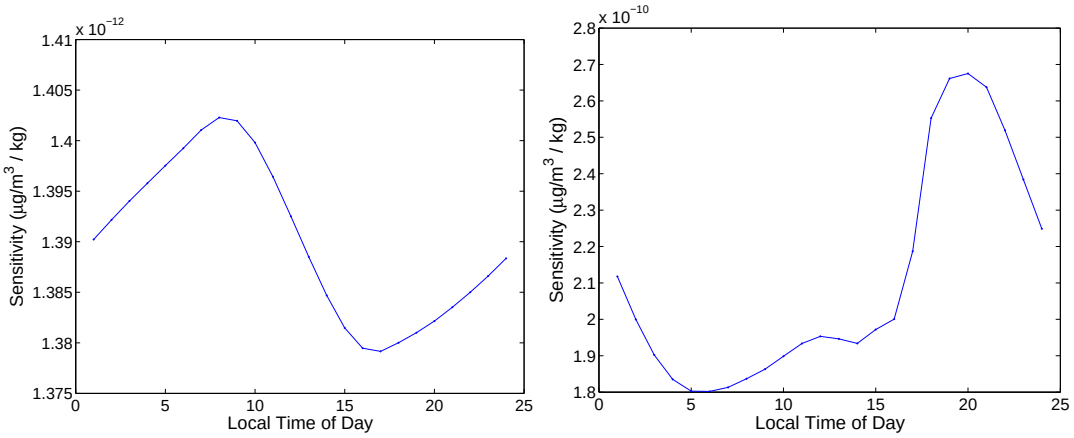

(a) Cruise level NO_X emissions

(b) Ground level NO_X emissions

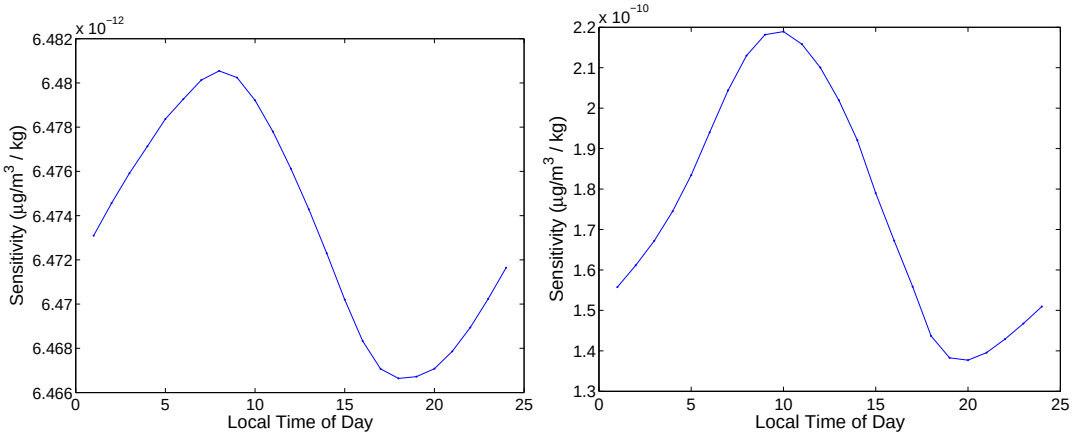

(c) Cruise level SO_X emissions

(d) Ground level SO_X emissions

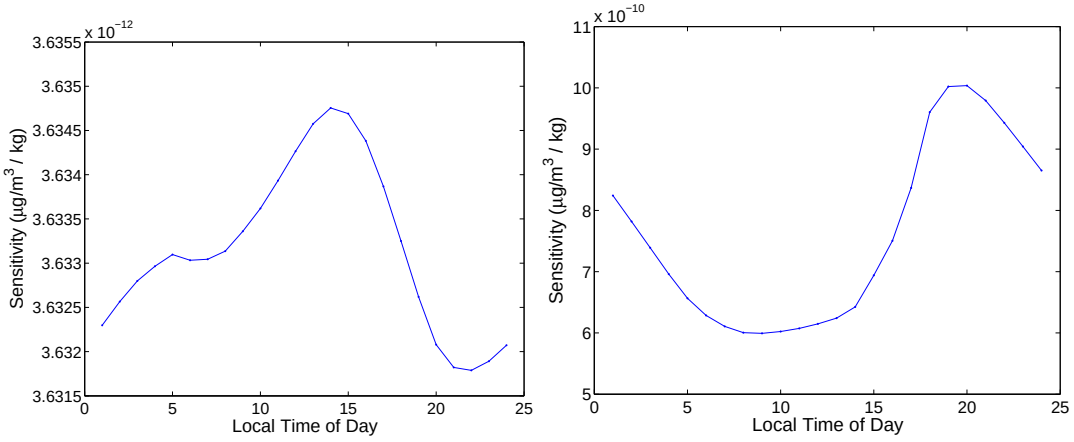

(e) Cruise level primary PM emissions

(f) Ground level primary PM emissions

Figure 3-10: Sensitivities of global surface PM concentration averaged over 365 days to various emissions at different local times of day for aviation

emissions of all three species (NO_X, SO_X, primary PM), the differences between the maximum and minimum averaged sensitivities maximum averaged sensitivities are less 2%, but for ground level emissions, the differences are about 50 to 60%. For NO_X and primary PM emissions, evening emissions create larger negative air quality impact than morning emissions, and morning emissions create larger negative impact for SO_X emissions.

3.5.2 Seasonal Cycle

Although the significance of diurnal cycle is observed only for ground level emissions, the seasonal variation is observed on both cruise emissions and ground level emissions as shown in Fig. 3-11. The highest seasonal variation occurs for cruise level NO_X emissions. The sensitivity in November is five times higher than the sensitivity in May. For primary PM, sensitivities to emissions in winter are about 50% larger than the ones in summer. With the exception of ground level SO_X emissions, all emissions (cruise level SO_X, cruise and ground level NO_X, and cruise and ground level primary PM) have higher sensitivities in winter than summer.

Although the sensitivities are spatially averaged by aircraft emissions, these values can also apply to other ground level emissions. The ground level aircraft emissions are located around airports, which are also located near cities. Thus, spatially weighting by aircraft emissions may be an adequate approximation for sensitivities to other ground level emissions. However, spatial weighting by other emissions should be performed when analyzing the ground emissions' impact on air quality in future work.

It could be argued that capturing the annual variation with only one-year simulation might be misleading. But a clear indication of cyclic behavior of sensitivities is shown: the sensitivities at the end of simulation, or March 31, 2007, match the sensitivities at the beginning of the simulation, or April 1, 2006. The understanding of the seasonal variation can be confirmed by running simulations in different year, a task left for future studies.

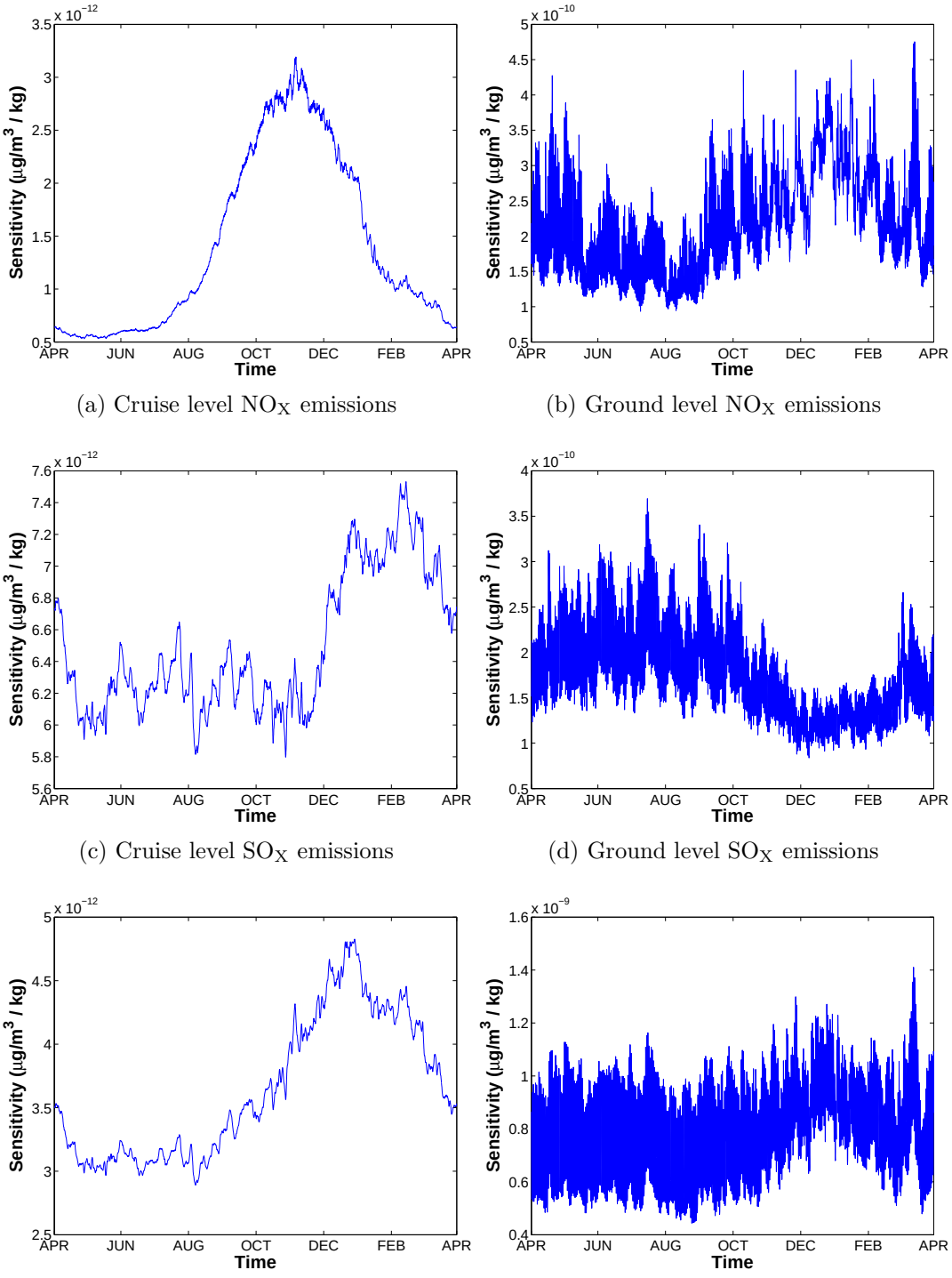

(a) Cruise level NO_X emissions

(b) Ground level NO_X emissions

(c) Cruise level SO_X emissions

(d) Ground level SO_X emissions

(e) Cruise level primary PM emissions

(f) Ground level primary PM emissions

Figure 3-11: Sensitivities of global surface PM concentration to various emissions at different times of year for aviation

3.6 Sensitivities of Each PM Species to Aircraft Emissions

This section looks at the sensitivity of each PM species to global aviation emissions. For three of the PM species (NO_3^-, SO_4^{2-}, NH_4^+), contributions from each of the aviation emission species are shown. Black carbon and organic carbon are primary PM species. They are directly emitted and do not react with other species in GEOS-Chem, so they are omitted in the tables below.

How to interpret Table 3.9 and Table 3.10 is explained here. The numbers in the first three rows and four columns represent how much change in PM species of the corresponding row is caused by aviation emissions of the given column. For example, the number in the second column and third row in Table 3.9 can be interpreted as the 21.7 % of ammonium increase due to aviation is caused by SO_X emission. The last column represents the portion of each of PM species change in the total PM concentration change due to aviation. So the number in the second row of the last column shows that sulfate increase contributes to 35.9% of total PM concentration change due to aviation emissions. The numbers in the last row represents how much of aviation induced PM is caused by each of the aircraft emitted PM precursors. The number in the last row of the first column shows that NO_X causes 77.5% of total PM concentration change due to aviation.

Comparing the individual PM species, nitrate aerosols have the largest contribution to the total PM concentration increase, followed closely by sulfate aerosols. Table 3.9 also indicates that NO_X makes a significant contribution to the formation of nitrate, sulfate, and ammonium. In contrast, SO_X emissions have an influence only on sulfate aerosols. Although increases in nitrate and sulfate aerosols due to aircraft activities are similar in their amounts, impact from NO_X is much larger than the impact from SO_X because NO_X is a precursor to various PM species whereas SO_X is a precursor to only sulfate.

Table 3.10 shows population-weighted PM concentration change due to aviation emissions. Whereas sulfate aerosols are 35.9% of PM concentration increase in Ta-

Table 3.9: Change in each PM species concentration due to aviation emissions (in %)

	NO_X	SO_X	HC	CO	Each PM species in total PM
NO_3^-	102.2	-2.5	0.1	0.2	41.2
SO_4^{2-}	51.0	49.2	0.1	-0.3	35.9
NH_4^+	78.3	21.7	0.1	-0.1	21.8
Total PM caused by each emission species	77.5	21.4	0.1	0.0	

ble 3.9, population exposure to sulfate aerosols is 10.8%. This means that sulfate aerosols formed from aviation SO_X emissions tend to reside in regions that are not heavily populated.

Table 3.10: Change in population exposure to each PM species due to aviation emissions (in %)

	NO_X	SO_X	HC	CO	Each PM species in total PM
NO_3^-	100.0	-0.4	0.2	0.2	65.7
SO_4^{2-}	53.0	47.8	0.1	-0.9	10.8
NH_4^+	91.9	7.9	0.2	0.0	23.0
Total PM caused by each emission species	92.6	6.7	0.2	0.1	

In order to verify the finding about the distributions of nitrate and sulfate, four forward simulations were run: a simulation with 1) full aviation emissions, 2) no aviation emissions, 3) full aviation emissions but excluding NO_X, and 4) full aviation emissions but excluding SO_X. Comparing the differences, the proportions of NO_X and SO_2 in each of the PM concentrations are analyzed, and distributions of nitrate and sulfate are plotted.

Fig. 3-12 shows the distributions of nitrate and sulfate aerosols formed by aircraft emissions. Fig. 3-12 confirms that nitrate aerosols are distributed in a populated area unlike the distribution of sulfate aerosols in tropic regions.

Table 3.10 shows that removing aircraft SO_X emissions completely in the world reduces the population exposure to increased PM concentration by 6.7 %, the amount SO_X contributes to global population exposure to PM.

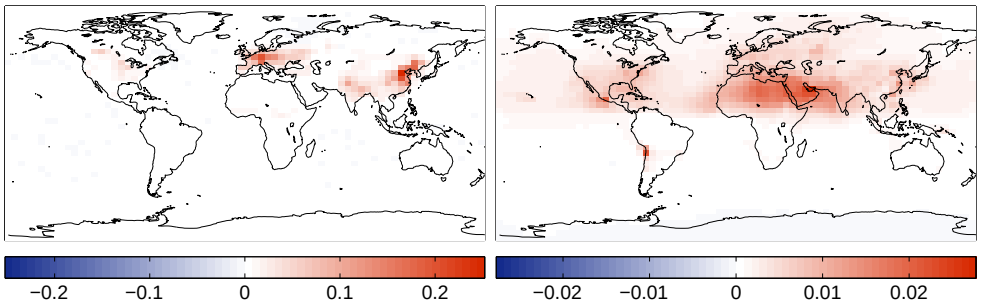

(a) NO_3^- (b) SO_4^{2-}

Figure 3-12: Change in annual average of the surface level nitrate and sulfate concentrations caused by aviation emissions simulated using the forward model of GEOS-Chem (in $\mu g/m^3$)

3.7 Second-order Sensitivities

In the above sections the direct impact of aircraft emissions on air quality has been calculated in numerical simulations. In addition to the first-order sensitivities, Woody et al. shows that a change in the background chemical composition, especially the availability of ammonia, changes the PM contribution of aviation [46]. With excess ammonia available, more HNO_3 can be neutralized, forming ammonium nitrate. In order to quantify the role of background emissions in changing the impact of aviation on air quality, the second-order sensitivities must be calculated.

$$\frac{d(J_{AV} - J_{noAV})}{dc} \approx \frac{dJ_{AV}}{dc} - \frac{dJ_{noAV}}{dc} \tag{3.7}$$

where $\frac{dJ_{AV}}{dc}$ is the sensitivity of an objective function to emissions calculated with aviation emissions and $\frac{dJ_{noAV}}{dc}$ is the sensitivity to emissions calculated without aviation emissions. After computing two sensitivities with aviation emissions on and off, taking the difference shows how the background emissions influence the magnitude of the impact of aviation on air quality and on premature mortalities.

As noted earlier in this section, having extra background emissions of ammonia will increase aviation's impact on air quality. The abundance of ammonia will increase the formation of PM, ammonium sulfate and ammonium nitrate. So the second-order sensitivities for ammonia is always positive as shown in Fig. 3-13.

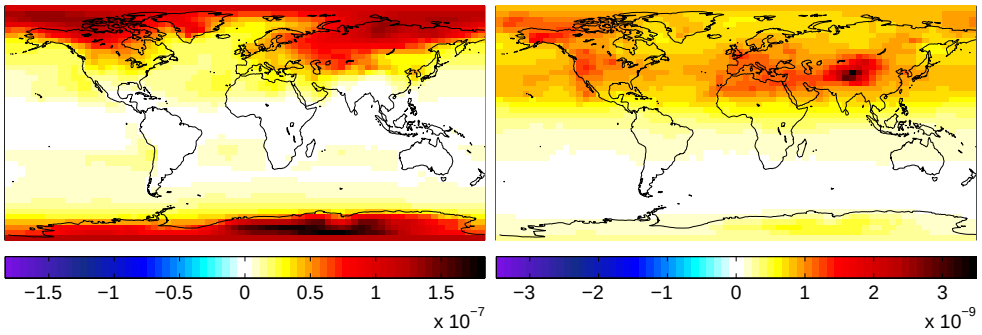

(a) First-order (b) Second-order

Figure 3-13: First- and second-order sensitivities of global surface PM concentration with respect to ammonia emissions (in $\mu g\,m^{-3}/kg\,hr^{-1}$)

Unlike ammonia, having extra NO_X emissions in the background would decrease aviation's impact as shown in Fig. 3-14. The factors leading to the negative second-order sensitivities are not studied in this thesis and can be studied in future work.

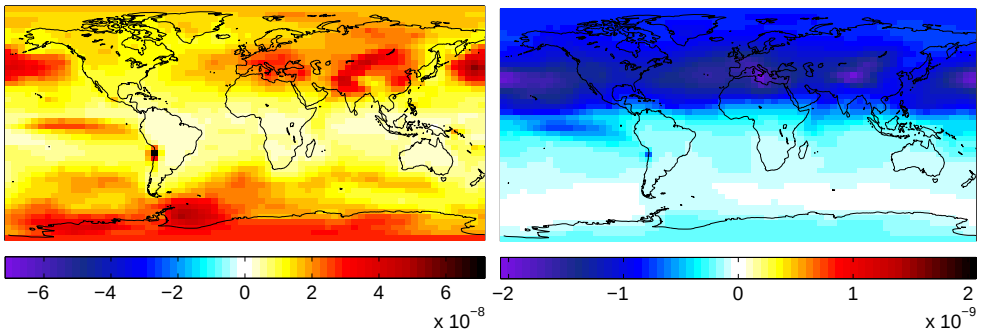

(a) First-order (b) Second-order

Figure 3-14: First- and second-order sensitivities of global surface PM concentration with respect to NO_X emissions (in $\mu g\,m^{-3}/kg\,hr^{-1}$)

Whereas the former two tracers only have either positive or negative second-order sensitivities, sulfur dioxide emissions have both positive and negative second-order effects as shown in Fig 3-15. In the Sahara, California, Middle East, and Greenland, the first-order sensitivities are larger and the second-order sensitivities are higher than other regions. These regions with relatively high sensitivities to SO_2 emissions are locations with low precipitation, either being a desert or an arctic desert. Unlike

these regions, the first-order sensitivities to SO_2 are lower in tropical regions and the second-order sensitivities are negative. Having more background emissions of SO_2 at locations with high precipitation decreases the aviation's impact on PM formation.

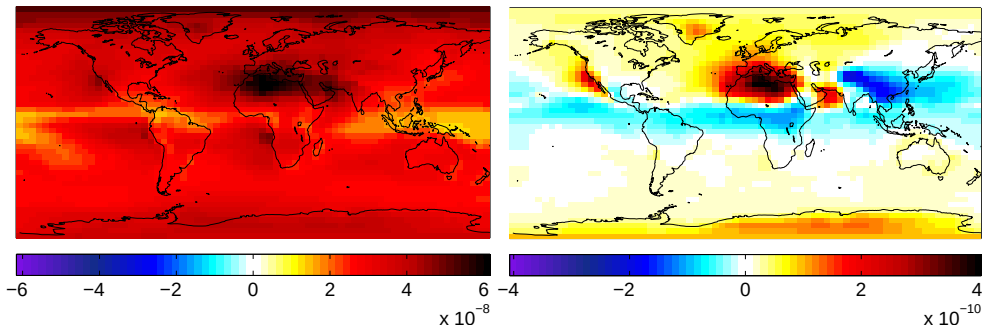

(a) First-order (b) Second-order

Figure 3-15: First- and second-order sensitivities of global surface PM concentration with respect to SO_2 emissions (in $\mu g\,m^{-3}/kg\,hr^{-1}$)

For the primary PM species, their contribution to PM concentration increase is linear. This is because primary PM in GEOS-Chem does not react with other species in the atmosphere, only being removed by wet deposition. The linearity of the sensitivities is confirmed in Fig. 3-16, showing the second-order sensitivities are zero everywhere. Thus, according to the atmosphere modeled by GEOS-Chem, having an extra unit of primary PM emissions does not change how aircraft emissions impact the air quality.

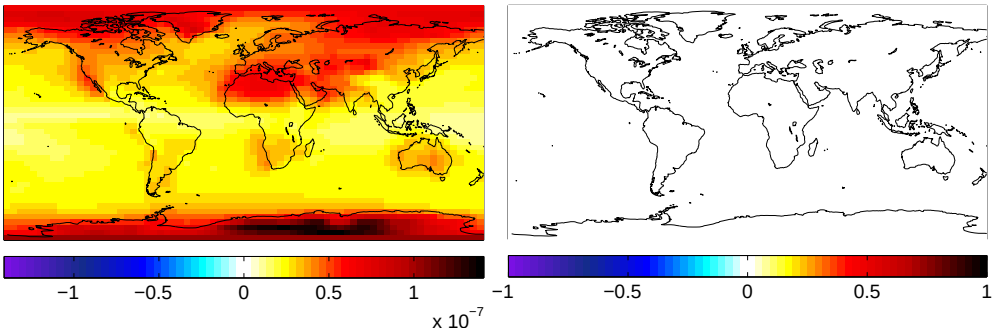

(a) First-order (b) Second-order

Figure 3-16: First- and second-order sensitivities of global surface PM concentration with respect to primary PM emissions (in $\mu g\,m^{-3}/kg\,hr^{-1}$)

There is an alternative explanation to the second-order sensitivities. The second-order sensitivities show the nonlinearities, which leads to the explanation of uncertainties. If the magnitude of the second-order sensitivities is large, uncertainties in the background emissions will translate to large uncertainties in the aviation's impact. Overestimation of background emissions where sensitivities are positive leads to overestimation of aviation's impacts. In contrast, overestimation of background emissions where sensitivities are negative leads to underestimation of aviation's impacts. This concept of uncertainties can be useful when giving uncertainty bounds for the model based on background emissions. Also, the second-order sensitivities show what species and what regions is it more important to have accurate emissions measurements to improve the accuracy of aircraft's influence on air quality and health of exposed population.

The second-order sensitivities with respect to all GEOS-Chem tracers, except the ones with zero sensitivities, are plotted in Appendix C.

Chapter 4

Conclusions and Future Work

Whereas one forward simulation computes the sensitivities of many outputs with respect to one input parameter, one adjoint simulation computes the sensitivities of a functional with respect to multiple input parameters. This trait makes the adjoint method very efficient at finding sensitivities of a few outputs to various inputs. Because the adjoint model finds the sensitivity of one functional objective function, a new adjoint simulation must be run whenever a new objective is introduced. For example, the sum of PM and the sum of population-weighted PM must be run separately in the adjoint simulation whereas population-weighted PM can be derived by post processing in the forward model simulation.

This thesis takes advantage of this feature of the adjoint method for studying the long-range transport of aerosols. This work further demonstrates the effectiveness of the adjoint method, opening possibilities for new research. The rest of this chapter summarizes the four main findings of this thesis and several areas for future work.

4.1 Conclusions

This thesis discusses the impacts of aircraft emissions on air quality and health.

4.1.1 Intercontinental Impacts

First-order sensitivities, or the impact on air quality due to aviation emissions, at varying longitude, latitude, and altitude were calculated. Aircraft emissions were correlated to approximately 12,150 premature mortalities in the world in 2006. About 8,760 mortalities were observed in Asia, and among the total Asian premature mortalities, less than a third are attributable to aircraft emissions in Asia. Pollutants from Europe and North America were transported to Asia whereas very small amount of Asian pollutants affected Europe. About 3,600 mortalities occurred in Europe, while Europe imported pollution from North America and Asia and exported to Asia. North America did not receive significant pollutants from foreign regions although it exported a significant portion to Europe and Asia. Whereas aircraft emissions in North America caused 3,400 mortalities globally in 2006, 490 occurred in the region.

4.1.2 Temporal Variation in Sensitivities

In addition to the variability of spatial sensitivities, sensitivities in time play a significant role in the amount of pollutants created. For the case of ground level NO_x emissions, emissions in the evening give the largest contribution to PM concentration increase, about twice the impact caused by the same emissions in the morning. Thus, regulating the ground level emissions differently at various times of day could potentially decrease the population's PM exposure. This idea can be generalized to regulation of non-aviation emissions. Unlike ground level emissions, sensitivities to cruise emissions at different times of day change less than 10%.

4.1.3 Proportion of the Impacts of Different Aircraft Emissions Species

About 78% of $PM_{2.5}$ formed due to aircraft emissions comes from NO_X emissions, and 21% originates from SO_X emissions. It is found that because nitrate is more concentrated in populated regions, compared to sulfate, the contribution of NO_X to health disbenefits is relatively larger at 90%.

4.1.4 Second-order Sensitivities

Comparison of the difference of sensitivities from two adjoint simulations produces the second-order derivatives. The second-order sensitivities can be used to show the sensitivity of air quality to the sensitivity of aircraft emissions, i.e., how variations in background atmospheric composition change the way aviation emissions impact the air quality. Results show that extra background ammonia emissions increase aviation's contribution to air pollution whereas extra background NO_X emissions decrease it.

4.2 Future Work

This section discusses limitations of this work and possible ways to address these limitations. The last section also introduces potential topics for future research using the adjoint model that can improve our understanding of aviation's air quality impact.

4.2.1 Limitations and Future Improvements

This study has several limitations. First, significant uncertainty exists resulting from the premature mortality calculation. The premature mortality calculation uses the average values for baseline incidence rate of mortalities and fraction of population over age 30. These coefficients differ greatly from region to region, and thus the use of average values results in imprecise mortality calculation. Because the distribution of various coefficients differs, premultiplying the coefficients to objective functions is required for more accurate mortality calculation.

Second, the grid resolution used in this thesis is $4^\circ \times 5^\circ$. As mentioned in Chapter 3, having a large grid size may underestimate the effect of LTO emissions. Thus, simulating on a finer resolution may lead to the calculation of the full LTO impact. Currently, the GEOS-Chem Adjoint community is developing the nested grid domain functionality for the adjoint code, and this development is expected to be completed in fall of 2011. Using the nested grid simulations, more extensive analysis can be

performed, including the difference of impact coming from LTO and cruise emissions. This limitation can also be improved when running with a finer resolution.

Third, GEOS-Chem is a tropospheric chemical transport model. The model includes a basic stratospheric chemistry module: LINOZ, a linearized ozone chemistry scheme. This scheme includes chemical reactions of only one tracer, modeling the cross-tropopause flux and ozone gradient near the tropopause. Because a portion of aircraft's emissions is emitted in the lower stratosphere, having a complete stratospheric chemistry module may lead to a better estimation. A stratospheric chemistry module is also being planned, which may aid future studies.

4.2.2 Potential Topics for Future Work

The potential topics to study the impact of emissions on the environment using the adjoint model are

1. implementing principal component analysis on meteorology,

2. finding the sensitivities of aerosol optical properties to emissions,

3. finding the sensitivities of radiative forcing and climate impact, and

4. exploring unexpected sensitivities and understanding the science behind them.

Using the principal component analysis (PCA), one can analyze the principal component, or the component that gives largest change in air quality or climate. Implementing the PCA in meteorology, the first principal component gives how the meteorology in average changes the aviation impact, and the second principal component shows how the global variation in meteorology together changes the aviation impact. In order to apply the PCA, multiple simulations must be run on different meteorological fields, requiring multi-year simulations. Emissions have climate impacts in addition to air quality impacts, and the climate impacts can be also studied using the adjoint model.

4.2.3 Policy Implications

Using the sensitivity information calculated by adjoint simulations, policy makers can implement effective policies for reducing PM concentrations. The impacts on air quality and health vary depending on time and location of emissions. Decreasing emissions at locations and times with high sensitivities results in larger reductions in PM concentration than reducing emissions with low sensitivities. Thus, policy makers should target reducing emissions with high sensitivities. One possible way is redistributing the emissions sources at locations and times with high sensitivities to locations and times with low sensitivities although this may not be practical or cost-effective in many cases.

Removing aircraft emissions solely in the receptor region reduces the aircraft emissions' impact by less than 50% in the same region. This suggests the importance and necessity of aircraft emission regulations at the global level.

THIS PAGE INTENTIONALLY LEFT BLANK

Bibliography

[1] Barrett, S. R. H., Britter, R. E., and Waitz, I. A., "Global mortality attributable to aircraft cruise emissions," *Environmental science & technology*, Vol. 44, No. 19, Oct. 2010, pp. 7736–42.

[2] Pope III, C. A., Burnett, R. T., Thun, M. J., Calle, E. E., Krewski, D., and Thurston, G. D., "Lung cancer, cardiopulmonary mortality, and long-term exposure to fine particulate air pollution," *The Journal of the American Medical Association*, Vol. 287, No. 9, 2002.

[3] Laden, F., Schwartz, J., Speizer, F. E., and Dockery, D. W., "Reduction in fine particulate air pollution and mortality: Extended follow-up of the Harvard Six Cities study," *American journal of respiratory and critical care medicine*, Vol. 173, No. 6, March 2006, pp. 667–72.

[4] Liu, J., Mauzerall, D. L., and Horowitz, L. W., "Evaluating inter-continental transport of fine aerosols:(2) Global health impact," *Atmospheric Environment*, Vol. 43, No. 28, Sept. 2009, pp. 4339–4347.

[5] Anenberg, S. C., West, J. J., Fiore, A. M., Jaffe, D. A., Prather, M. J., Bergmann, D., Cuvelier, K., Dentener, F. J., Duncan, B. N., Gauss, M., Hess, P., Jonson, J. E., Lupu, A., Mackenzie, I. A., Marmer, E., Park, R. J., Sanderson, M. G., Schultz, M., Shindell, D. T., Szopa, S., Vivanco, M. G., Wild, O., and Zeng, G., "Intercontinental impacts of ozone pollution on human mortality," *Environmental science & technology*, Vol. 43, No. 17, Sept. 2009, pp. 6482–7.

[6] Holloway, T., Fiore, A., and Hastings, M. G., "Intercontinental transport of air pollution: will emerging science lead to a new hemispheric treaty?" *Environmental science & technology*, Vol. 37, No. 20, Oct. 2003, pp. 4535–42.

[7] ICAO, "Environmental Report 2007," Tech. rep., International Civil Aviation Organization, 2007.

[8] ICAO, "Environment Report, 2010," Tech. rep., International Civil Aviation Organization, 2010.

[9] IPCC, "Aviation and the Global Atmosphere," Tech. rep., Intergovernmental Panel on Climate Change, Cambridge, UK, 1999.

[10] Rojo, J. J., *Future Trends in Local Air Quality Impacts of Aviation*, Master's thesis, Massachusetts Institute of Technology, 2007.

[11] Mahashabde, A., Wolfe, P., Ashok, A., Dorbian, C., He, Q., Fan, A., Lukachko, S., Mozdzanowska, A., Wollersheim, C., Barrett, S. R. H., Locke, M., and Waitz, I. A., "Assessing the environmental impacts of aircraft noise and emissions," *Progress in Aerospace Sciences*, Vol. 47, No. 1, Jan. 2011, pp. 15–52.

[12] Waitz, I., Lukachko, S., Willcox, K., Belobaba, P., Garcia, E., Hollingsworth, P., Mavris, D., Harback, K., Morser, F., and Steinbach, M., "Architecture Study for the Aviation Environmental Portfolio Management Tool prepared by Architecture Study for the Aviation Environmental Portfolio Management Tool," Tech. Rep. June, U.S. Federal Aviation Administration, 2006.

[13] EPA, "2006 National Ambient Air Quality Standards for Particle Pollution," Tech. rep., U.S. Environmental Protection Agency, 2006.

[14] EPA, "Review of the National Ambient Air Quality Standards for Particulate Matter: Policy Assessment of Scientific and Technical Information: OAQPS Staff Paper," Tech. rep., U.S. Environmental Protection Agency, Office of the Air Quality Planning and Standards, Research Triangle Park, NC, 2005.

[15] EPA, "Review of the National Ambient Air Quality Standards for Ozone: Policy Assessment of Scientific and Technical Information OAQPS Staff Paper," Tech. rep., U.S. Environmental Protection Agency, Office of Air Quality Planning and Standards, Research Triangle Park, NC, 2007.

[16] Pope III, C. A. and Dockery, D. W., "Health Effects of Fine Particulate Air Pollution: Lines that Connect," *Journal of the Air & Waste Management Association*, 2006, pp. 709 –742.

[17] Wey, C. C., Anderson, B. E., Wey, C., Miake-Lye, R. C., Whitefield, P., and Howard, R., "Overview on the Aircraft Particle Emissions Experiment," *Journal of Propulsion and Power*, Vol. 23, No. 5, Sept. 2007, pp. 898–905.

[18] Jun, M., *Microphysical Modeling of Ultrafine Hydrocarbon-Containing Aerosols in Aircraft Emissions*, Ph.D. thesis, Massachusetts Institute of Technology, 2011.

[19] Leibensperger, E. M., Mickley, L. J., Jacob, D. J., and Barrett, S. R. H., "Intercontinental influence of NOx and CO emissions on particulate matter air quality," *Atmospheric Environment*, Vol. 45, No. 19, April 2011, pp. 3318–3324.

[20] Seinfeld, J. H. and Pandis, S. N., *Atmospheric Chemistry and Physics - From Air Pollution to Climate Change*, John Wiley & Sons., Hoboken, New Jersey, 2nd ed., 2006.

[21] Holve, D. J. and Chapman, J., "Real-Time Soot (black carbon) Concentration and Size by Light Scattering," *Aircraft Particle Emissions eXperiment(APEX)*, American Association for Aerosols Research, 2005.

[22] Holland, M., Hurley, F., Hunt, A., and Watkiss, P., "Methodology for the Cost-Benefit Analysis for CAFE: Volume 3: Uncertainty in the CAFE CBA: Methods and First Analysis," Tech. Rep. 1, AEA Technology Environment, 2005.

[23] Sequeira, C. J., *An Assessment of the Health Implications of Aviation Emissions Regulations*, Master's thesis, Massachusetts Institute of Technology, 2008.

[24] Ratliff, G., Sequeira, C., Waitz, I., Ohsfeldt, M., Thrasher, T., and Thompson, T., "Aircraft Impacts on Local and Regional Air Quality in the United States Aircraft Impacts on Local and Regional Air Quality in the United States," Tech. Rep. October, 2009.

[25] Nadarajah, S. K. and Jameson, A., "A comparison of the continuous and discrete adjoint approach to automatic aerodynamic optimization," *AIAA*, Vol. 0667, 2000.

[26] Singh, K., Eller, P., Sandu, A., Henze, D., Bowman, K., Kopacz, M., and Lee, M., "Towards the Construction of a Standard Adjoint GEOS-Chem Model," ACM High Performance Computing Conference, 2000.

[27] Henze, D. K., Hakami, A., and Seinfeld, J. H., "Development of the adjoint of GEOS-Chem," *Atmospheric Chemistry and Physics*, 2007, pp. 2413–2433.

[28] Damian, V., Sandu, A., Damian, M., Potra, F., and Carmichael, G. R., "The kinetic preprocessor KPP-a software environment for solving chemical kinetics," *Computers & Chemical Engineering*, Vol. 26, No. 11, Nov. 2002, pp. 1567–1579.

[29] Jacob, D. J., "Heterogeneous chemistry and tropospheric ozone," *Atmospheric Environment*, Vol. 34, No. 12-14, 2000, pp. 2131–2159.

[30] Binkowski, F. S. and Roselle, S. J., "Models-3 Community Multiscale Air Quality (CMAQ) model aerosol component 1. Model description," *Journal of Geophysical Research*, Vol. 108, No. D6, 2003.

[31] Zhang, Y., Seigneur, C., Seinfeld, J. H., Jacobson, M., Clegg, S. L., and Binkowski, F. S., "A comparative review of inorganic aerosol thermodynamic equilibrium modules: similarities, differences, and their likely causes," *Atmospheric Environment*, Vol. 34, No. 1, Jan. 2000, pp. 117–137.

[32] Bey, I., Jacob, D. J., Yantosca, R. M., Logan, J. A., Field, B. D., Fiore, A. M., Li, Q., Liu, H. Y., Mickley, L. J., and Schultz, M. G., "Global modeling of tropospheric chemistry with assimilated meteorology: Model description and evaluation," *Journal of Geophysical Research*, Vol. 106, No. D19, 2001, pp. 23073–23095.

[33] Park, R. J., Jacob, D. J., Chin, M., and Martin, R. V., "Sources of carbonaceous aerosols over the United States and implications for natural visibility," *Journal of Geophysical Research*, Vol. 108, No. D12, 2003.

[34] Park, R. J., Jacob, D. J., Field, B. D., Yantosca, R. M., and Chin, M., "Natural and transboundary pollution influences on sulfate-nitrate-ammonium aerosols in the United States: Implications for policy," *Journal of Geophysical Research*, Vol. 109, No. D15, 2004.

[35] Fiore, A. M., Dentener, F. J., Wild, O., Cuvelier, C., Schultz, M. G., Hess, P., Textor, C., Schulz, M., Doherty, R. M., Horowitz, L. W., MacKenzie, I. A., Sanderson, M. G., Shindell, D. T., Stevenson, D. S., Szopa, S., Van Dingenen, R., Zeng, G., Atherton, C., Bergmann, D., Bey, I., Carmichael, G., Collins, W. J., Duncan, B. N., Faluvegi, G., Folberth, G., Gauss, M., Gong, S., Hauglustaine, D., Holloway, T., Isaksen, I. S. A., Jacob, D. J., Jonson, J. E., Kaminski, J. W., Keating, T. J., Lupu, A., Marmer, E., Montanaro, V., Park, R. J., Pitari, G., Pringle, K. J., Pyle, J. A., Schroeder, S., Vivanco, M. G., Wind, P., Wojcik, G., Wu, S., and Zuber, A., "Multimodel estimates of intercontinental source-receptor relationships for ozone pollution," *Journal of Geophysical Research*, Vol. 114, No. D4, Feb. 2009, pp. 1–21.

[36] Wu, S., Duncan, B. N., Jacob, D. J., Fiore, A. M., and Wild, O., "Chemical nonlinearities in relating intercontinental ozone pollution to anthropogenic emissions," *Geophysical Research Letters*, Vol. 36, No. 5, March 2009, pp. 1–5.

[37] McLinden, C. A., Olsen, S. C., Hannegan, B., Wild, O., Prather, M. J., and Sundet, J., "Stratospheric ozone in 3-D models: A simple chemistry and the cross-tropopause flux," *Journal of Geophysical Research*, Vol. 105, No. D11, 2000, pp. 14653–14665.

[38] Henze, D. K., Seinfeld, J. H., and Shindell, D. T., "Inverse modeling and mapping US air quality influences of inorganic PM 2.5 precursor emissions using the adjoint of GEOS-Chem," *Atmospheric Chemistry and Physics*, 2009, pp. 5877–5903.

[39] Zhang, L., Jacob, D. J., Kopacz, M., Henze, D. K., Singh, K., and Jaffe, D. A., "Intercontinental source attribution of ozone pollution at western U.S. sites using an adjoint method," *Geophysical Research Letters*, Vol. 36, No. 11, June 2009, pp. 1–5.

[40] Kopacz, M., Mauzerall, D. L., Wang, J., Leibensperger, E. M., Henze, D. K., and Singh, K., "Origin and radiative forcing of black carbon transported to the Himalayas and Tibetan Plateau," *Atmospheric Chemistry and Physics*, Vol. 11, No. 6, March 2011, pp. 2837–2852.

[41] Noel, G., Allaire, D., Jacobson, S., Willcox, K., and Cointin, R., "Assessment of the Aviation Environmental Design Tool," *Eighth USA/Europe Air Traffic Management Research and Development Seminar (ATM2009)*, 2009.

[42] Roof, C., Hansen, A., Fleming, G., Thrasher, T., Nguyen, A., Hall, C., Dinges, E., Bea, R., Grandi, F., Kim, B., Usdrowski, S., and Hollingsworth, P., "Aviation

Environmental Design Tool (AEDT) System Architecture," Tech. rep., Federal Aviation Adminiatration Office of Environment and Energy, 2007.

[43] Brunelle-yeung, E., *The Impacts of Aviation Emissions on Human Health through Changes in Air Quality and UV Irradiance*, Master's thesis, Massachusetts Institute of Technology, 2009.

[44] Masek, T., *A Response Surface Model of the Air Quality Impacts of Aviation*, Master's thesis, Massachusetts Institue of Technology, 2008.

[45] Tarrason, L., Jonson, J. E., Berntsen, T. K., and Rypdal, K., "Study on air quality impacts of non-LTO emissions from aviation," Tech. Rep. 3, Center for International Climate and Environmental Research - Oslo, Oslo, 2002.

[46] Woody, M., Baek, B. H., Adelman, Z., Omary, M., Lam, Y. F., West, J. J., and Arunachalam, S., "An assessment of Aviations contribution to current and future fine particulate matter in the United States," *Atmospheric Environment*, Vol. 45, No. 20, June 2011, pp. 3424–3433.

THIS PAGE INTENTIONALLY LEFT BLANK

Appendix A

Conversion between Discrete and Continuous Adjoint Variables

This chapter of appendix explains the conversion between the continuous and discrete adjoint variables that were briefly mentioned in Chapter 2.2.3. The continuous and discrete adjoint variables often do not represent the same physical qualities, requiring conversion factors moving from one to another.

The change in objective function can be written in terms of the continuous adjoint variables as in Eq. A.1 and the discrete adjoint variables as in Eq. A.2:

$$\delta J = \int \delta\phi^C \, \hat{\phi}^C \, dV \tag{A.1}$$

$$\delta J = \sum_i \delta\phi_i^D \, \hat{\phi}_i^D \tag{A.2}$$

Relating the two equations, the discrete and continuous adjoint variables can be related.

$$\hat{\phi}_i^D \approx \int_{V_i} \hat{\phi}^C \, dV \approx \hat{\phi}^C V_i \tag{A.3}$$

Therefore, when moving from discrete to continuous adjoint variables or vice versa, multiplications or divisions by the volumes of the cells are needed, respectively.

GEOS-Chem Adjoint uses a continuous adjoint approach for the transport module

and a discrete adjoint approach for all other modules, including chemistry, emission, convection, and deposition. As used in GEOS-Chem's transport module, the conversion between the two adjoint variables will be demonstrated using Finite Volume Method.

A simple one dimensional advection equation is given as an example.

$$\frac{\partial \rho}{\partial t} + v\frac{\partial \rho}{\partial x} = 0$$

Integrating the equation for finite volume method, discretizing the equation, and denoting flux with F, the equation becomes

$$\frac{\partial}{\partial t}\int \rho \, dx = -(F_{i+\frac{1}{2}} - F_{i-\frac{1}{2}}) \tag{A.4}$$

$$\bar{\rho}_i^{n+1} = \bar{\rho}_i^n - \frac{\triangle t}{\triangle x_i}(F_{i+\frac{1}{2}} - F_{i-\frac{1}{2}}) \tag{A.5}$$

where $\bar{\rho}_i = \frac{1}{\triangle x_i}\int_i \rho dx$. The first order upwind scheme sets $F_{i+\frac{1}{2}} = \bar{\rho}_i$ and $F_{i-\frac{1}{2}} = \bar{\rho}_{i-1}$ if $v > 0$. Then the equation becomes

$$\bar{\rho}_i^{n+1} = \bar{\rho}_i^n - \frac{v\triangle t}{\triangle x_i}(\bar{\rho}_i^n - \bar{\rho}_{i-1}^n) \tag{A.6}$$

It can be rewritten in the matrix form, $\underline{\bar{\rho}}^{n+1} = (I - A)\,\underline{\bar{\rho}}^n$, where

$$A = \begin{bmatrix} \frac{U\triangle t}{\triangle x_1} & 0 & 0 & 0 & 0 \\ -\frac{U\triangle t}{\triangle x_2} & \frac{U\triangle t}{\triangle x_2} & 0 & 0 & 0 \\ 0 & -\frac{U\triangle t}{\triangle x_3} & \ddots & 0 & \vdots \\ 0 & 0 & \ddots & \frac{U\triangle t}{\triangle x_{n-1}} & 0 \\ 0 & \dots & 0 & -\frac{U\triangle t}{\triangle x_n} & \frac{U\triangle t}{\triangle x_n} \end{bmatrix}$$

In the continuous adjoint model, the wind direction is reversed to transport the sensitivities, $\hat{\bar{\rho}}$, backward. The adjoint version of Eq. A.6 becomes

$$\hat{\bar{\rho}}_i^{n+1} = \hat{\bar{\rho}}_i^n + \frac{v\triangle t}{\triangle x_i}(\hat{\bar{\rho}}_{i+1}^n - \hat{\bar{\rho}}_i^n) \tag{A.7}$$

The equivalent matrix form is $\underline{\hat{\rho}}^{n+1} = (I - B)\,\underline{\hat{\rho}}^{n}$ where

$$B = \begin{bmatrix} \frac{U\triangle t}{\triangle x_1} & -\frac{U\triangle t}{\triangle x_1} & 0 & 0 & 0 \\ 0 & \frac{U\triangle t}{\triangle x_2} & -\frac{U\triangle t}{\triangle x_2} & 0 & 0 \\ 0 & 0 & \ddots & \ddots & \vdots \\ 0 & 0 & \ddots & \frac{U\triangle t}{\triangle x_{n-1}} & -\frac{U\triangle t}{\triangle x_{n-1}} \\ 0 & 0 & \dots & 0 & \frac{U\triangle t}{\triangle x_n} \end{bmatrix}$$

Note that the matrix A is not equal to the transpose of B if we do not have the same discretization of space. For the advection in east-west direction, the volumes of neighboring cells are similar, having slight differences due to the different heights of the neiboring boxes. But for the advection in north-south direction, the volume of neighboring cells can be vastly different, especially near polar regions. The conversion between the matrices A and B can be perfomred by left and right multipling matrix B with matrices V and V^{-1}, where V contains the volume of each cell in diagonal entries. As shown in $A = B_2^T = (VBV^{-1})^T$, conversion from discrete to we must first divide the adjoint variable by the volume of each of the grid boxes, advect the adjoint variables, and then multiply by the volume after transport. Dividing by volume of each cell is moving from discrete to continuous adjoint, and multiplying by volume is a step of moving from continuous to discrete adjoint.

Fig. A-1 shows large sensitivities of $PM_{2.5}$ in the US with respect to emissions in the North Pole. The large sensitivities in areas where grid size differences are alrge were caused by the omission of unit conversion between the two adjoint variables. Going towards the polar regions, cell size decreases at a rapid rate, causing the grid box difference to be large.

Implementing what was discussed in this section fixed the problem, as shown in Fig. A-2. As expected, the sensitivities in the non-polar regions are very similar because the neighboring cells of equatorial region have similar volumes. But the large sensitivities in the North Pole are removed in Fig. A-2.

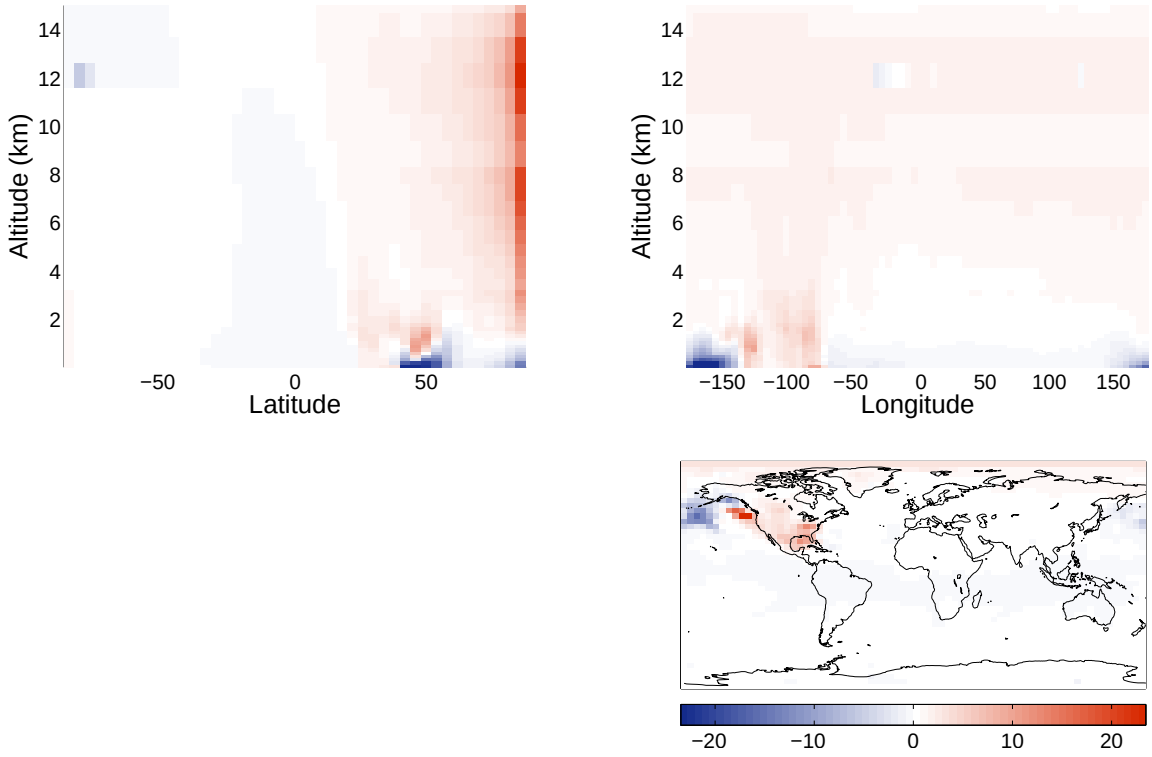

Figure A-1: Resulting sensitivities from running with incorrect unit conversion

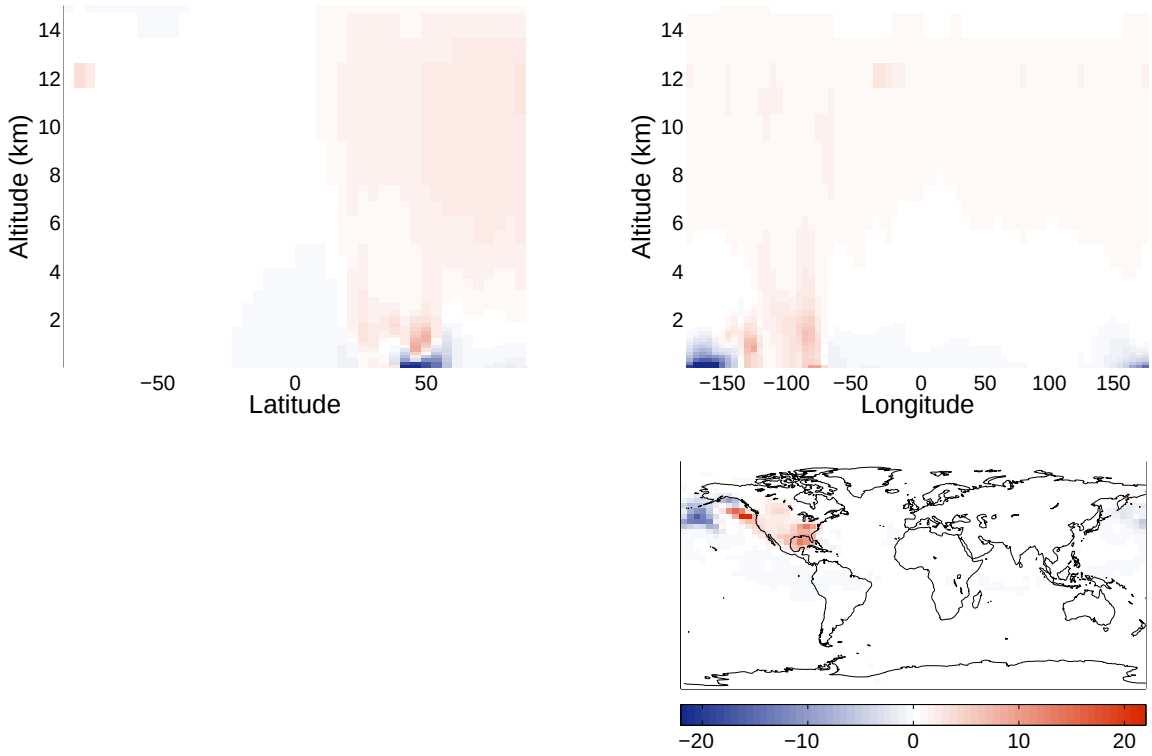

Figure A-2: Resulting sensitivities from running with correct unit conversion

Appendix B

Sensitivity Plots

This appendix lists the plots of 1) sensitivities of surface PM concentration in various regions (the US, North America, Europe, Asia, the world) with respect to aircraft emissions (NO_X, SO_X, HC, CO, primary PM) at all locations and altitudes and 2) sensitivities of population exposure to PM in various regions (the US, North America, Europe, Asia, the world) with respect to aircraft emissions (NO_X, SO_X, HC, CO, primary PM) at all latitudes, longitudes, and altitudes. Three subfigures in each figure represent sensitivities that are averaged over all latitudes, longitudes, and altitudes.

B.1 Sensitivities of Surface PM Concentration

This section shows the sensitivities of surface PM concentration in various regions (the US, North America, Europe, Asia, the world) with respect to several aircraft emissions (NO_X, SO_X, HC, CO, primary PM).

B.1.1 Sensitivities of Surface PM concentration in the US to Aircraft Emissions

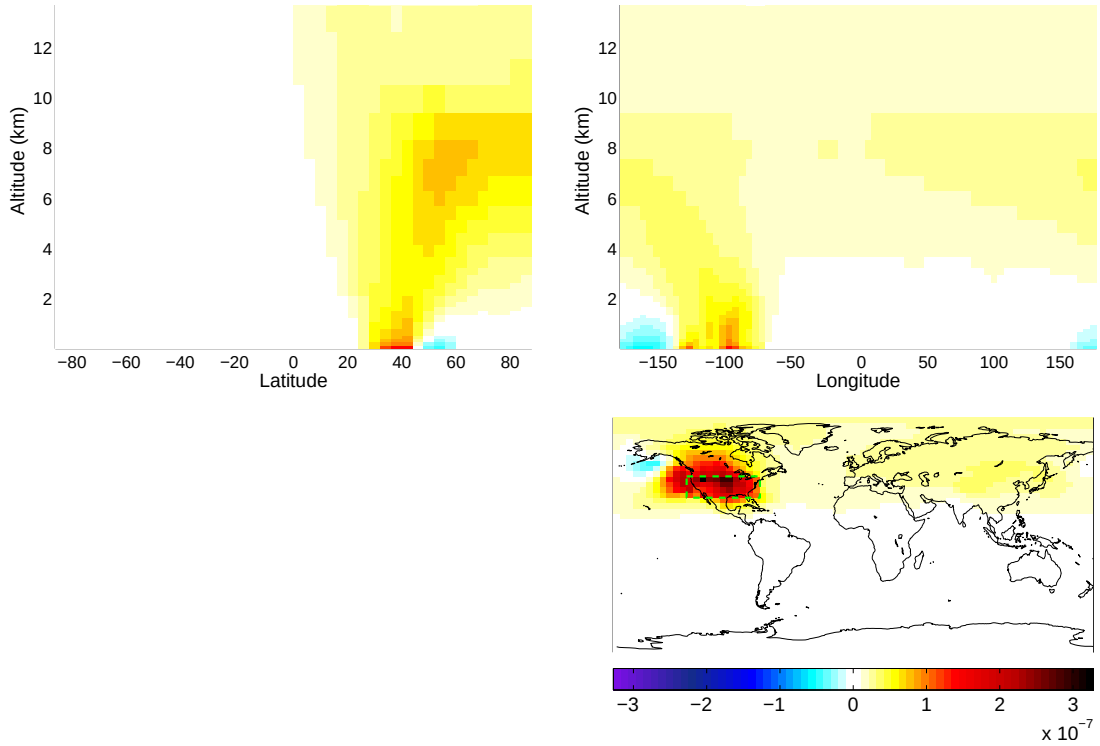

Figure B-1: Sensitivities of surface PM concentration in the US to NO_X emissions (in $\mu g\,m^{-3}/kg\,hr^{-1}$)

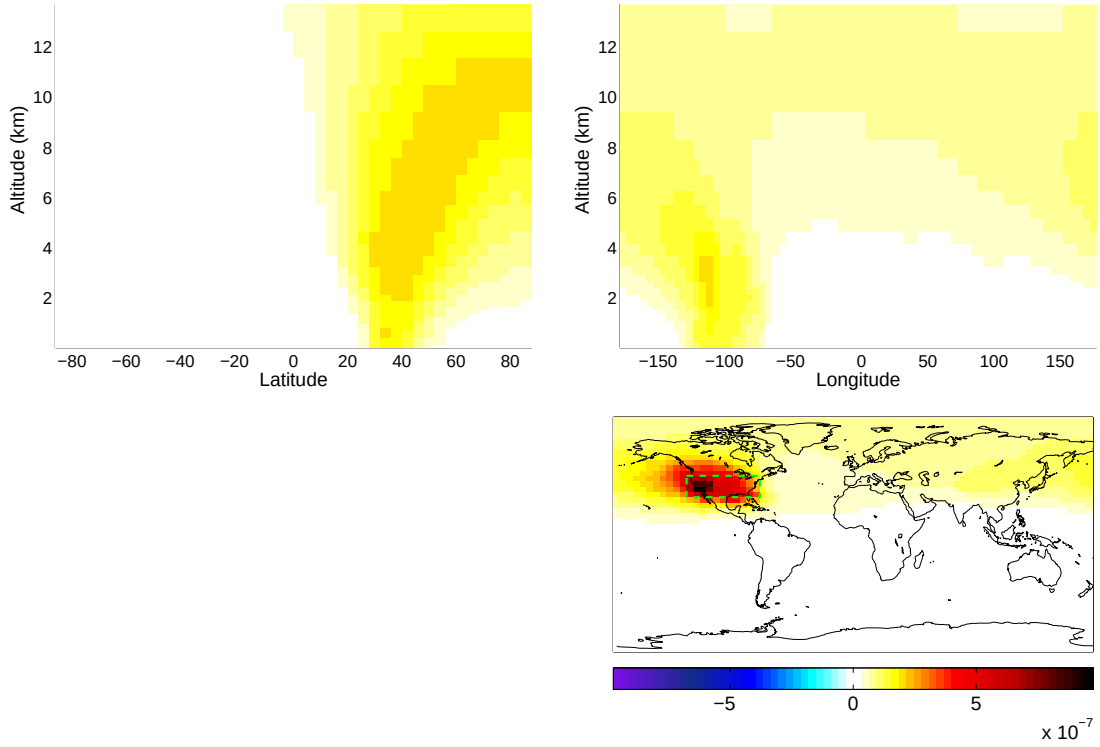

Figure B-2: Sensitivities of surface PM concentration in the US to SO_X emissions (in $\mu g\,m^{-3}/kg\,hr^{-1}$)

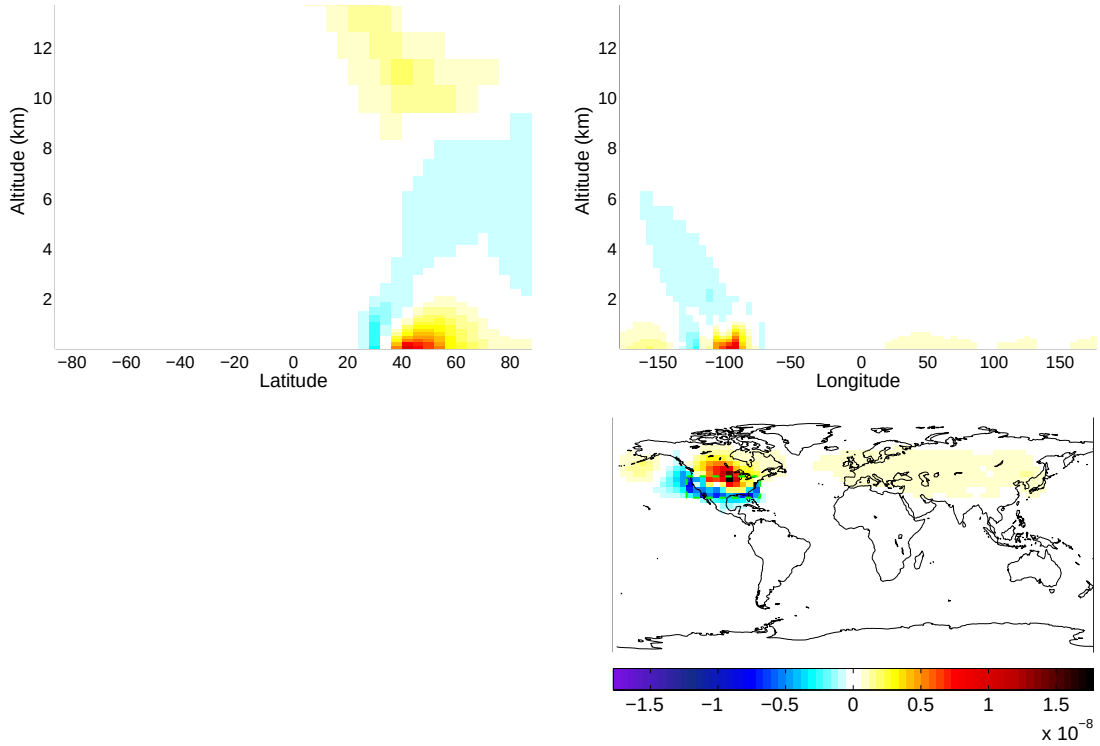

Figure B-3: Sensitivities of surface PM concentration in the US to HC emissions (in $\mu g\,m^{-3}/kg\,hr^{-1}$)

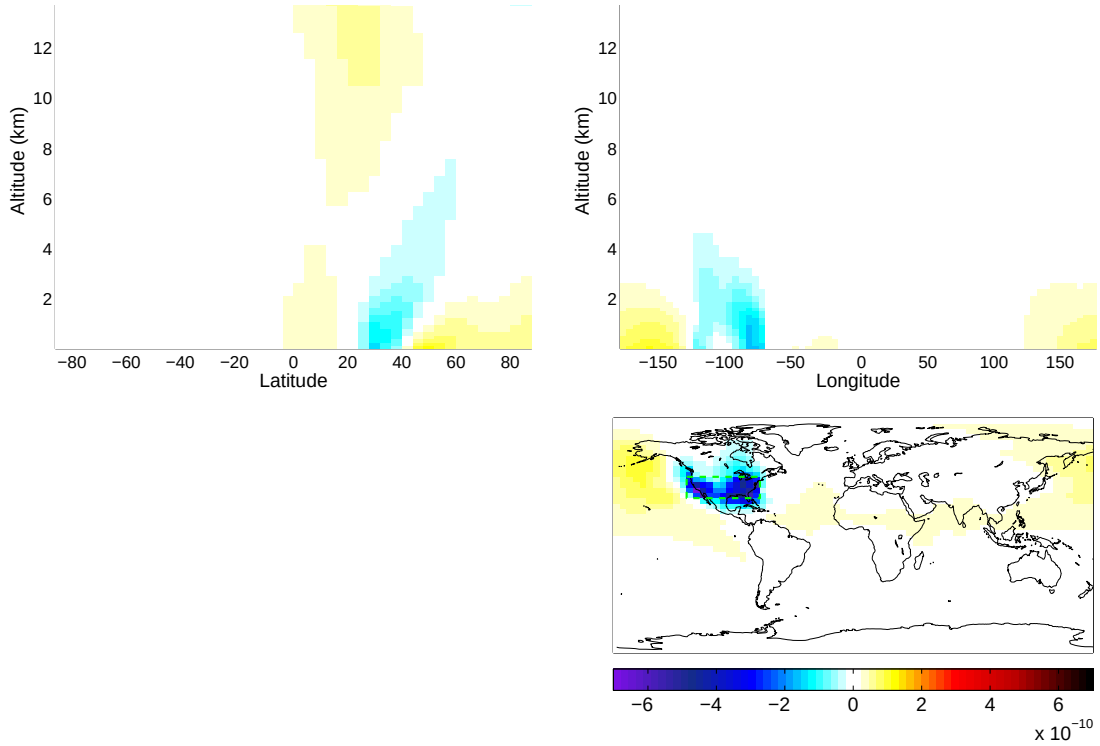

Figure B-4: Sensitivities of surface PM concentration in the US to CO emissions (in $\mu g\,m^{-3}/kg\,hr^{-1}$)

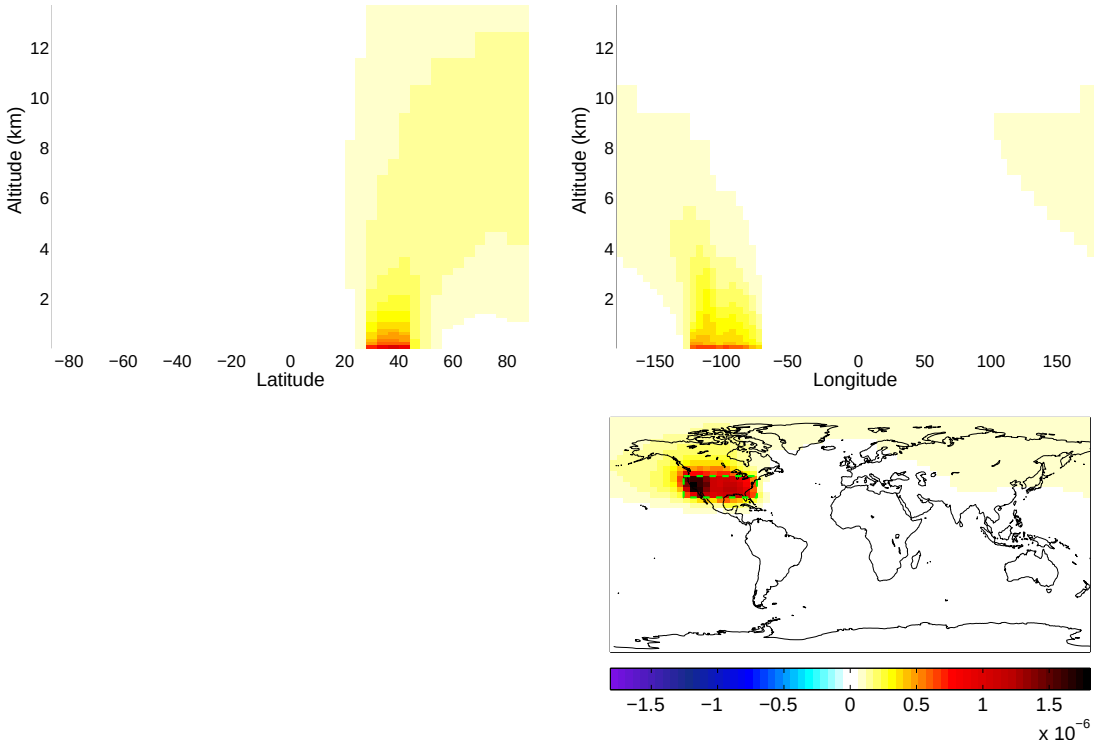

Figure B-5: Sensitivities of surface PM concentration in the US to primary PM emissions (in $\mu g\,m^{-3}/kg\,hr^{-1}$)

B.1.2 Sensitivities of Surface PM concentration in North America to Aircraft Emissions

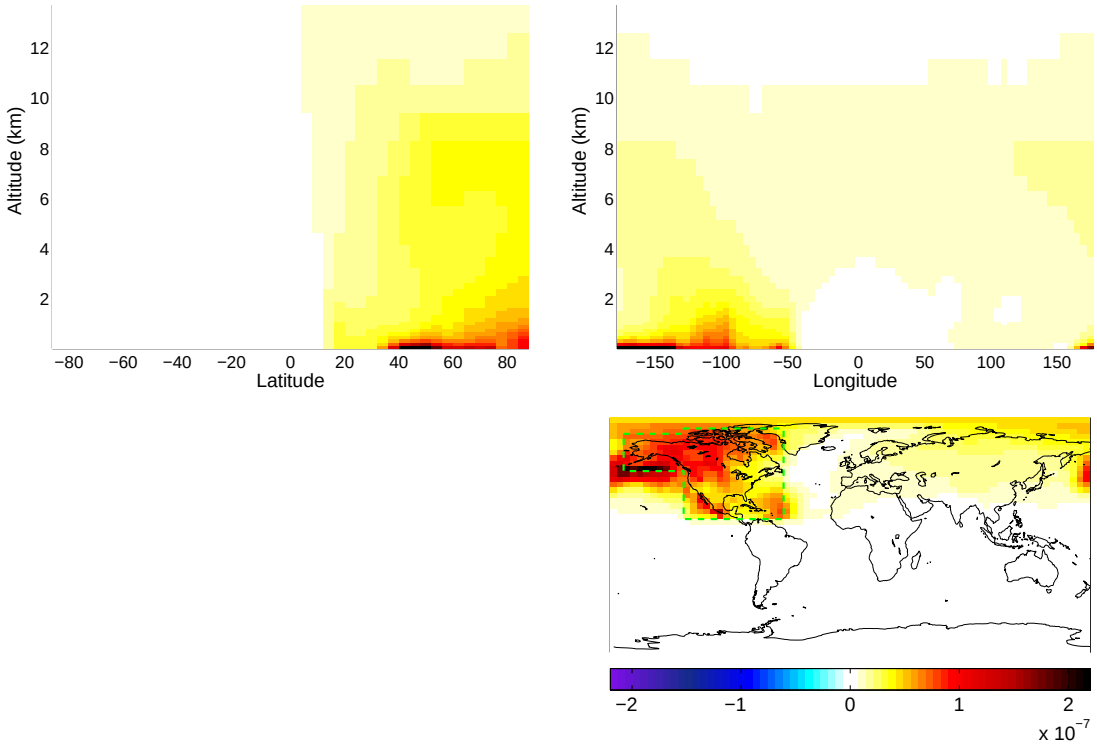

Figure B-6: Sensitivities of surface PM concentration in North America to NO_X emissions (in $\mu g\,m^{-3}/kg\,hr^{-1}$)

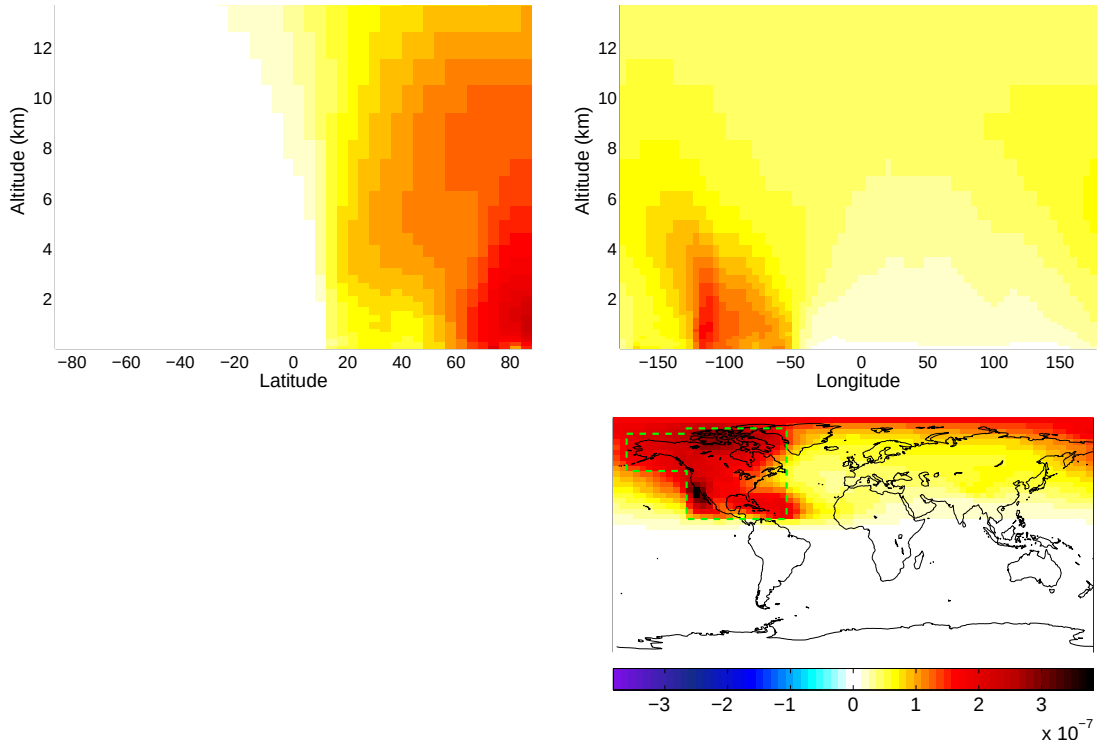

Figure B-7: Sensitivities of surface PM concentration in North America to SO_X emissions (in $\mu g\,m^{-3}/kg\,hr^{-1}$)

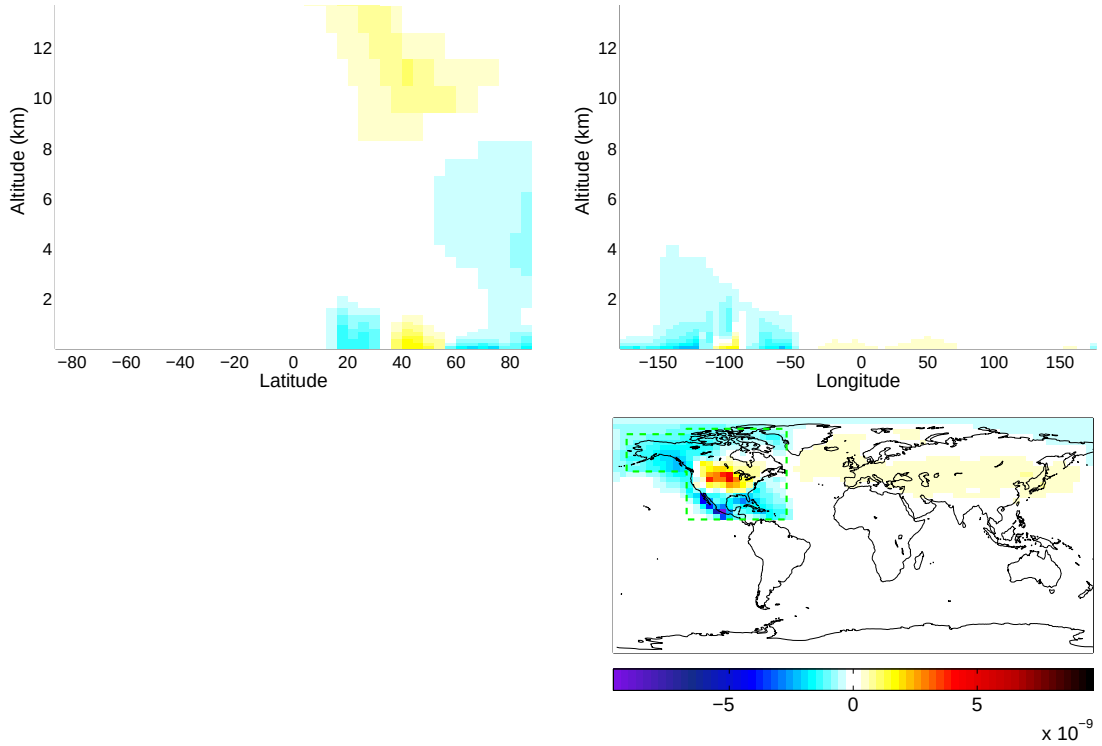

Figure B-8: Sensitivities of surface PM concentration in North America to HC emissions (in $\mu g\,m^{-3}/kg\,hr^{-1}$)

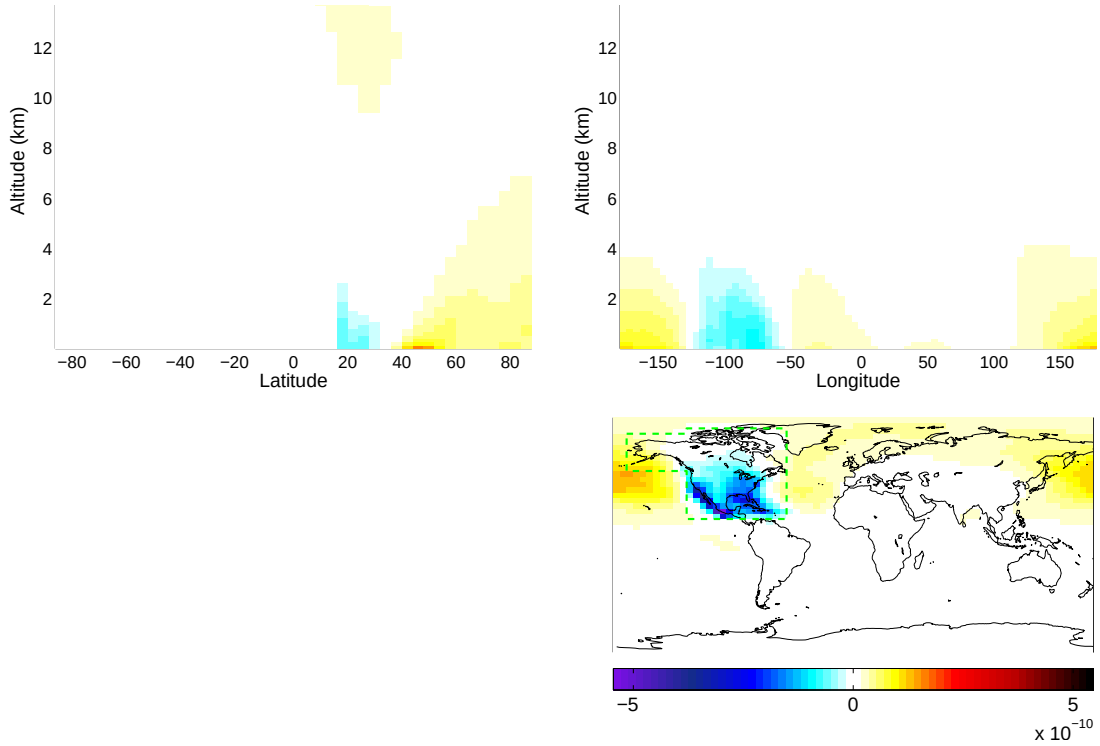

Figure B-9: Sensitivities of surface PM concentration in North America to CO emissions (in $\mu g\,m^{-3}/kg\,hr^{-1}$)

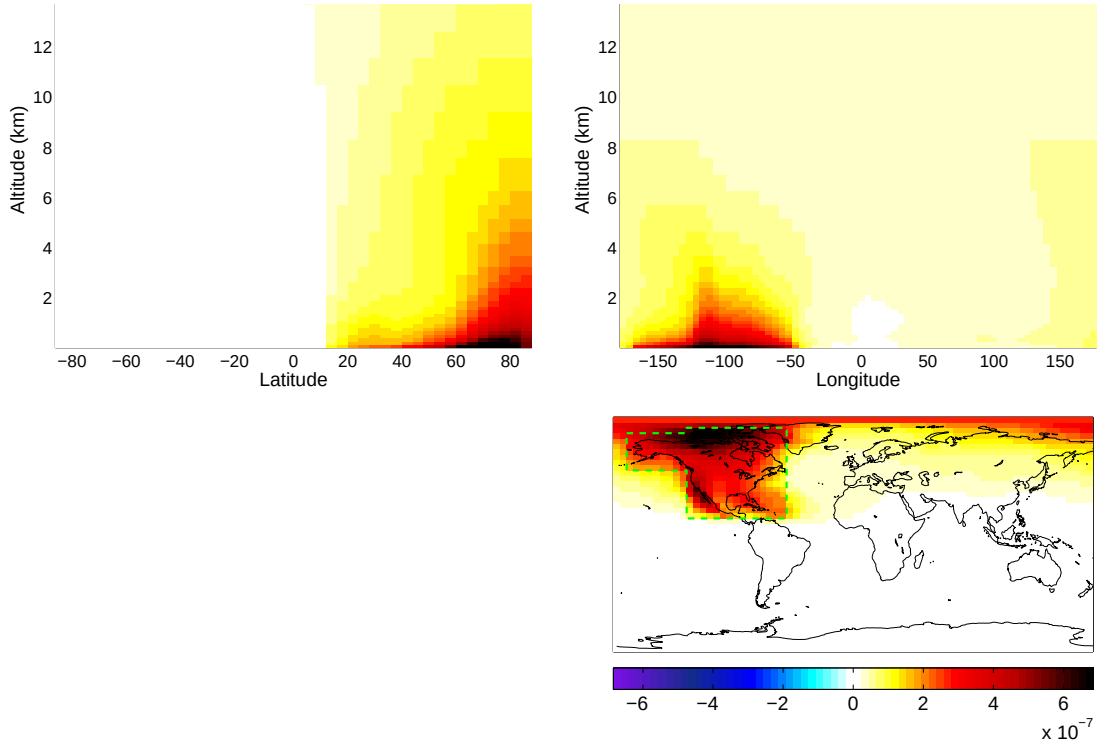

Figure B-10: Sensitivities of surface PM concentration in North America to primary PM emissions (in $\mu g\,m^{-3}/kg\,hr^{-1}$)

B.1.3 Sensitivities of Surface PM concentration in Europe to Aircraft Emissions

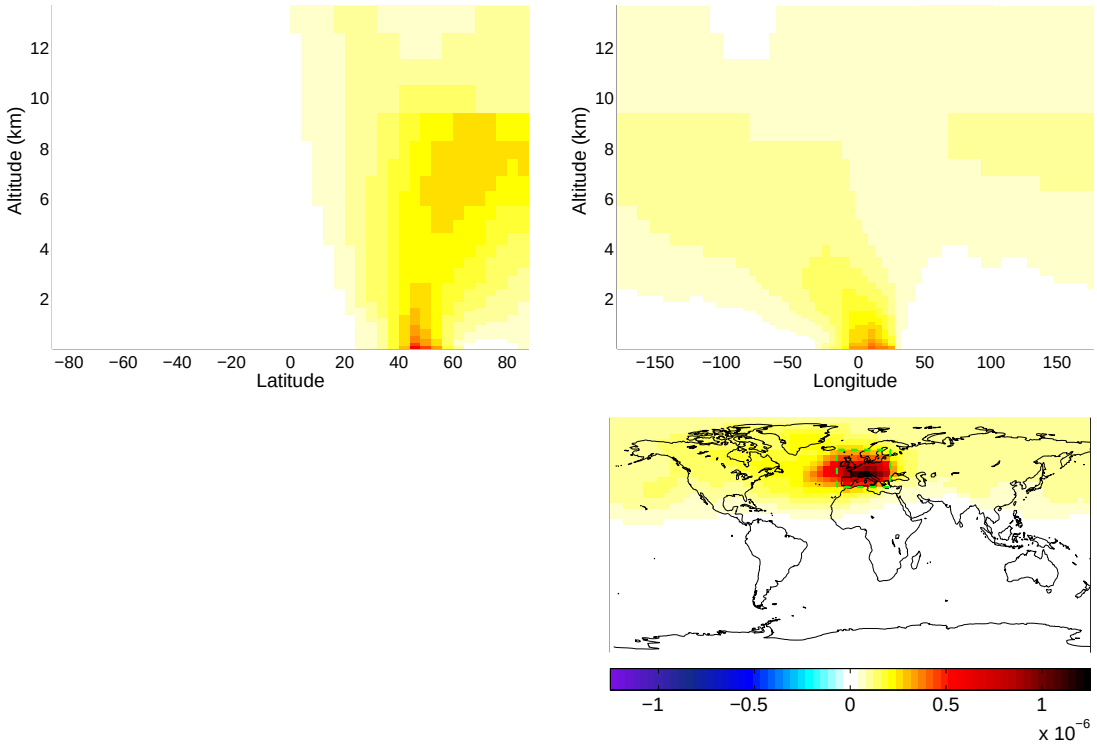

Figure B-11: Sensitivities of surface PM concentration in Europe to NO_X emissions (in $\mu g\,m^{-3}/kg\,hr^{-1}$)

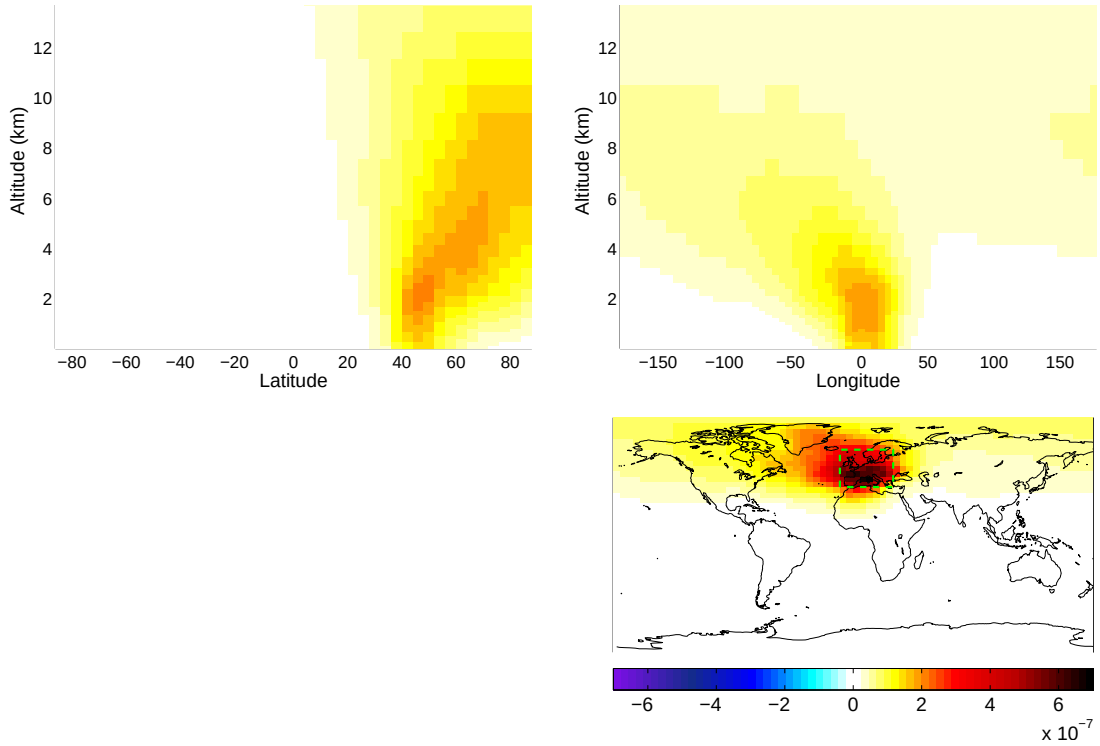

Figure B-12: Sensitivities of surface PM concentration in Europe to SO_X emissions (in $\mu g\,m^{-3}/kg\,hr^{-1}$)

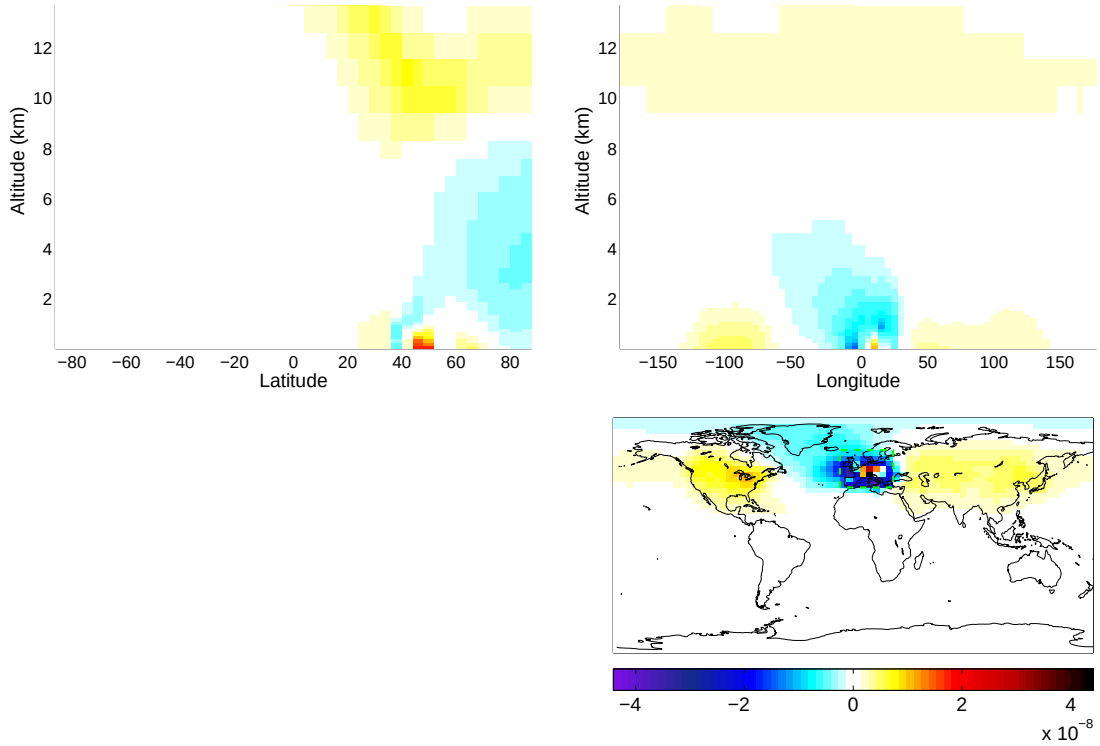

Figure B-13: Sensitivities of surface PM concentration in Europe to HC emissions (in $\mu g\,m^{-3}/kg\,hr^{-1}$)

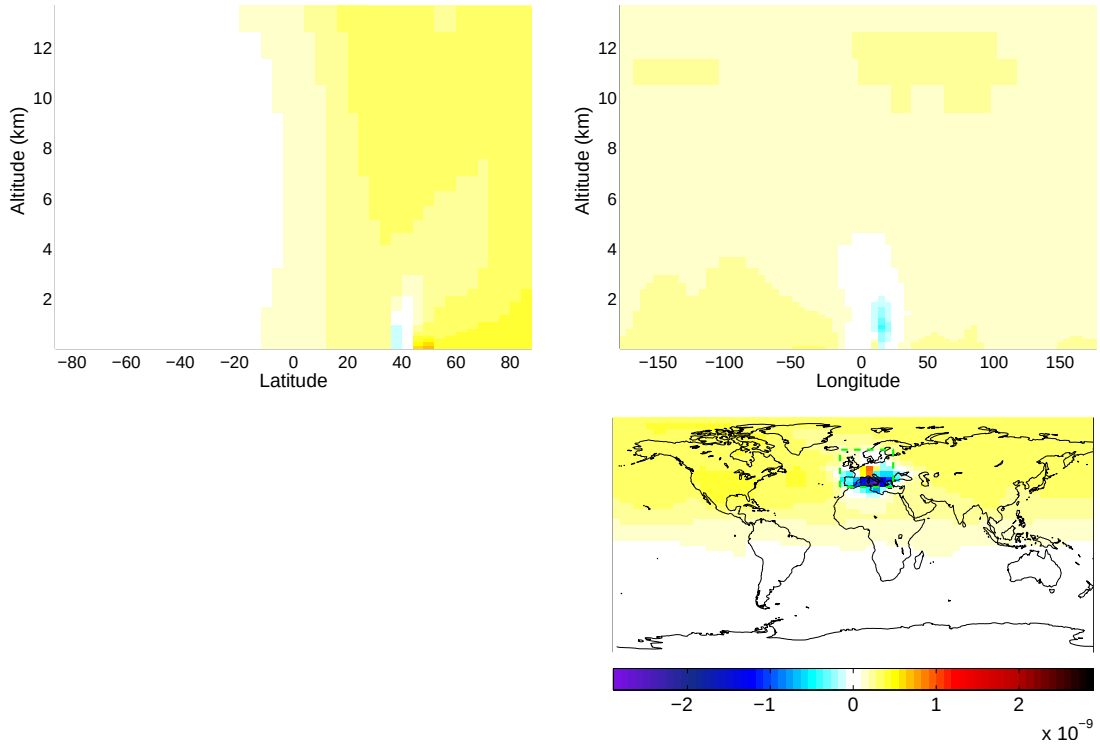

Figure B-14: Sensitivities of surface PM concentration in Europe to CO emissions (in $\mu g\,m^{-3}/kg\,hr^{-1}$)

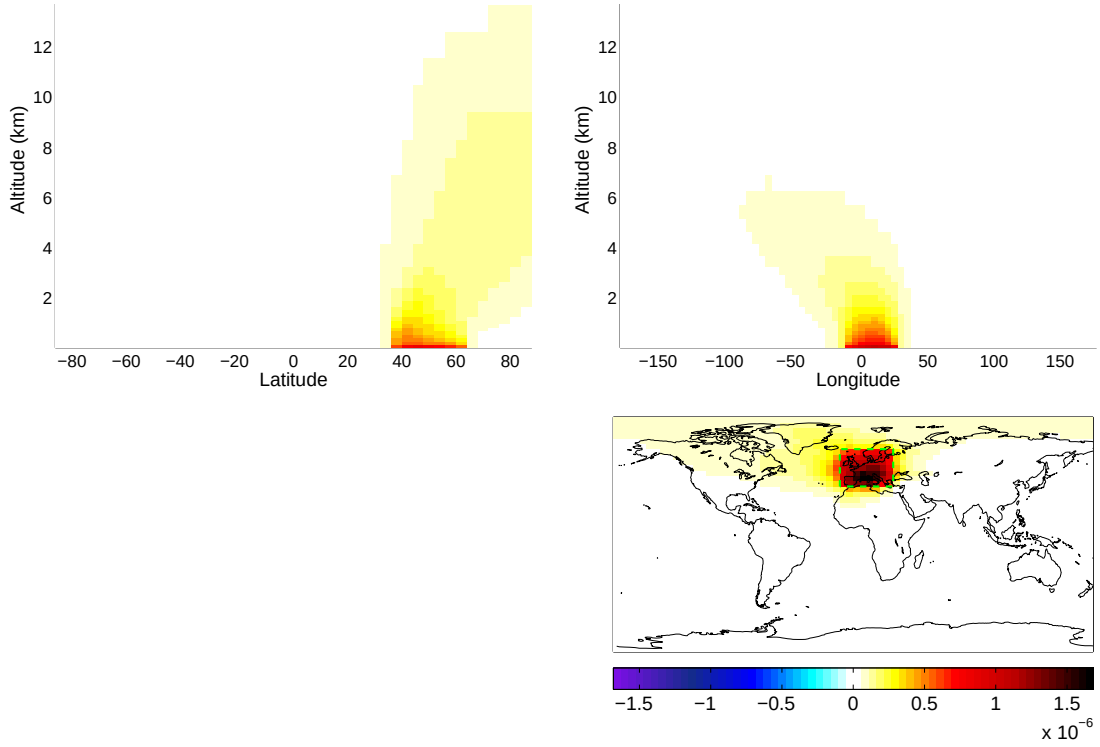

Figure B-15: Sensitivities of surface PM concentration in Europe to primary PM emissions (in $\mu g\,m^{-3}/kg\,hr^{-1}$)

B.1.4 Sensitivities of Surface PM concentration in Asia to Aircraft Emissions

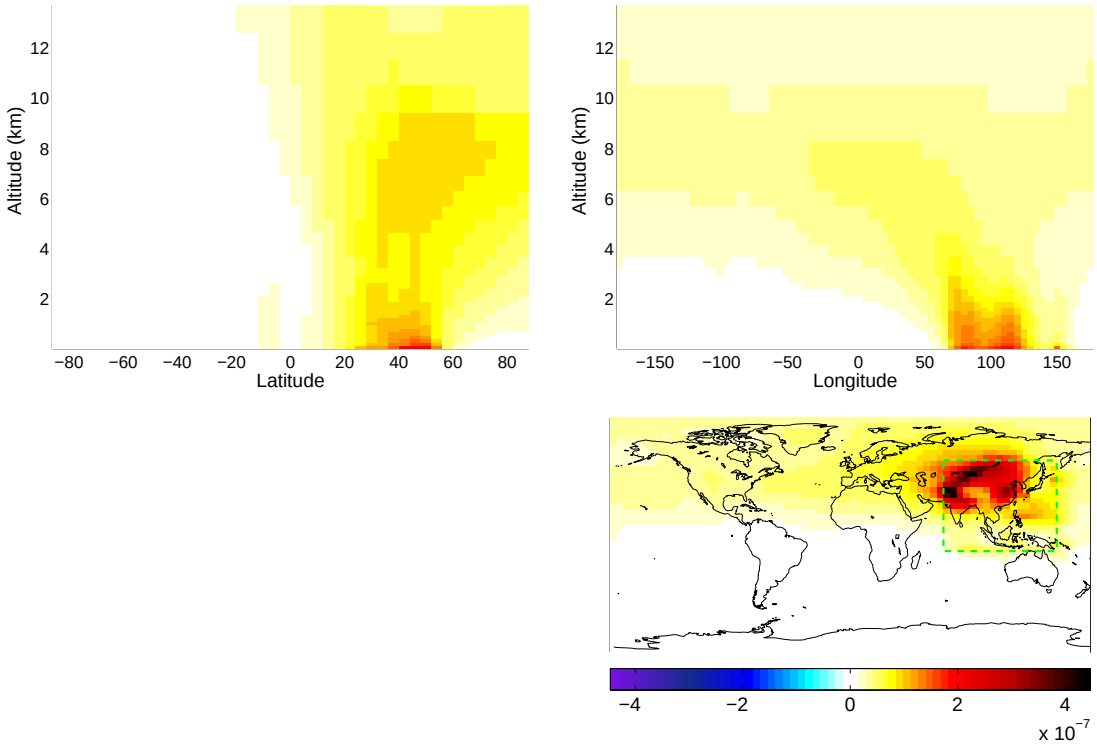

Figure B-16: Sensitivities of surface PM concentration in Asia to NO_X emissions (in $\mu g\,m^{-3}/kg\,hr^{-1}$)

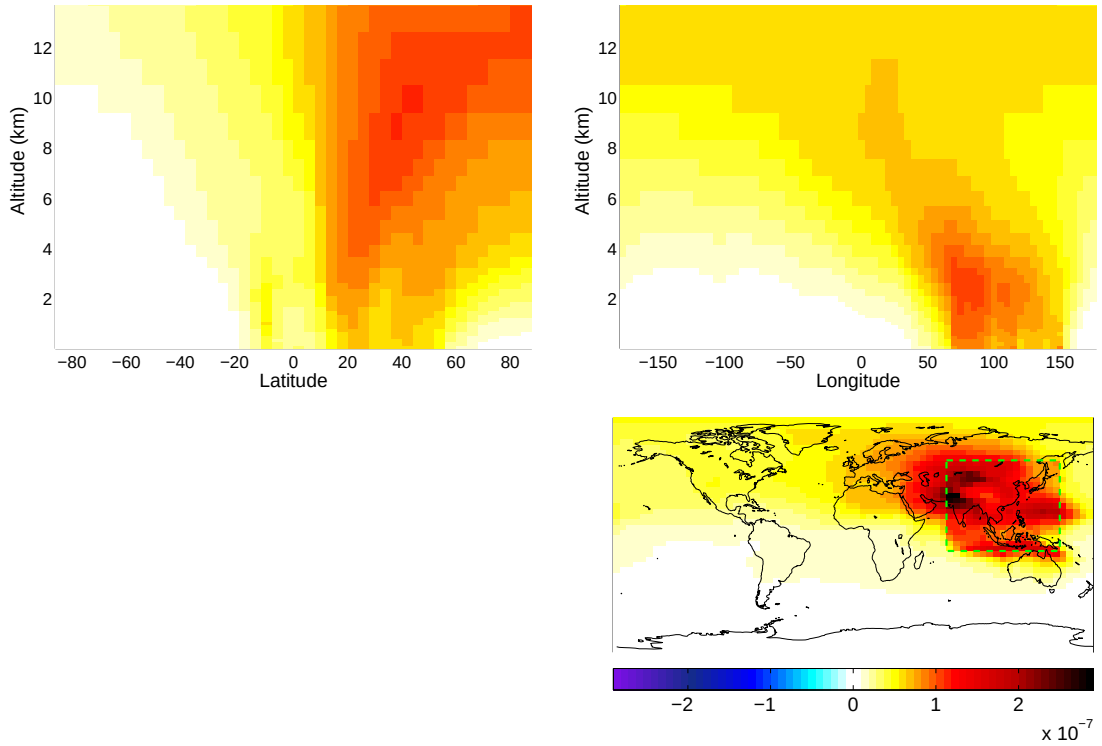

Figure B-17: Sensitivities of surface PM concentration in Asia to SO_X emissions (in $\mu g\,m^{-3}/kg\,hr^{-1}$)

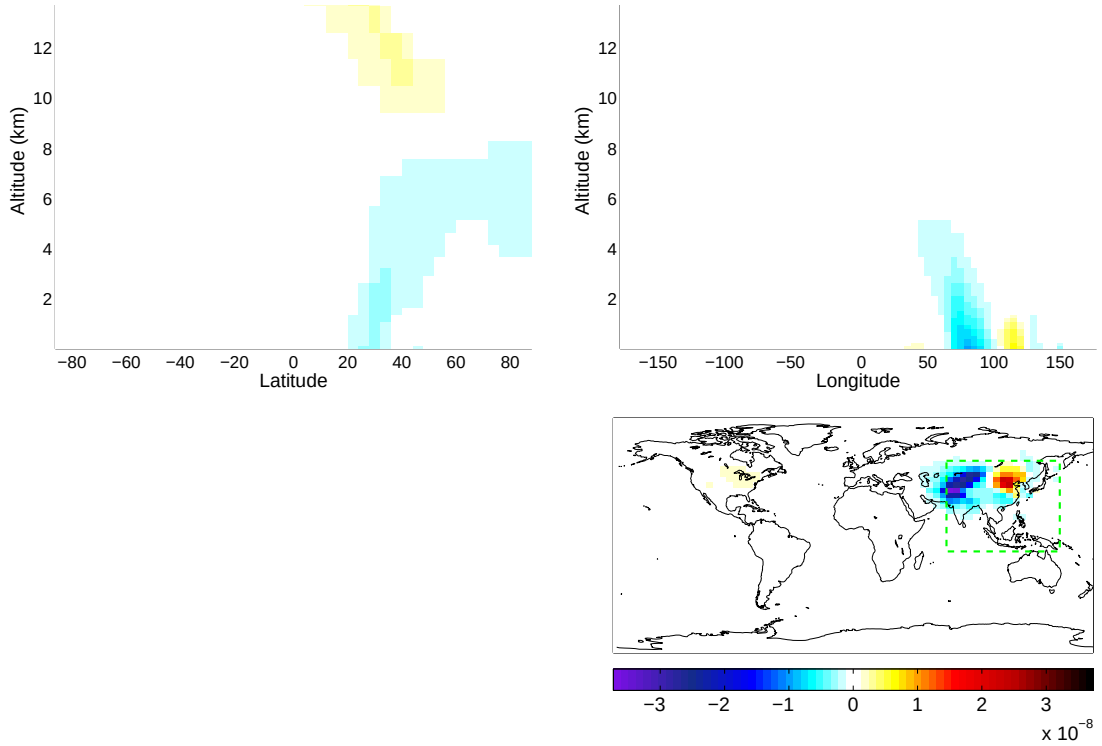

Figure B-18: Sensitivities of surface PM concentration in Asia to HC emissions (in $\mu g\,m^{-3}/kg\,hr^{-1}$)

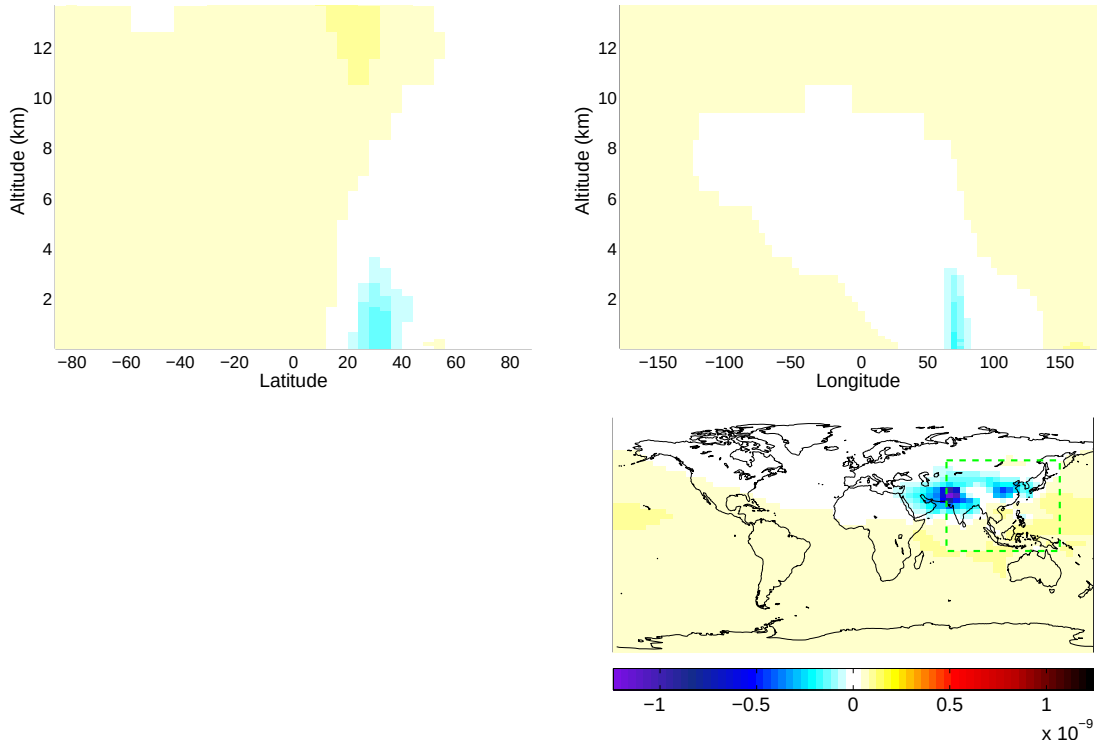

Figure B-19: Sensitivities of surface PM concentration in Asia to CO emissions (in $\mu g\,m^{-3}/kg\,hr^{-1}$)

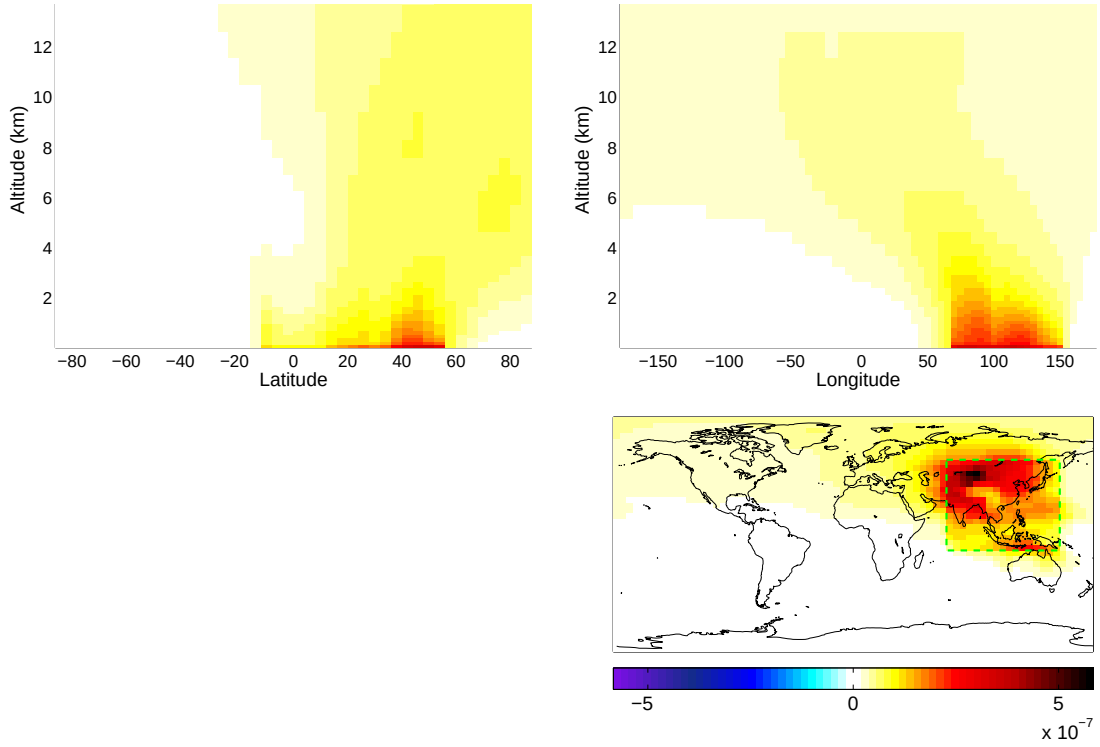

Figure B-20: Sensitivities of surface PM concentration in Asia to primary PM emissions (in $\mu g\,m^{-3}/kg\,hr^{-1}$)

B.1.5 Sensitivities of Surface PM concentration in the World to Aircraft Emissions

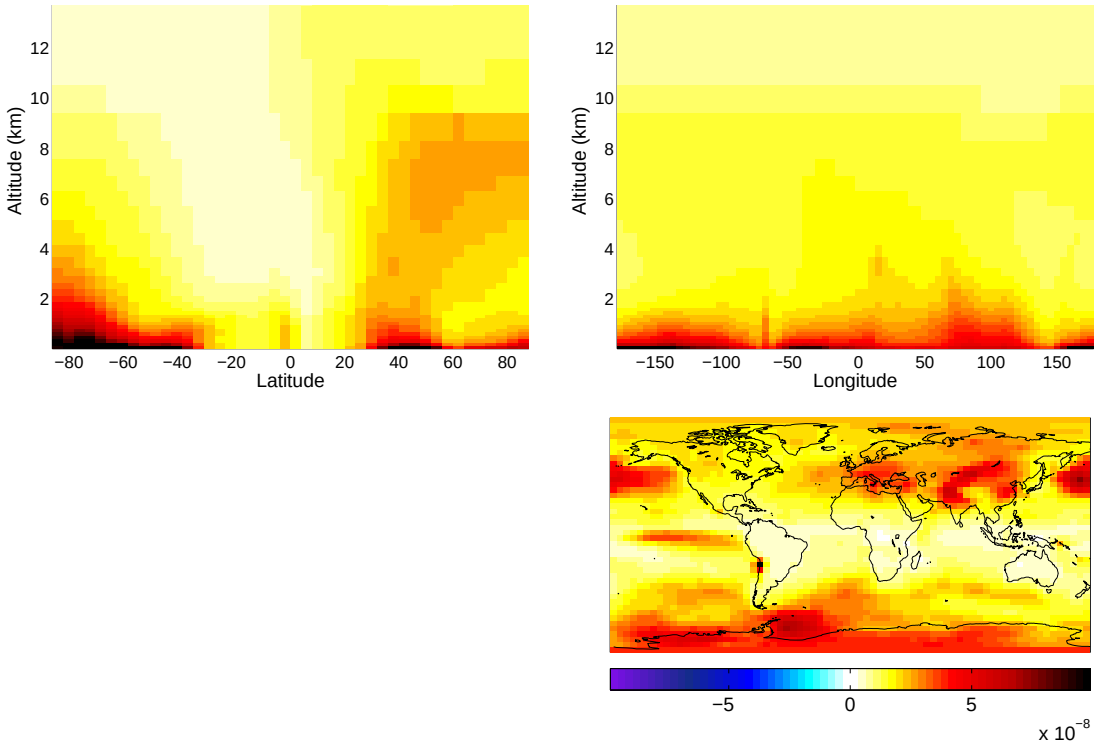

Figure B-21: Sensitivities of surface PM concentration in the world to NO_X emissions (in $\mu g\,m^{-3}/kg\,hr^{-1}$)

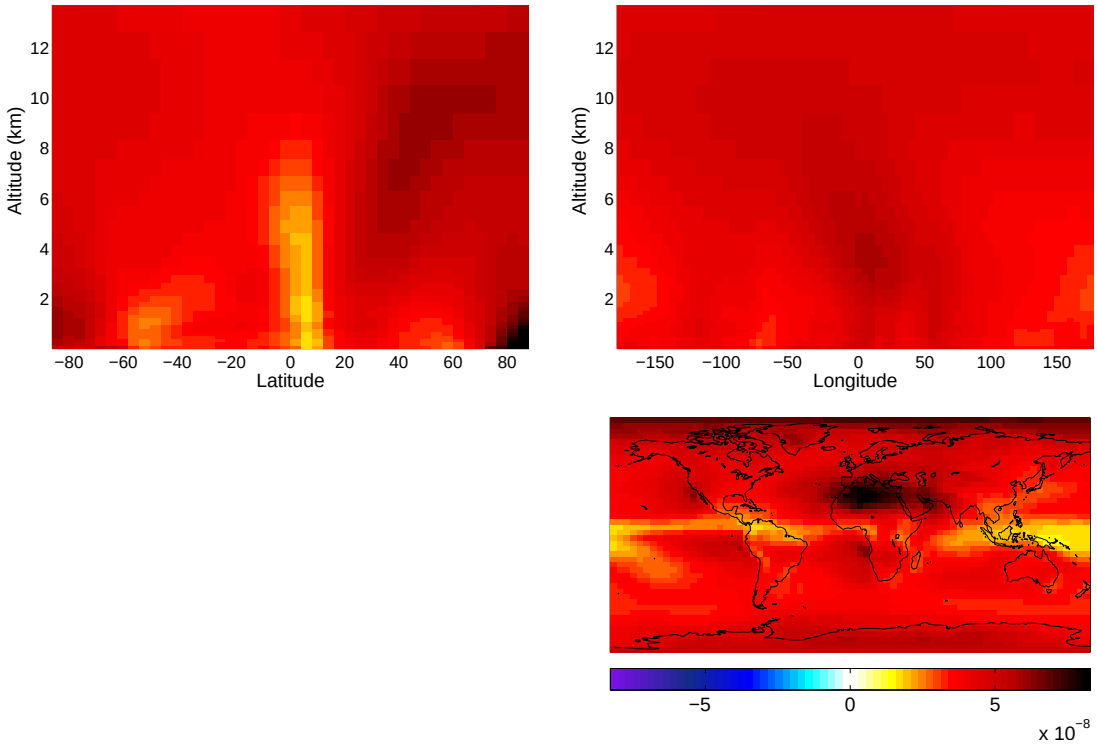

Figure B-22: Sensitivities of surface PM concentration in the world to SO_X emissions (in $\mu g\,m^{-3}/kg\,hr^{-1}$)

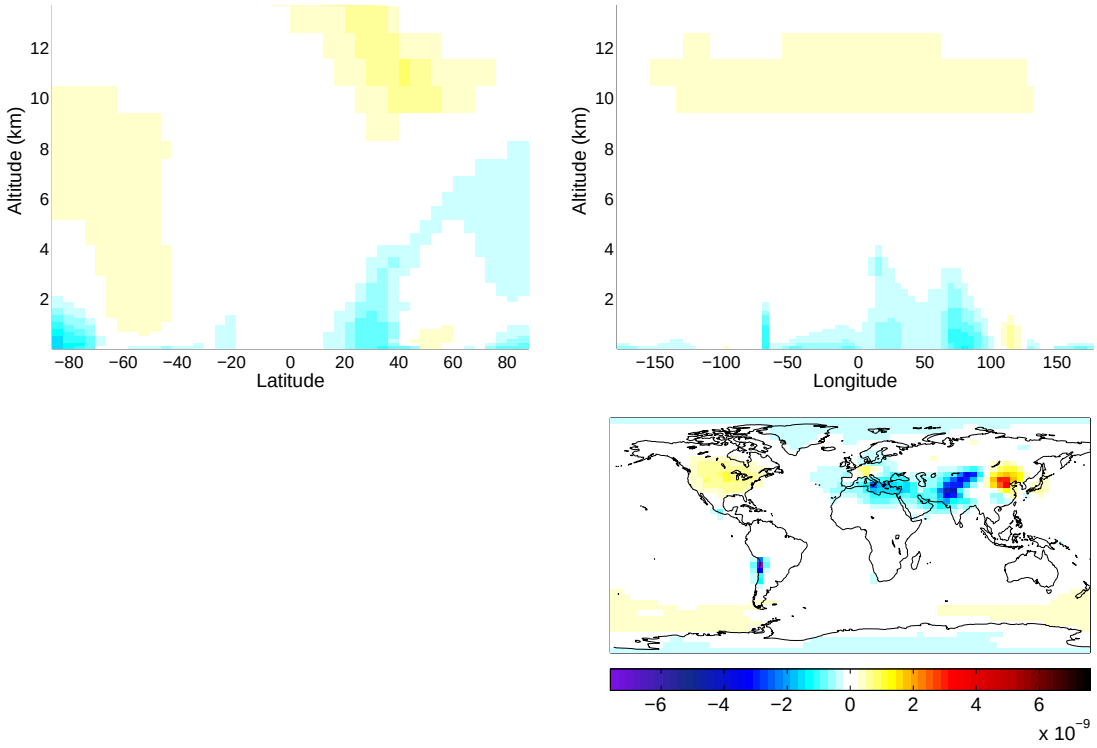

Figure B-23: Sensitivities of surface PM concentration in the world to HC emissions (in $\mu g\,m^{-3}/kg\,hr^{-1}$)

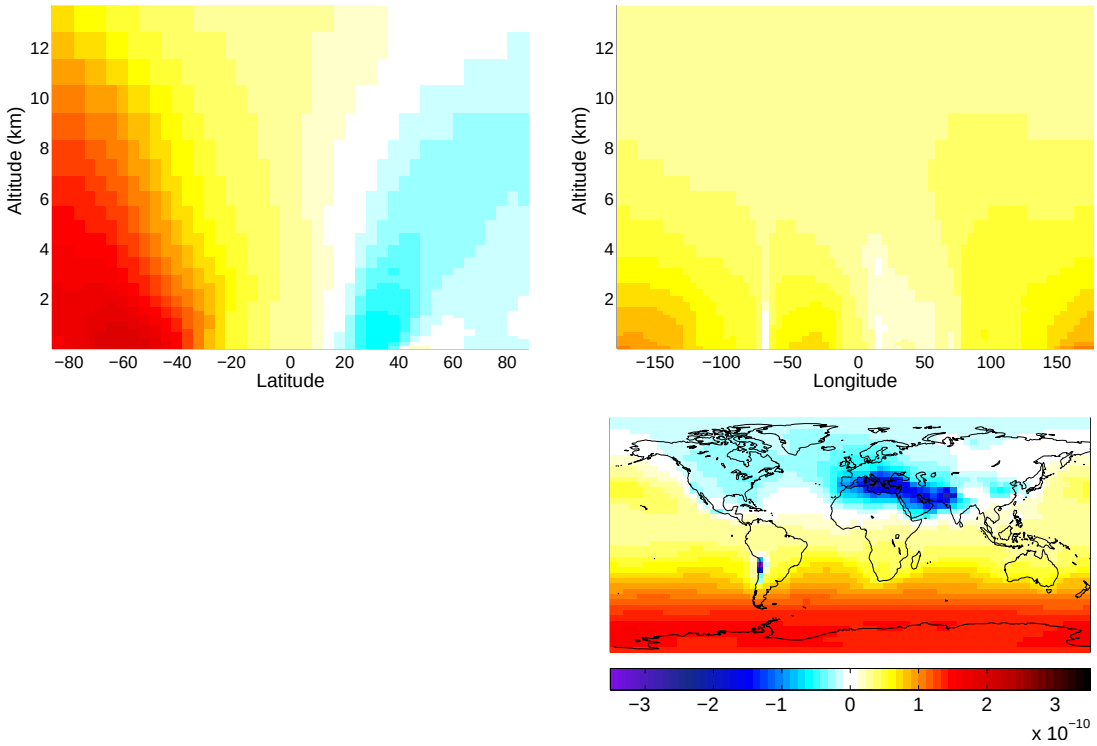

Figure B-24: Sensitivities of surface PM concentration in the world to CO emissions (in $\mu g\,m^{-3}/kg\,hr^{-1}$)

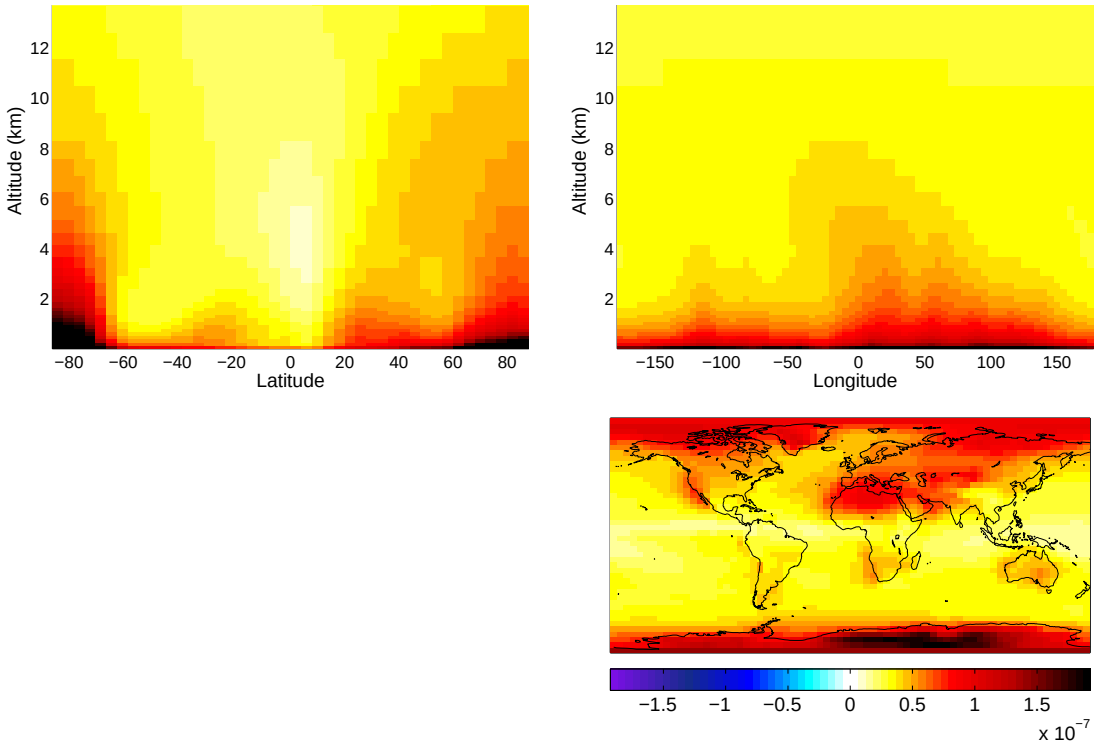

Figure B-25: Sensitivities of surface PM concentration in the world to primary PM emissions (in $\mu g\,m^{-3}/kg\,hr^{-1}$)

B.2 Sensitivities of Population Exposure to PM

This section shows the sensitivities of population exposure to PM in various regions (the US, North America, Europe, Asia, the world) with respect to several aircraft emissions (NO_X, SO_X, HC, CO, primary PM).

B.2.1 Sensitivities of Population Exposure to PM in the US to Aircraft Emissions

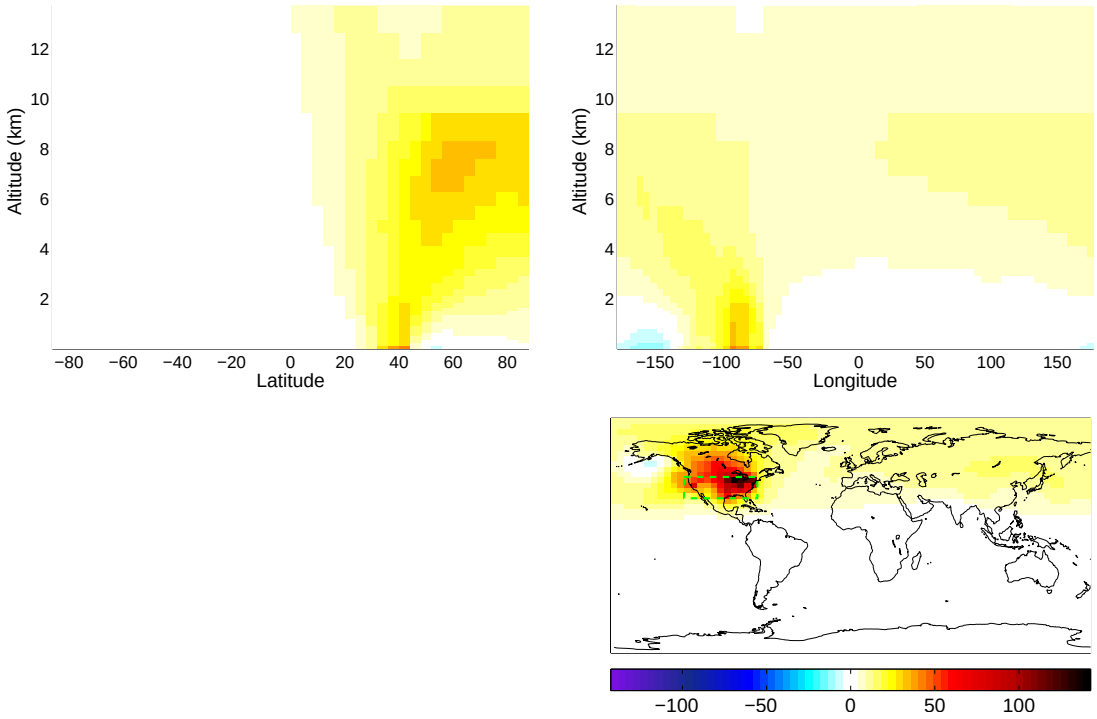

Figure B-26: Sensitivities of population exposure to PM in the US to NO_X emissions (in $\text{ppl} \cdot \mu\text{g}\,\text{m}^{-3}/\text{kg}\,\text{hr}^{-1}$)

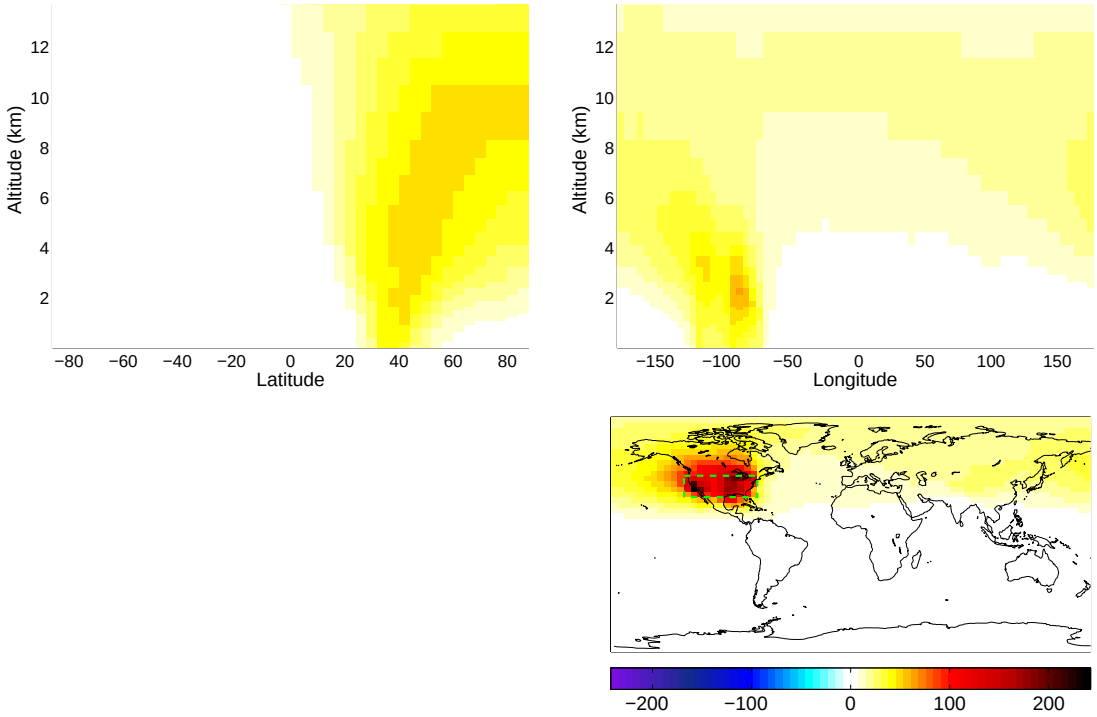

Figure B-27: Sensitivities of population exposure to PM in the US to SO_X emissions (in $\text{ppl} \cdot \mu\text{g}\,\text{m}^{-3}/\text{kg}\,\text{hr}^{-1}$)

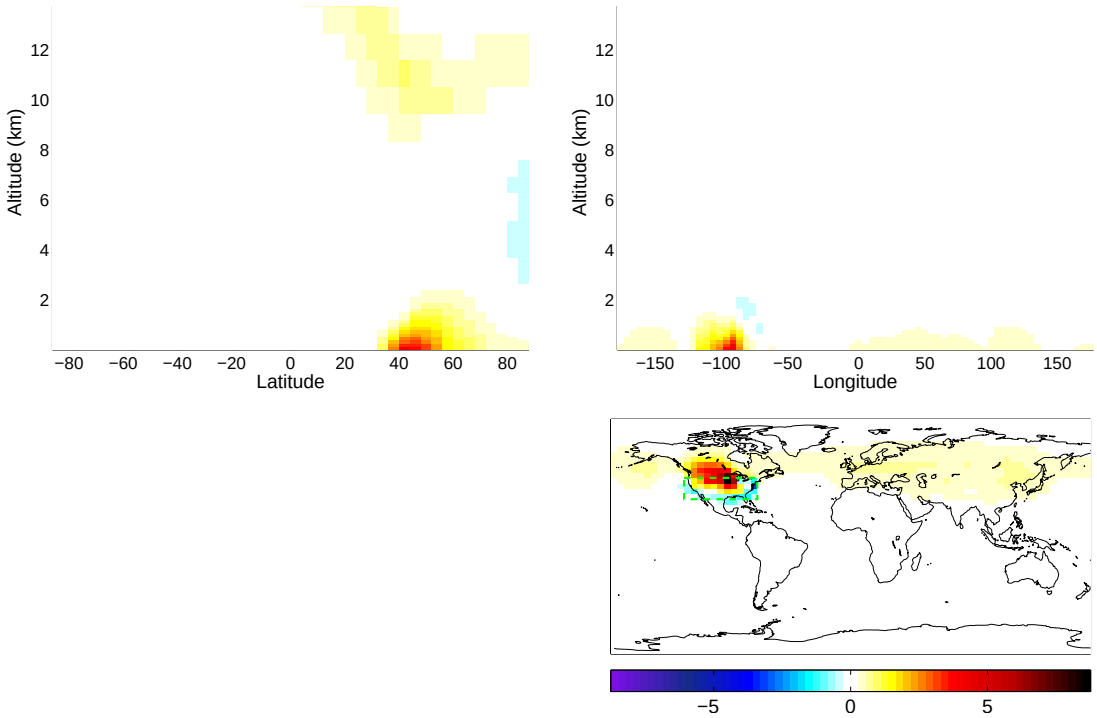

Figure B-28: Sensitivities of population exposure to PM in the US to HC emissions (in $\text{ppl} \cdot \mu\text{g}\,\text{m}^{-3}/\text{kg}\,\text{hr}^{-1}$)

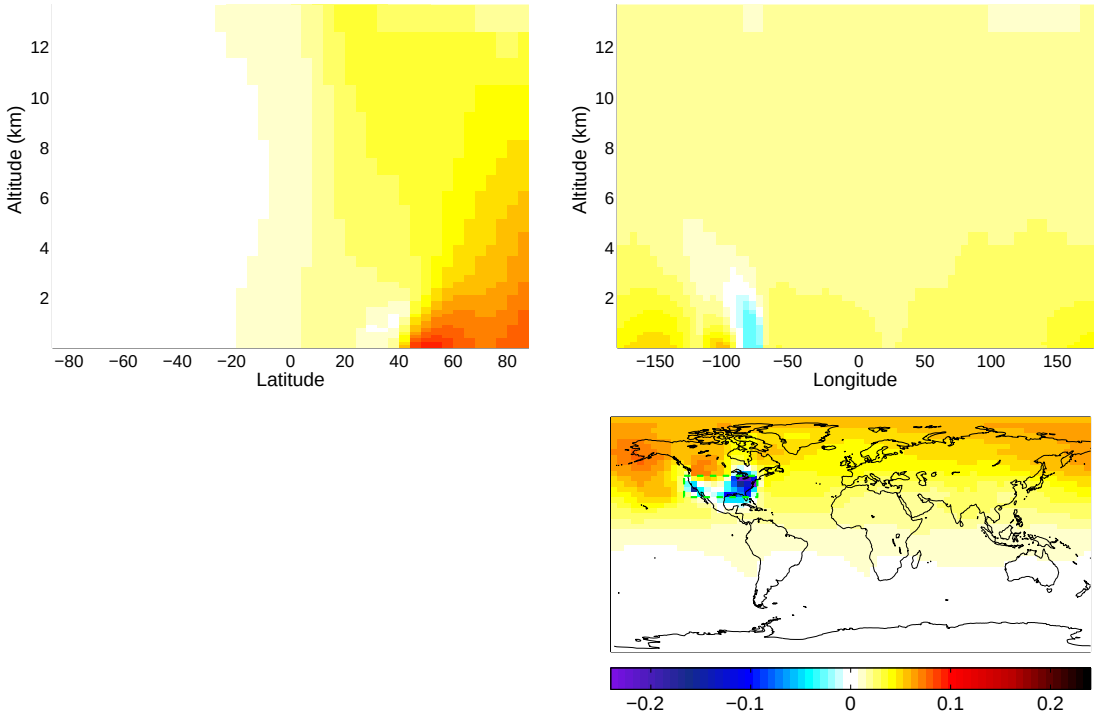

Figure B-29: Sensitivities of population exposure to PM in the US to CO emissions (in $\text{ppl} \cdot \mu\text{g}\,\text{m}^{-3}/\text{kg}\,\text{hr}^{-1}$)

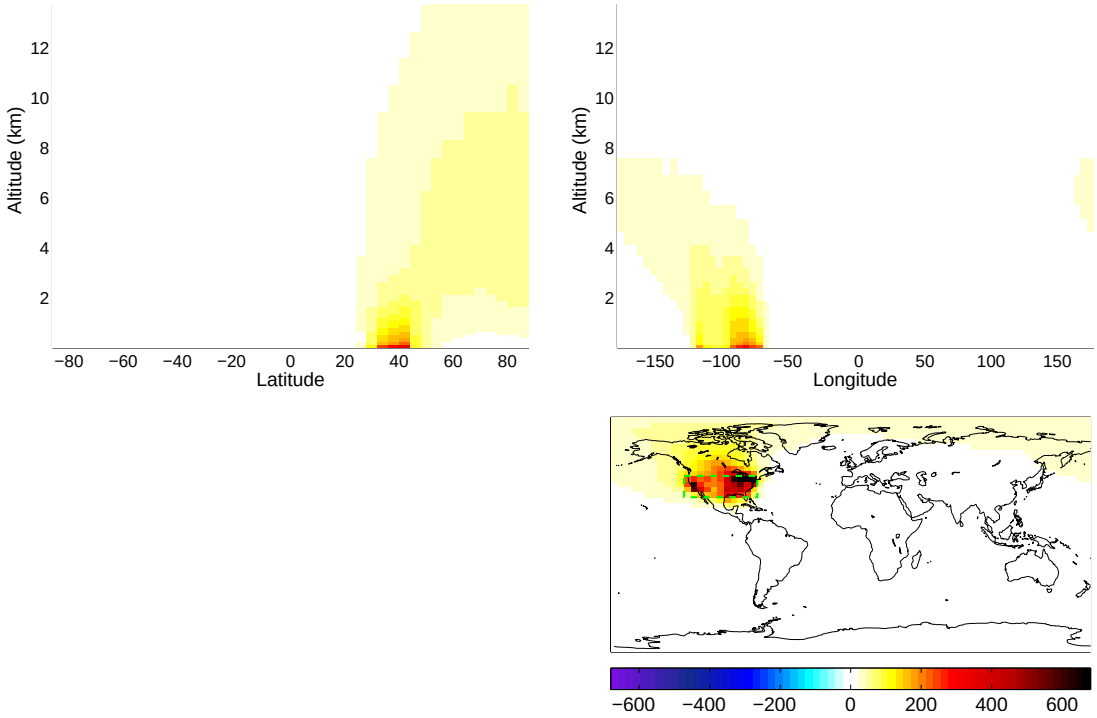

Figure B-30: Sensitivities of population exposure to PM in the US to primary PM emissions (in $\text{ppl} \cdot \mu\text{g}\,\text{m}^{-3}/\text{kg}\,\text{hr}^{-1}$)

B.2.2 Sensitivities of Population Exposure to PM in North America to Aircraft Emissions

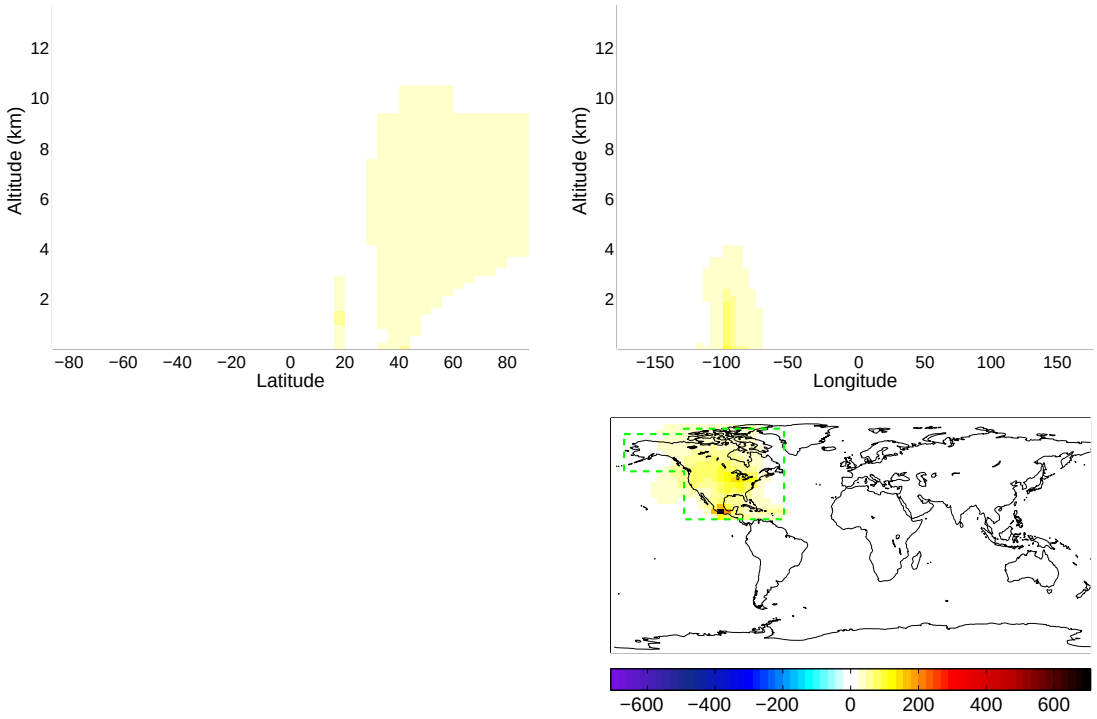

Figure B-31: Sensitivities of population exposure to PM in North America to NO_X emissions (in $\text{ppl} \cdot \mu\text{g}\,\text{m}^{-3}/\text{kg}\,\text{hr}^{-1}$)

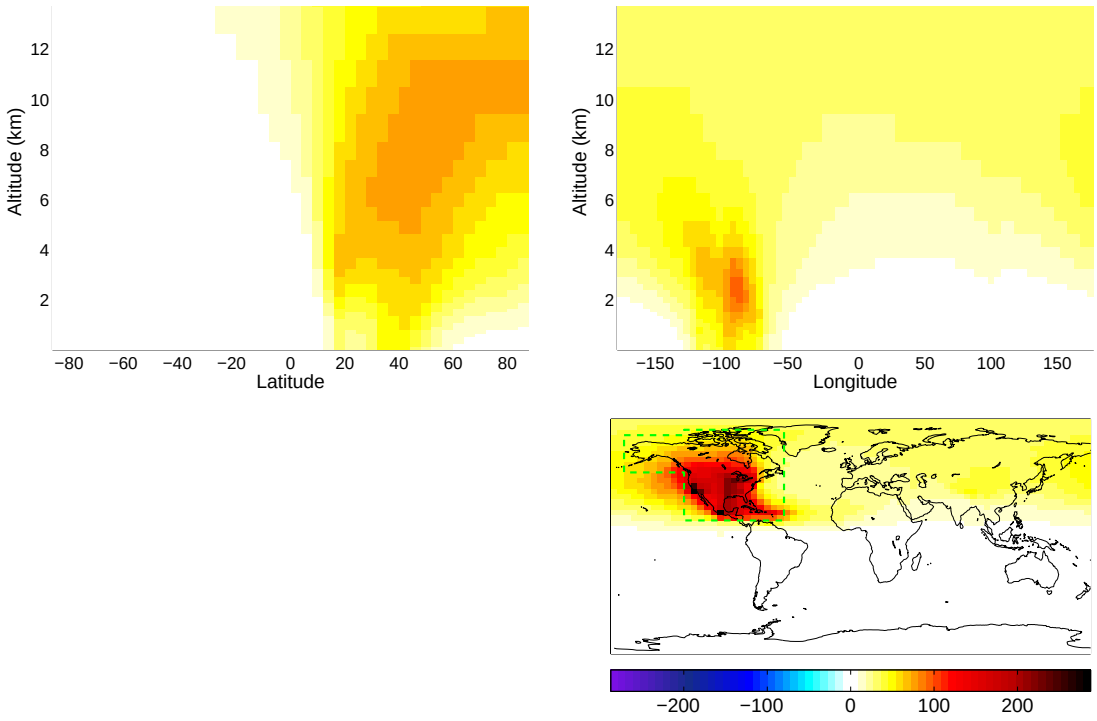

Figure B-32: Sensitivities of population exposure to PM in North America to SO_X emissions (in $\text{ppl} \cdot \mu\text{g}\,\text{m}^{-3}/\text{kg}\,\text{hr}^{-1}$)

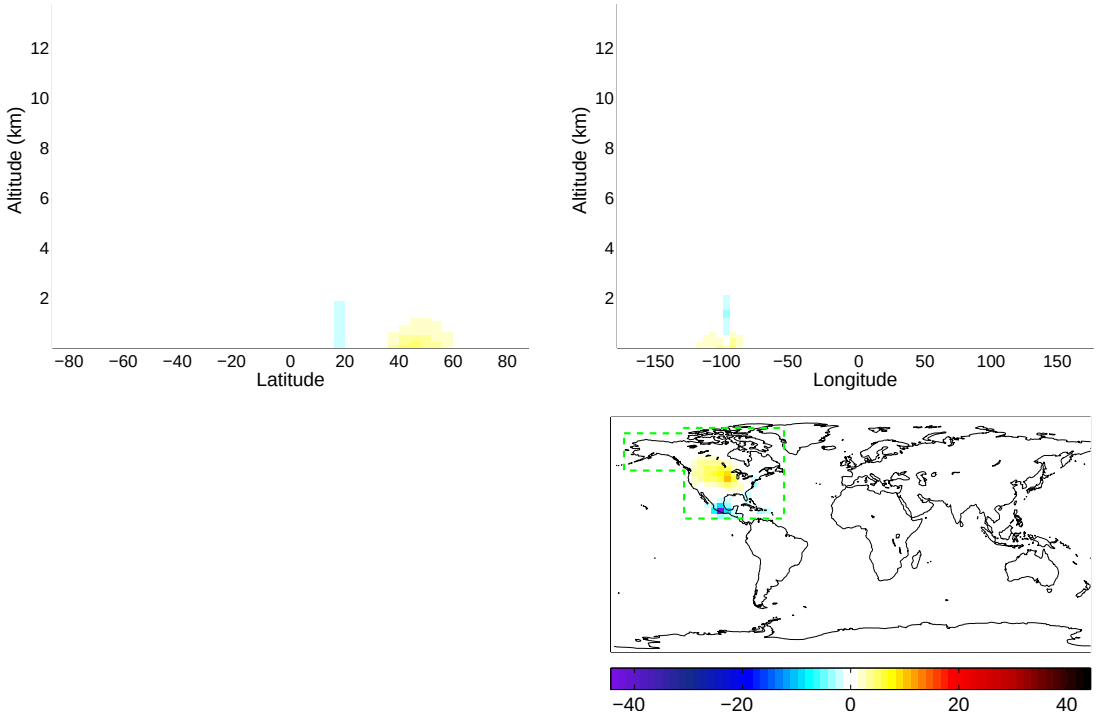

Figure B-33: Sensitivities of population exposure to PM in North America to HC emissions (in $\text{ppl} \cdot \mu\text{g}\,\text{m}^{-3}/\text{kg}\,\text{hr}^{-1}$)

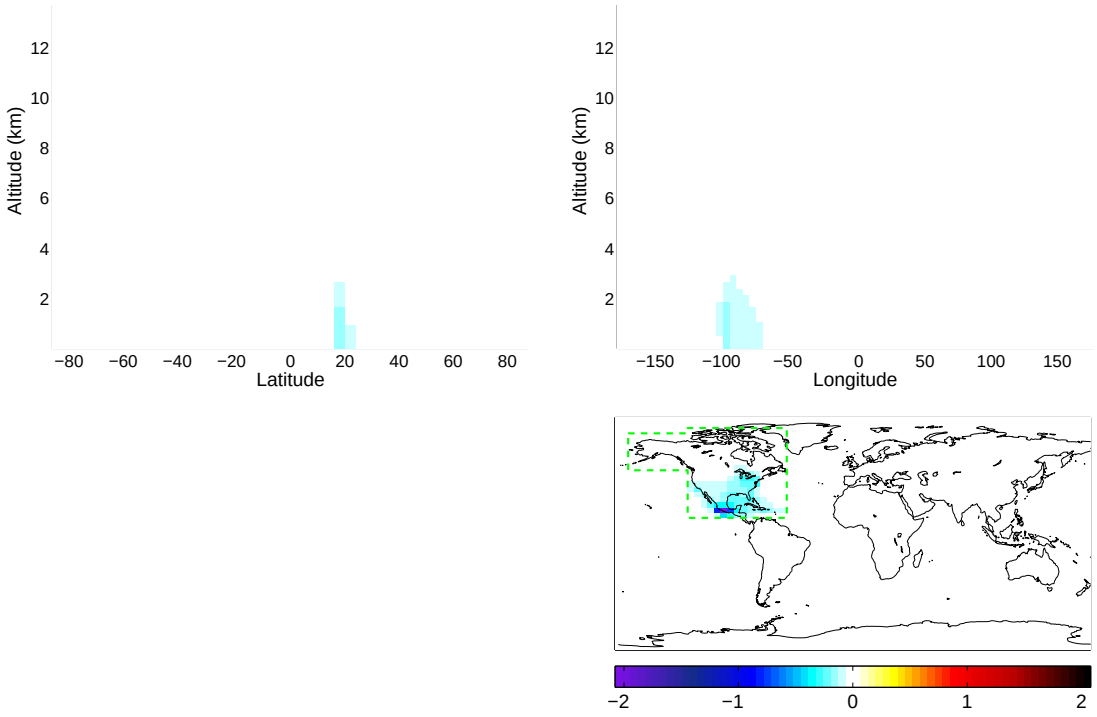

Figure B-34: Sensitivities of population exposure to PM in North America to CO emissions (in $\text{ppl} \cdot \mu\text{g}\,\text{m}^{-3}/\text{kg}\,\text{hr}^{-1}$)

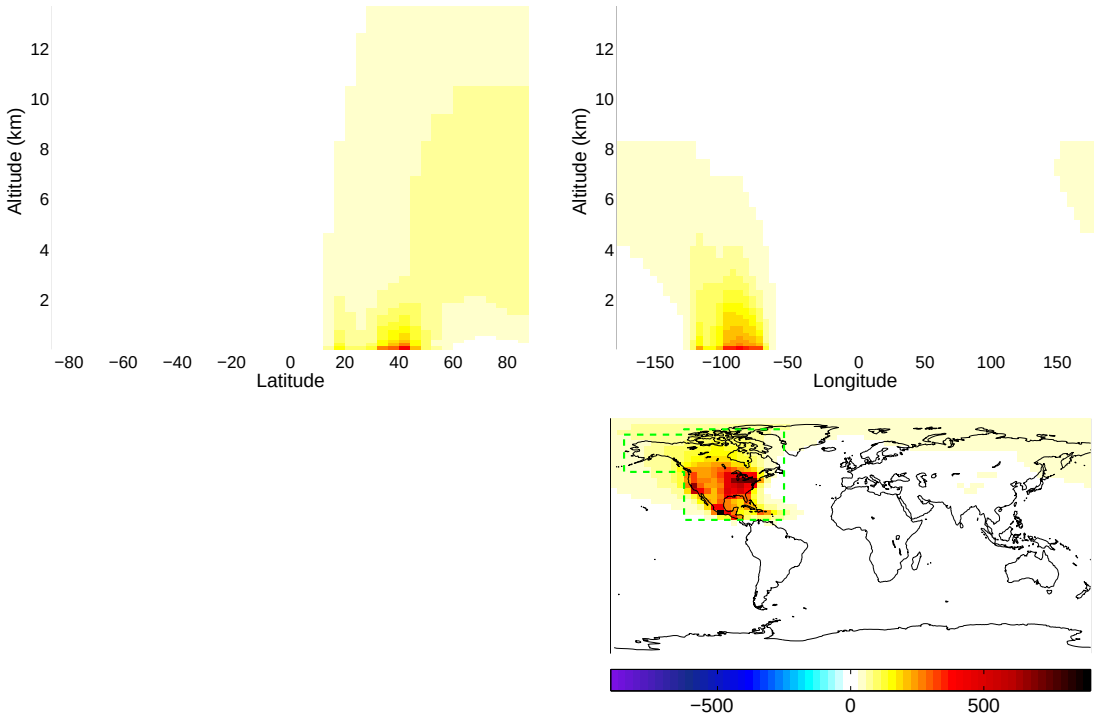

Figure B-35: Sensitivities of population exposure to PM in North America to primary PM emissions (in $\text{ppl} \cdot \mu\text{g}\,\text{m}^{-3}/\text{kg}\,\text{hr}^{-1}$)

B.2.3 Sensitivities of Population Exposure to PM in Europe to Aircraft Emissions

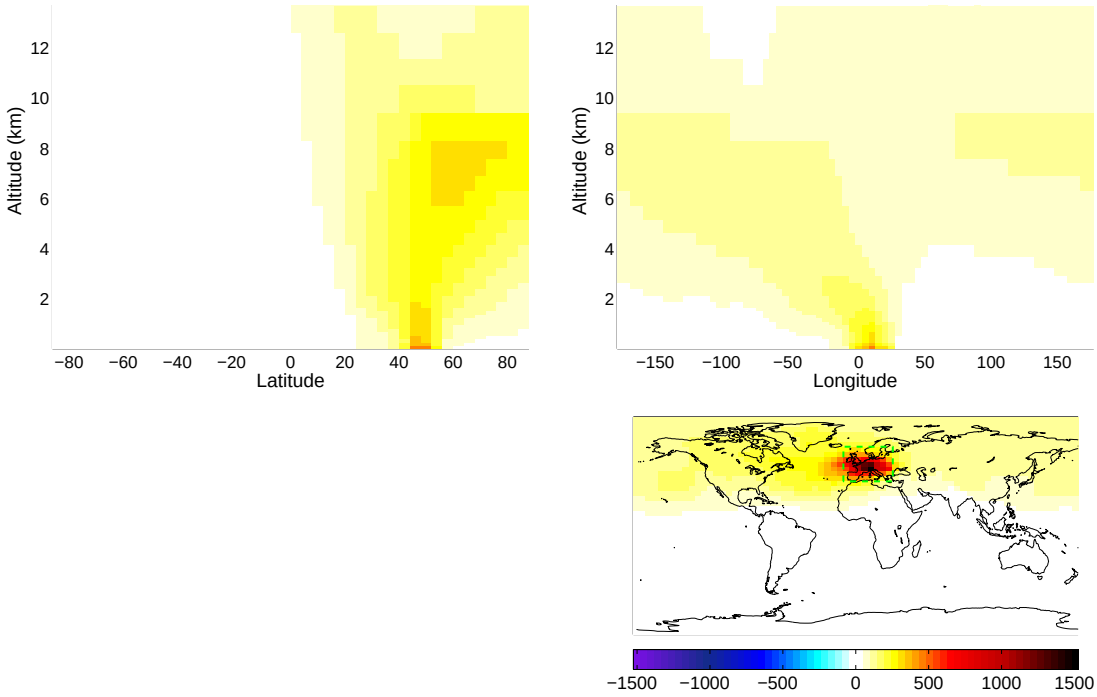

Figure B-36: Sensitivities of population exposure to PM in Europe to NO_X emissions (in $\text{ppl} \cdot \mu\text{g}\,\text{m}^{-3}/\text{kg}\,\text{hr}^{-1}$)

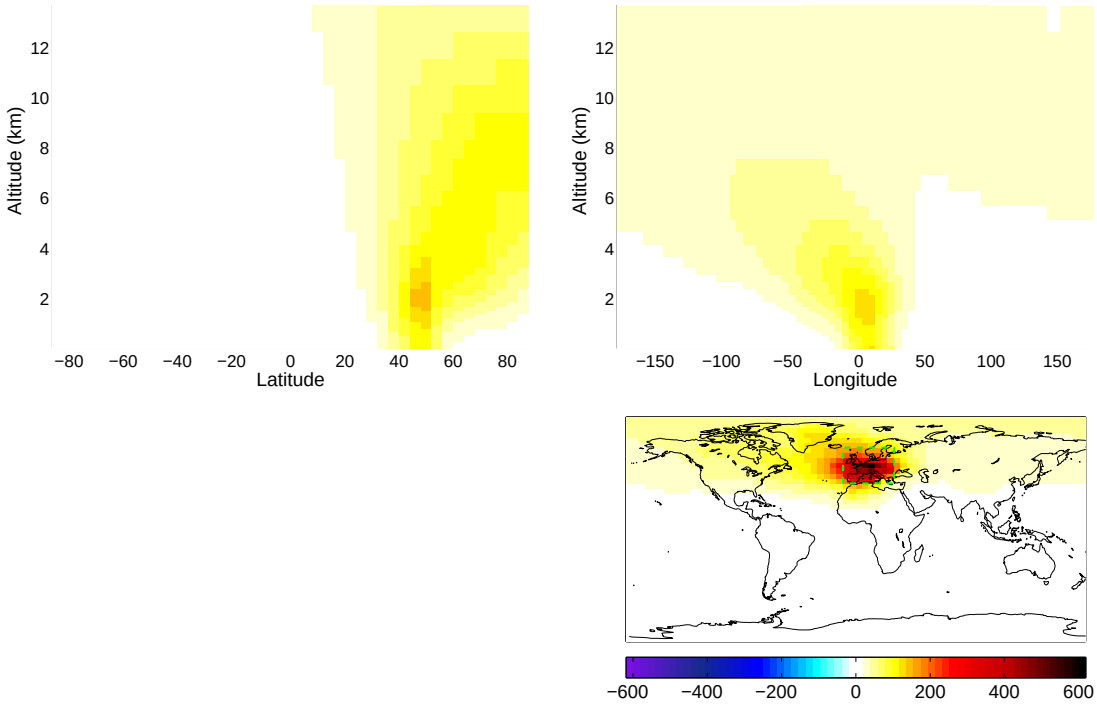

Figure B-37: Sensitivities of population exposure to PM in Europe to SO_X emissions (in $\text{ppl} \cdot \mu\text{g}\,\text{m}^{-3}/\text{kg}\,\text{hr}^{-1}$)

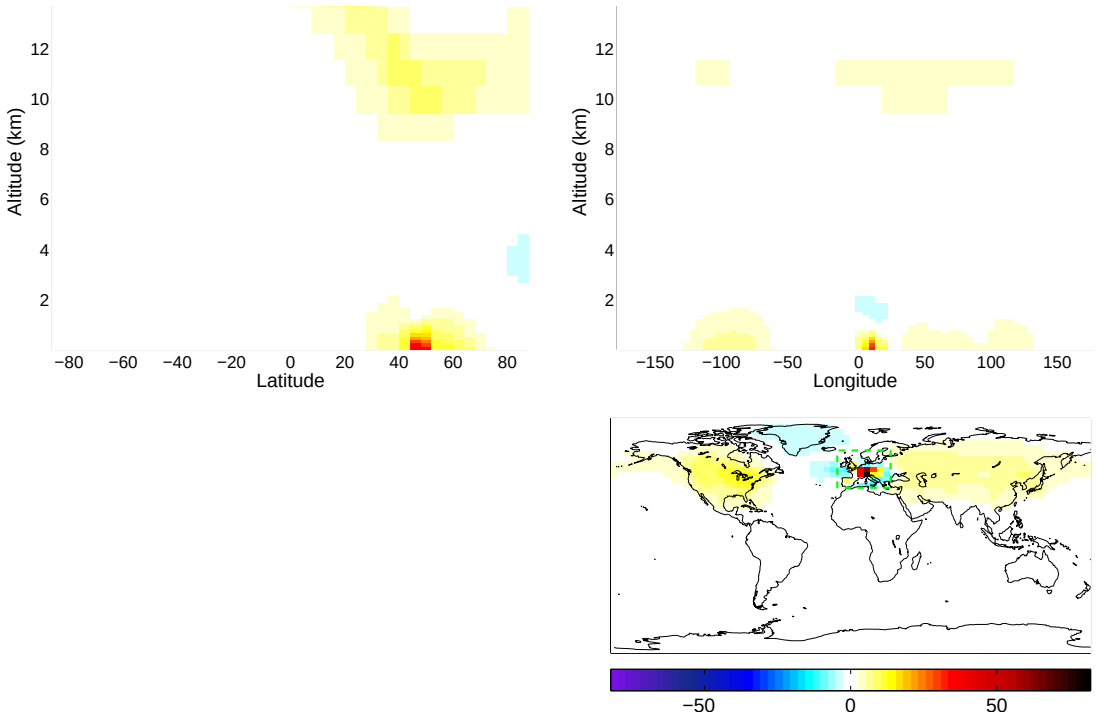

Figure B-38: Sensitivities of population exposure to PM in Europe to HC emissions (in $\text{ppl} \cdot \mu\text{g}\,\text{m}^{-3}/\text{kg}\,\text{hr}^{-1}$)

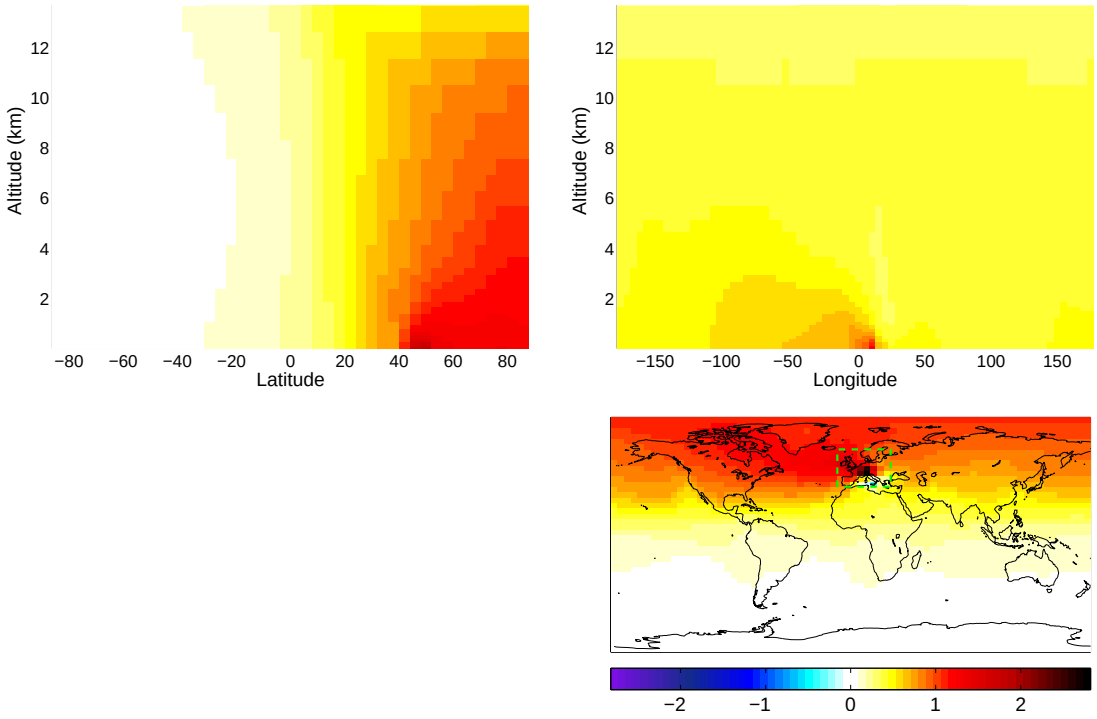

Figure B-39: Sensitivities of population exposure to PM in Europe to CO emissions (in $\text{ppl} \cdot \mu\text{g}\,\text{m}^{-3}/\text{kg}\,\text{hr}^{-1}$)

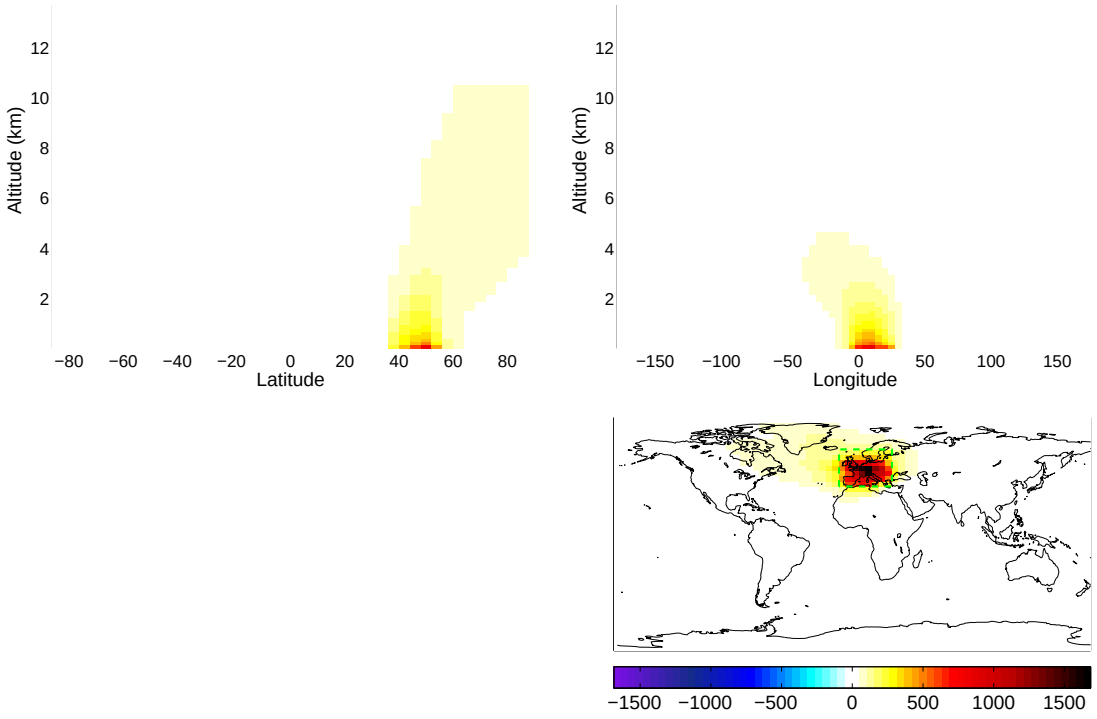

Figure B-40: Sensitivities of population exposure to PM in Europe to primary PM emissions (in $\text{ppl} \cdot \mu\text{g}\,\text{m}^{-3}/\text{kg}\,\text{hr}^{-1}$)

B.2.4 Sensitivities of Population Exposure to PM in Asia to Aircraft Emissions

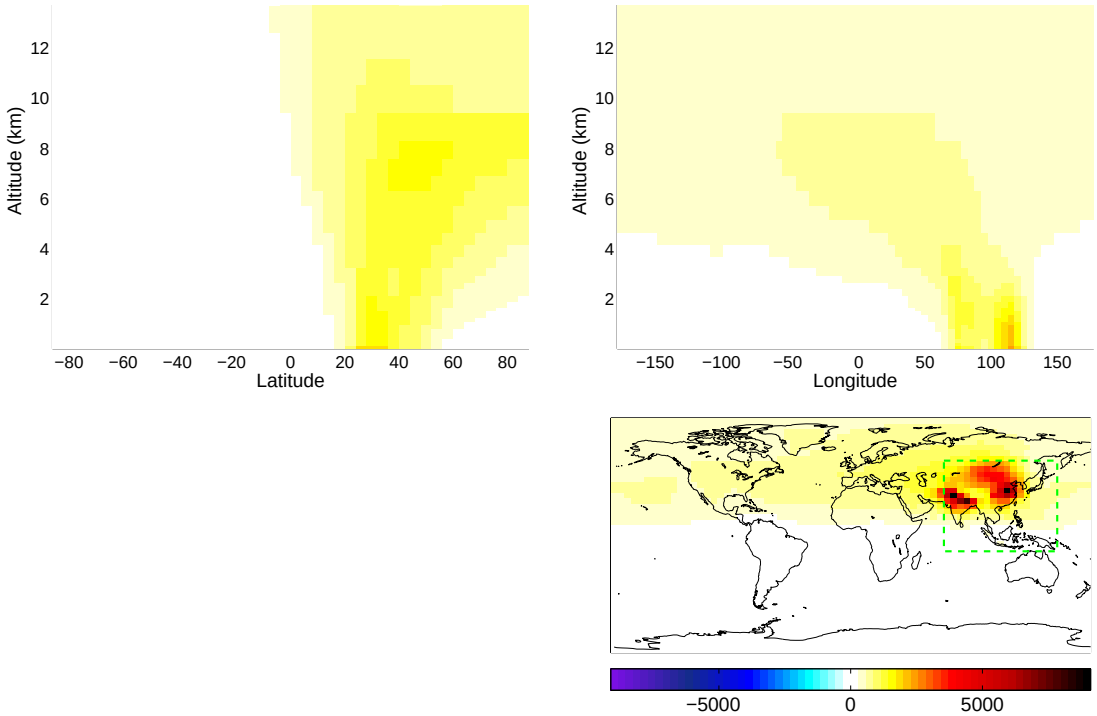

Figure B-41: Sensitivities of population exposure to PM in Asia to NO_X emissions (in $\text{ppl} \cdot \mu\text{g}\,\text{m}^{-3}/\text{kg}\,\text{hr}^{-1}$)

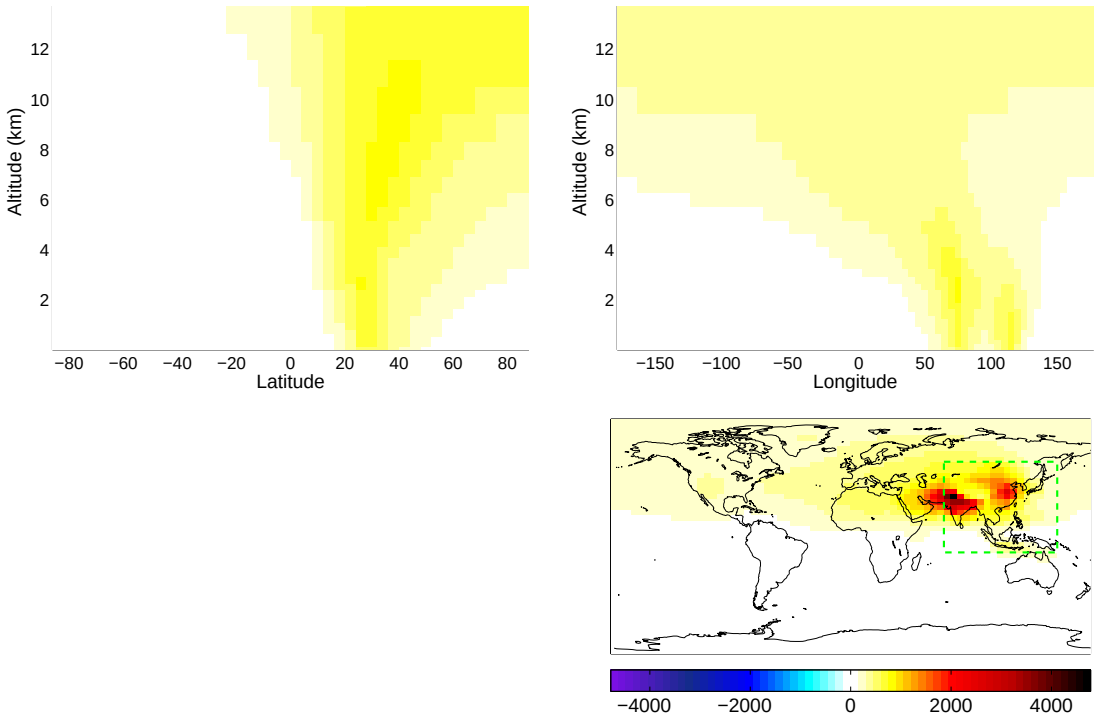

Figure B-42: Sensitivities of population exposure to PM in Asia to SO_X emissions (in $\text{ppl} \cdot \mu\text{g}\,\text{m}^{-3}/\text{kg}\,\text{hr}^{-1}$)

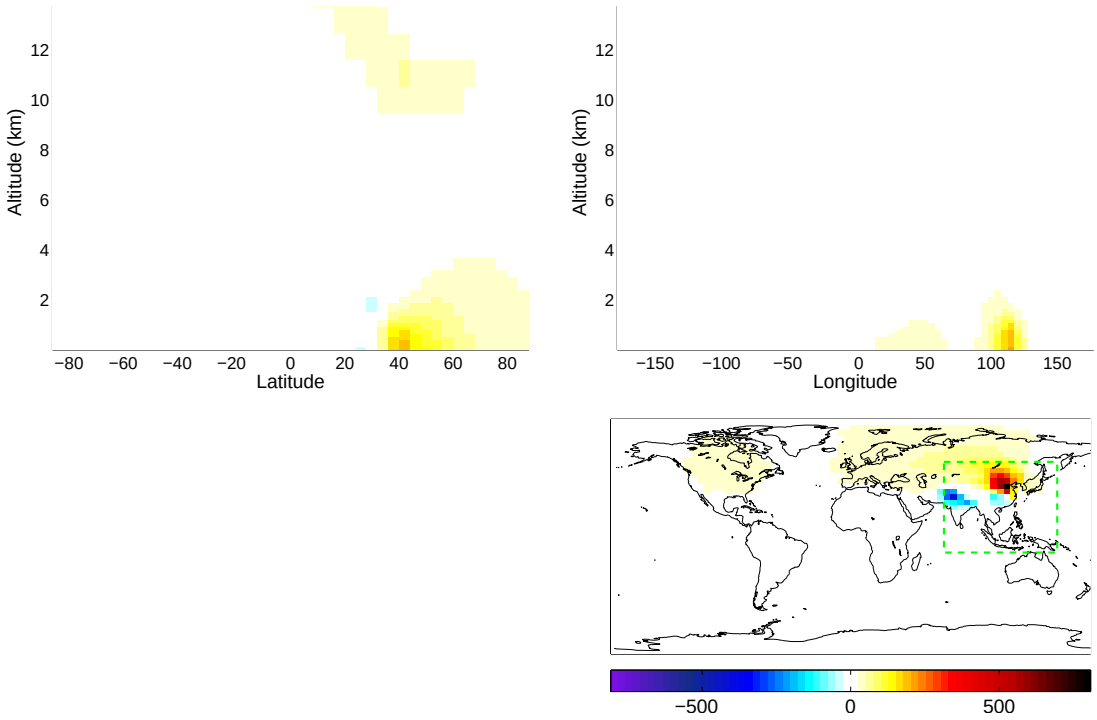

Figure B-43: Sensitivities of population exposure to PM in Asia to HC emissions (in $\text{ppl} \cdot \mu\text{g}\,\text{m}^{-3}/\text{kg}\,\text{hr}^{-1}$)

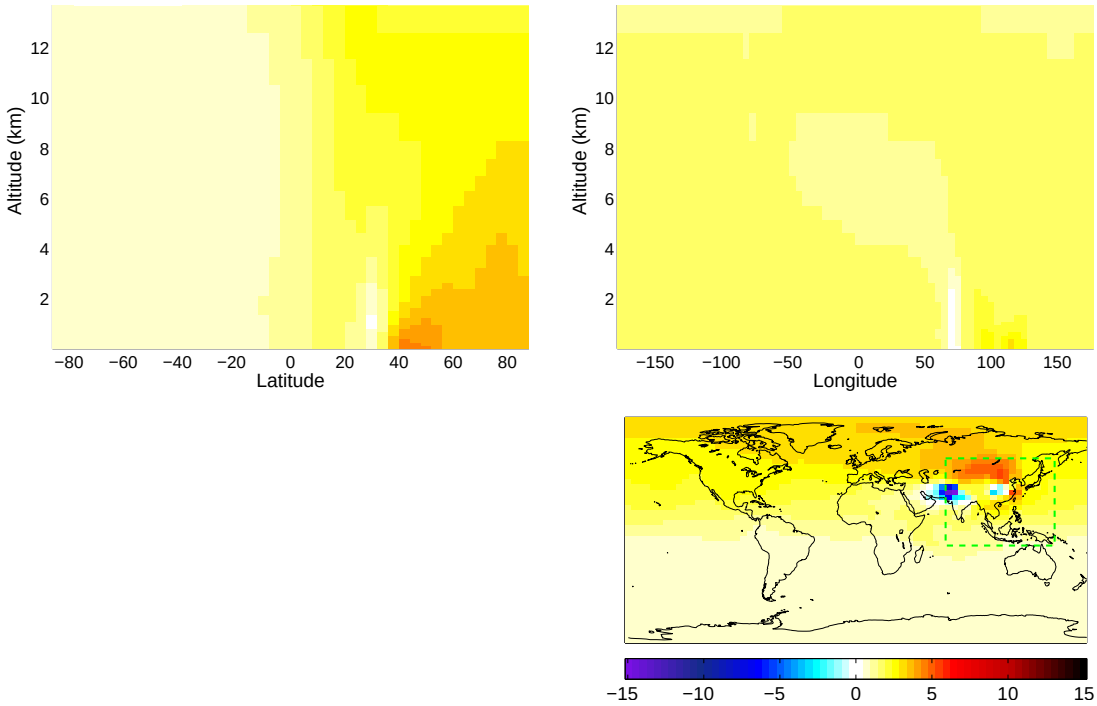

Figure B-44: Sensitivities of population exposure to PM in Asia to CO emissions (in $\text{ppl} \cdot \mu\text{g}\,\text{m}^{-3}/\text{kg}\,\text{hr}^{-1}$)

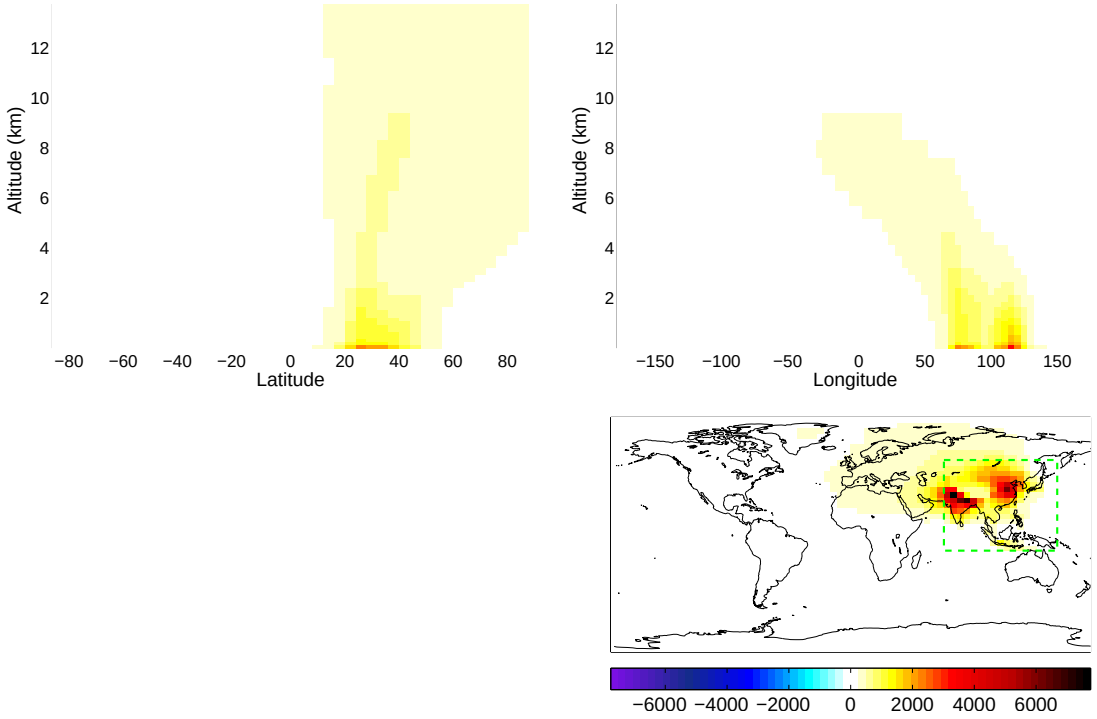

Figure B-45: Sensitivities of population exposure to PM in Asia to primary PM emissions (in $\text{ppl} \cdot \mu\text{g}\,\text{m}^{-3}/\text{kg}\,\text{hr}^{-1}$)

B.2.5 Sensitivities of Population Exposure to PM in the World to Aircraft Emissions

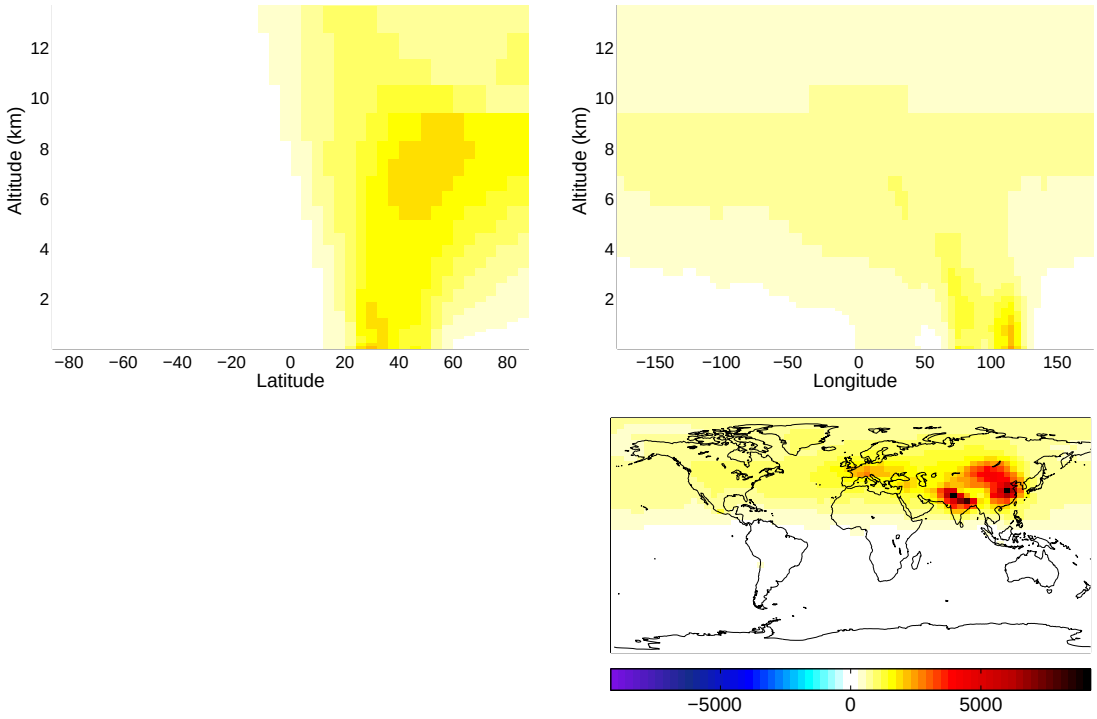

Figure B-46: Sensitivities of population exposure to PM in the world to NO_X emissions (in $\text{ppl} \cdot \mu\text{g}\,\text{m}^{-3}/\text{kg}\,\text{hr}^{-1}$)

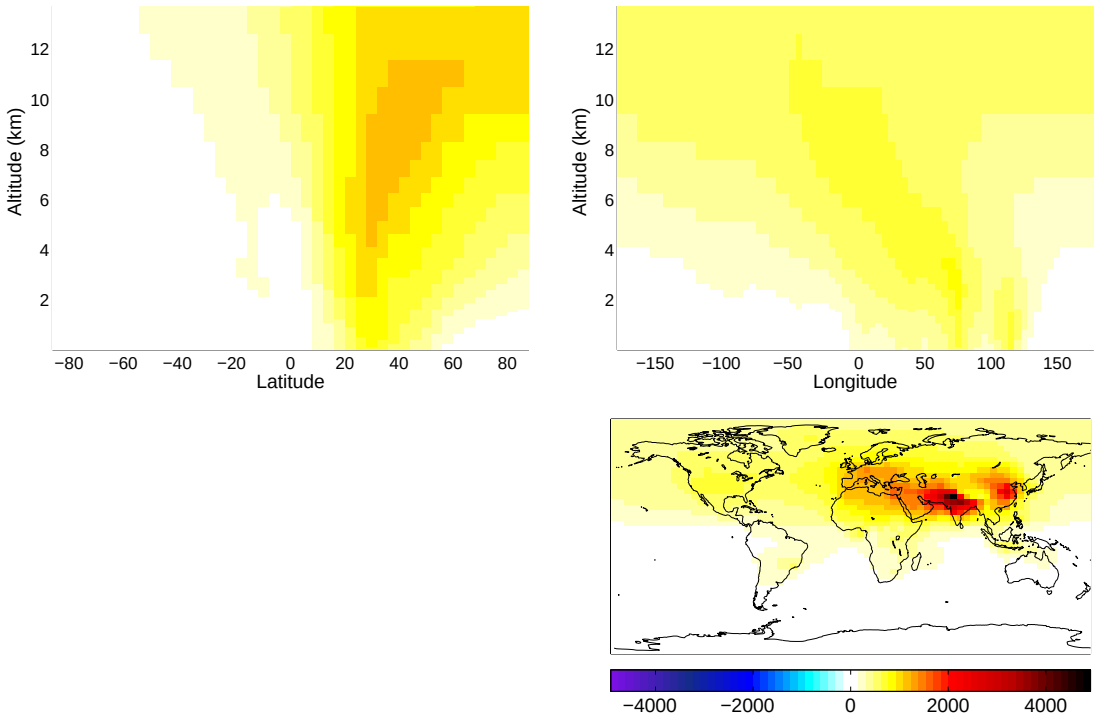

Figure B-47: Sensitivities of population exposure to PM in the world to SO_X emissions (in $\text{ppl} \cdot \mu\text{g}\,\text{m}^{-3}/\text{kg}\,\text{hr}^{-1}$)

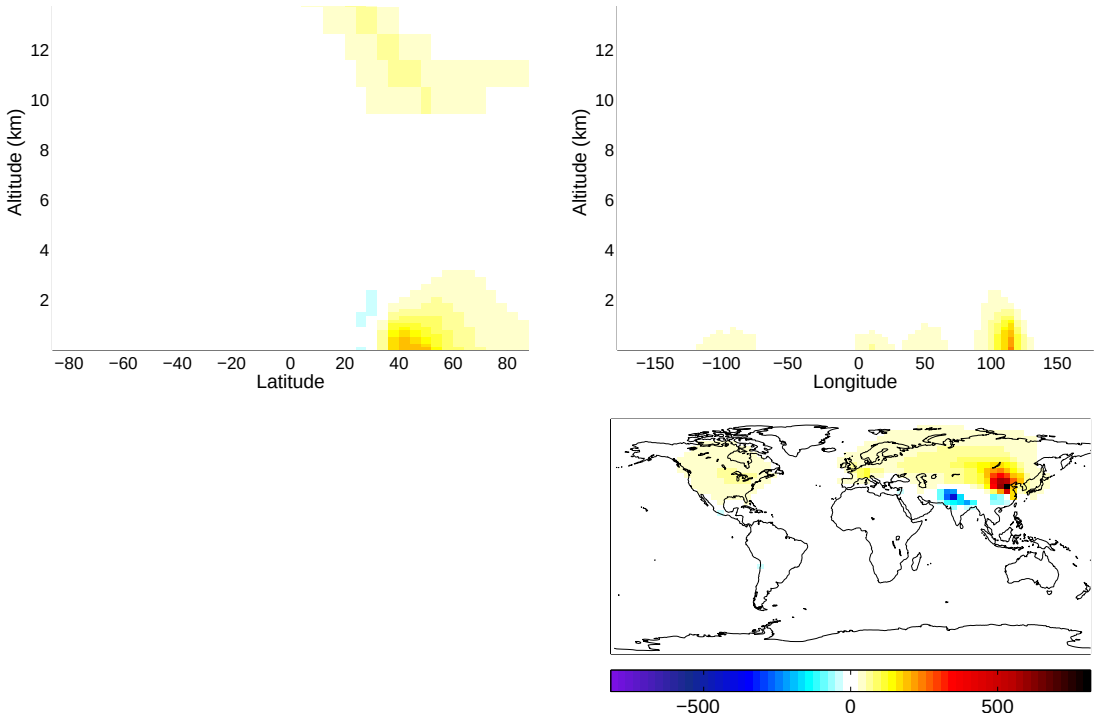

Figure B-48: Sensitivities of population exposure to PM in the world to HC emissions (in $\text{ppl} \cdot \mu\text{g}\,\text{m}^{-3}/\text{kg}\,\text{hr}^{-1}$)

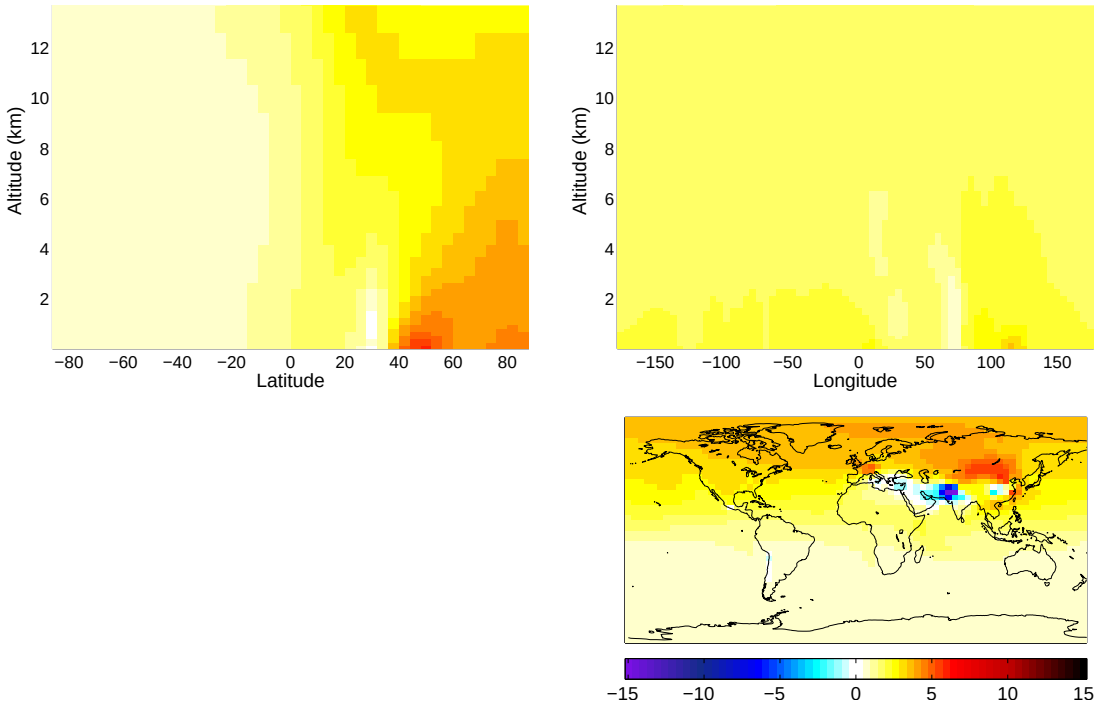

Figure B-49: Sensitivities of population exposure to PM in the world to CO emissions (in $\text{ppl} \cdot \mu\text{g}\,\text{m}^{-3}/\text{kg}\,\text{hr}^{-1}$)

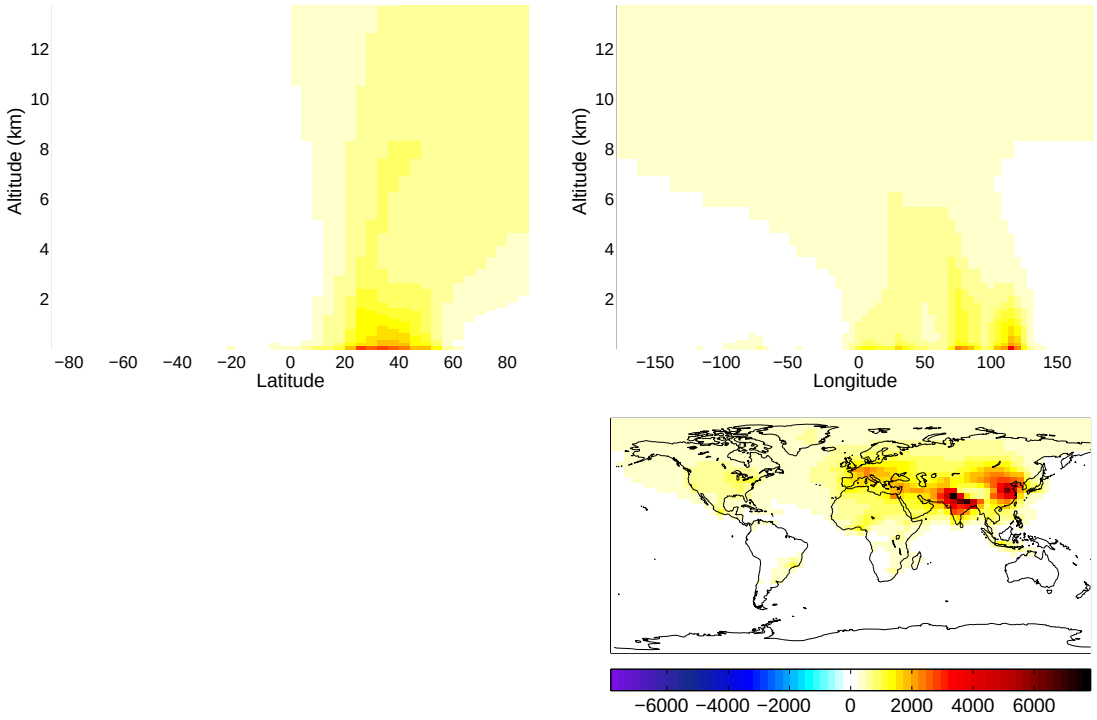

Figure B-50: Sensitivities of population exposure to PM in the world to primary PM emissions (in $\text{ppl} \cdot \mu\text{g}\,\text{m}^{-3}/\text{kg}\,\text{hr}^{-1}$)

THIS PAGE INTENTIONALLY LEFT BLANK

Appendix C

Second-order Sensitivity Plots

This appendix shows the first-order and second-order sensitivities. All figures show the first- and second-order sensitivities of global surface PM concentration with respect to emissions averaged over all altitudes.

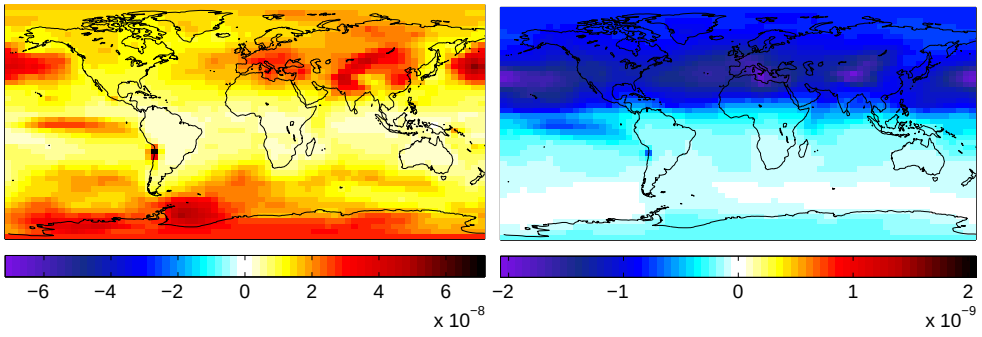

(a) First-order (b) Second-order

Figure C-1: First- and second-order sensitivities of global surface PM concentration with respect to NO_X emissions (in $\mu g\,m^{-3}/kg\,hr^{-1}$)

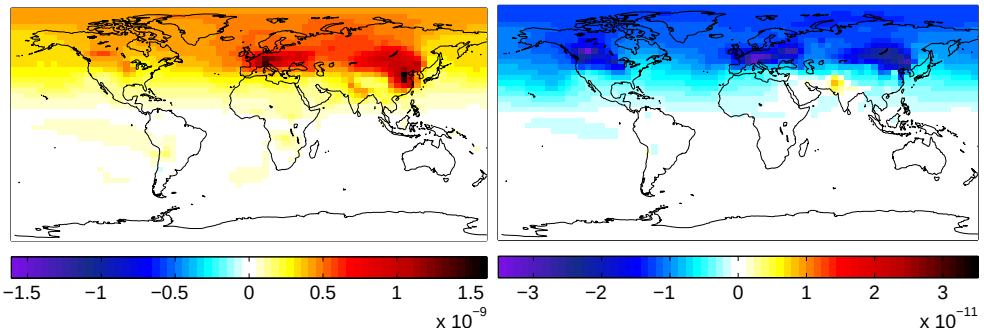

(a) First-order (b) Second-order

Figure C-2: First- and second-order sensitivities of global surface PM concentration with respect to O_X emissions (in $\mu g\,m^{-3}/kg\,hr^{-1}$)

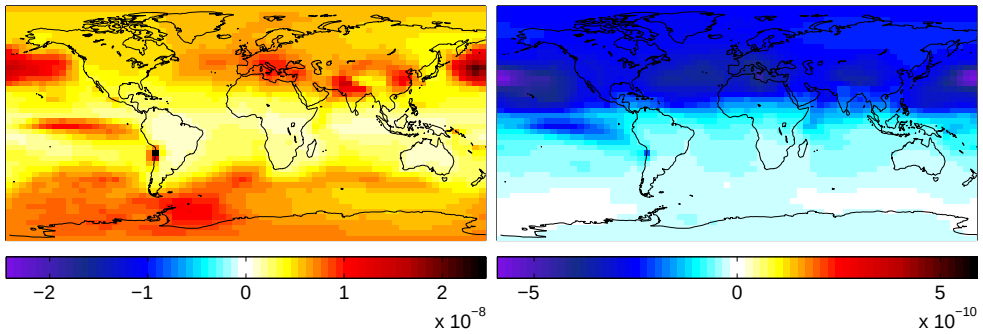

(a) First-order (b) Second-order

Figure C-3: First- and second-order sensitivities of global surface PM concentration with respect to PAN emissions (in $\mu g\,m^{-3}/kg\,hr^{-1}$)

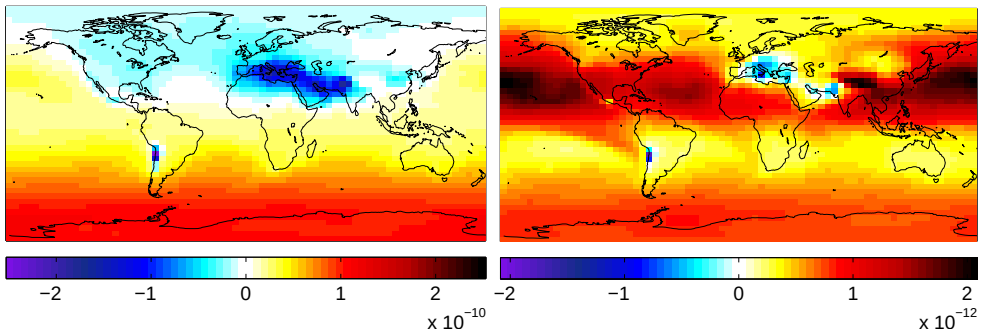

(a) First-order (b) Second-order

Figure C-4: First- and second-order sensitivities of global surface PM concentration with respect to CO emissions (in $\mu g\,m^{-3}/kg\,hr^{-1}$)

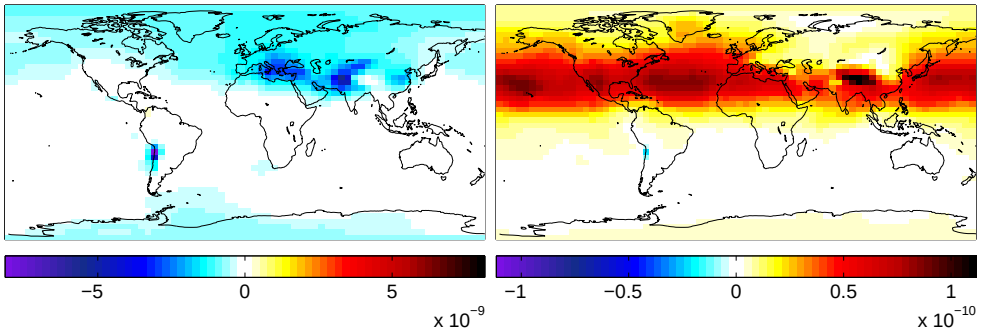

(a) First-order (b) Second-order

Figure C-5: First- and second-order sensitivities of global surface PM concentration with respect to ALK4 emissions (in $\mu g\,m^{-3}/kg\,hr^{-1}$)

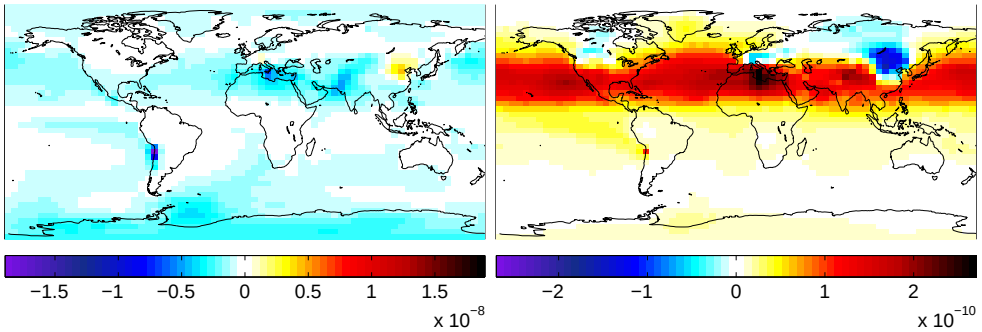

(a) First-order (b) Second-order

Figure C-6: First- and second-order sensitivities of global surface PM concentration with respect to ISOP emissions (in $\mu g\,m^{-3}/kg\,hr^{-1}$)

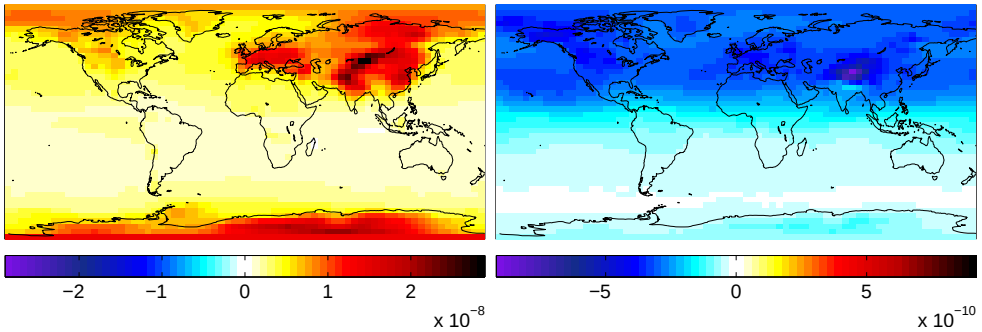

(a) First-order (b) Second-order

Figure C-7: First- and second-order sensitivities of global surface PM concentration with respect to HNO_3 emissions (in $\mu g\,m^{-3}/kg\,hr^{-1}$)

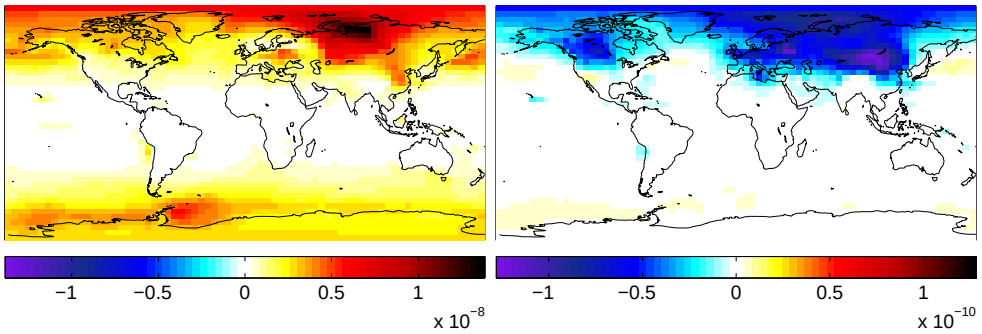

(a) First-order (b) Second-order

Figure C-8: First- and second-order sensitivities of global surface PM concentration with respect to H_2O_2 emissions (in $\mu g\,m^{-3}/kg\,hr^{-1}$)

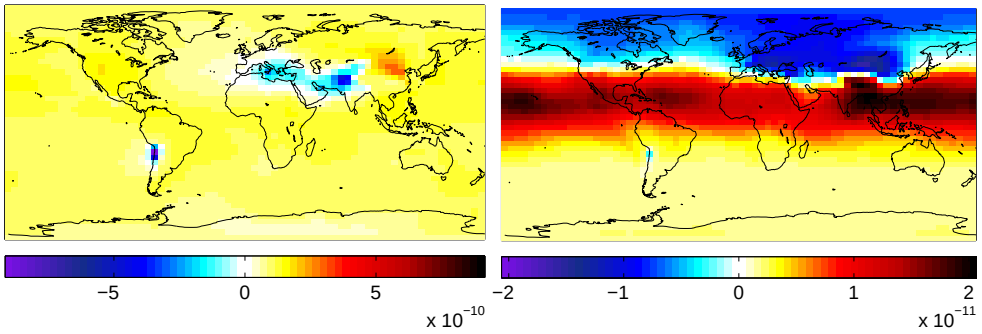

(a) First-order (b) Second-order

Figure C-9: First- and second-order sensitivities of global surface PM concentration with respect to ACET emissions (in $\mu g\,m^{-3}/kg\,hr^{-1}$)

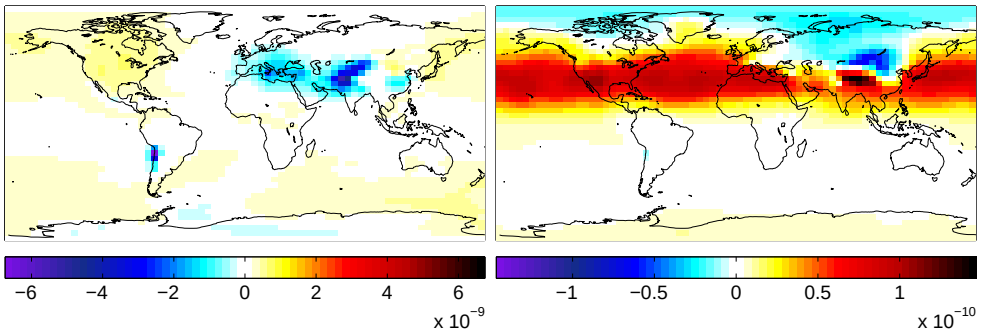

(a) First-order (b) Second-order

Figure C-10: First- and second-order sensitivities of global surface PM concentration with respect to MEK emissions (in $\mu g\,m^{-3}/kg\,hr^{-1}$)

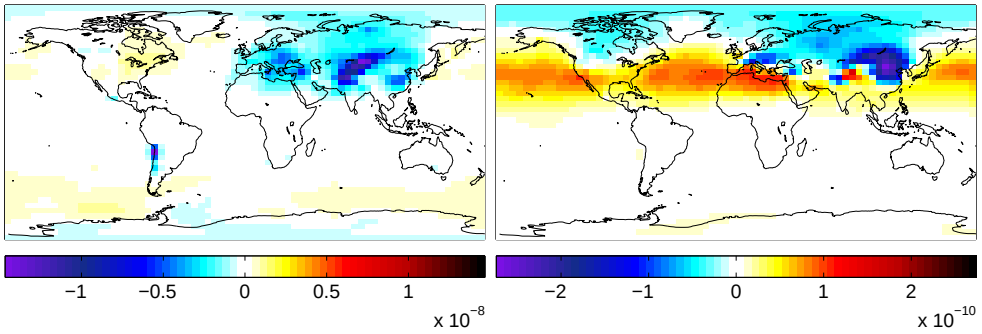

(a) First-order (b) Second-order

Figure C-11: First- and second-order sensitivities of global surface PM concentration with respect to ALD2 emissions (in $\mu g\,m^{-3}/kg\,hr^{-1}$)

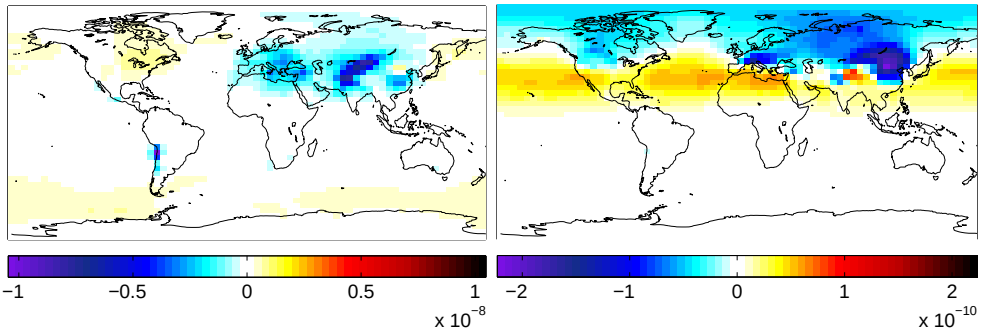

(a) First-order (b) Second-order

Figure C-12: First- and second-order sensitivities of global surface PM concentration with respect to RCHO emissions (in $\mu g\,m^{-3}/kg\,hr^{-1}$)

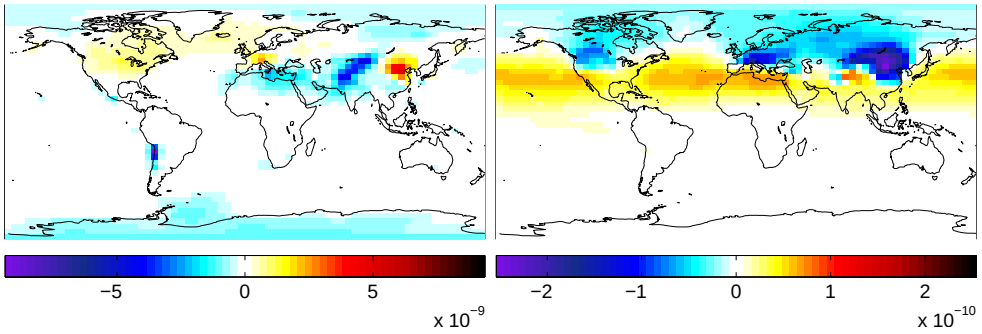

(a) First-order (b) Second-order

Figure C-13: First- and second-order sensitivities of global surface PM concentration with respect to MVK emissions (in $\mu g\,m^{-3}/kg\,hr^{-1}$)

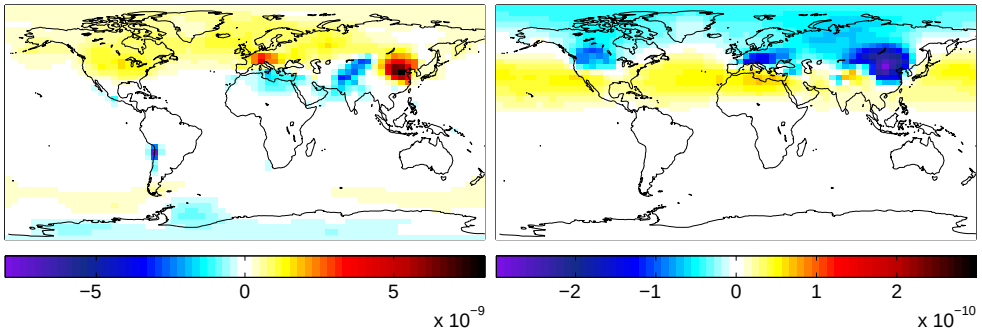

(a) First-order (b) Second-order

Figure C-14: First- and second-order sensitivities of global surface PM concentration with respect to MACR emissions (in $\mu g\,m^{-3}/kg\,hr^{-1}$)

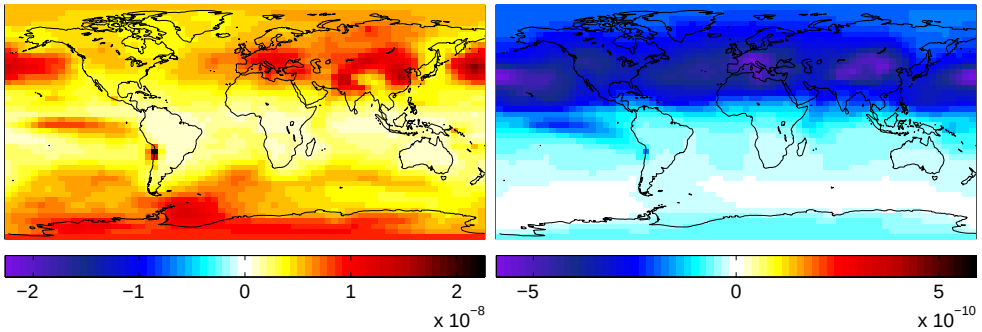

(a) First-order (b) Second-order

Figure C-15: First- and second-order sensitivities of global surface PM concentration with respect to PMN emissions (in $\mu g\,m^{-3}/kg\,hr^{-1}$)

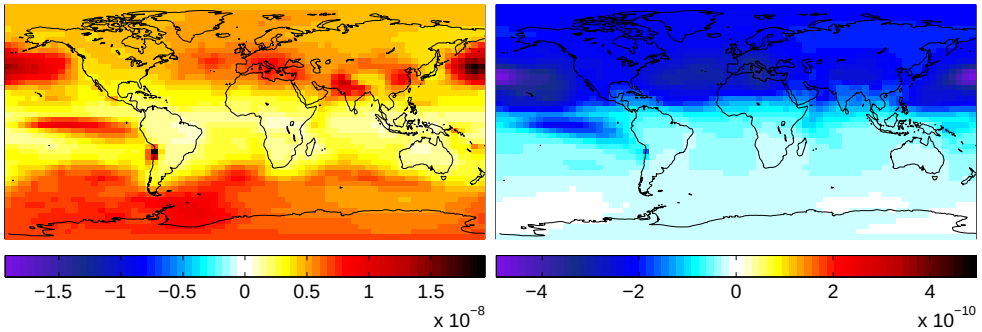

(a) First-order (b) Second-order

Figure C-16: First- and second-order sensitivities of global surface PM concentration with respect to PPN emissions (in $\mu g\,m^{-3}/kg\,hr^{-1}$)

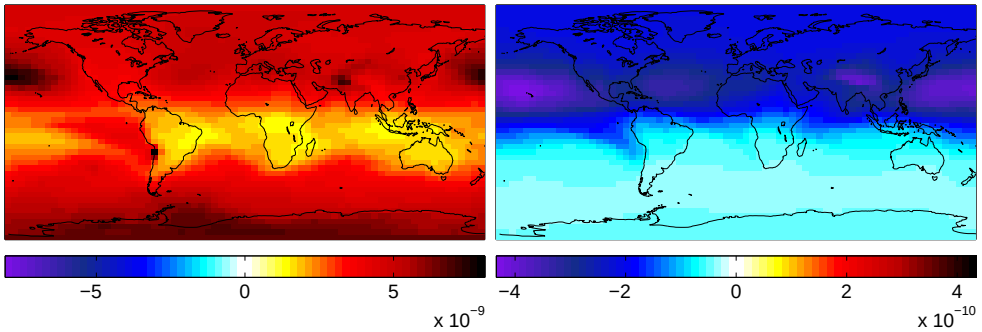

(a) First-order (b) Second-order

Figure C-17: First- and second-order sensitivities of global surface PM concentration with respect to R4N2 emissions (in $\mu g\,m^{-3}/kg\,hr^{-1}$)

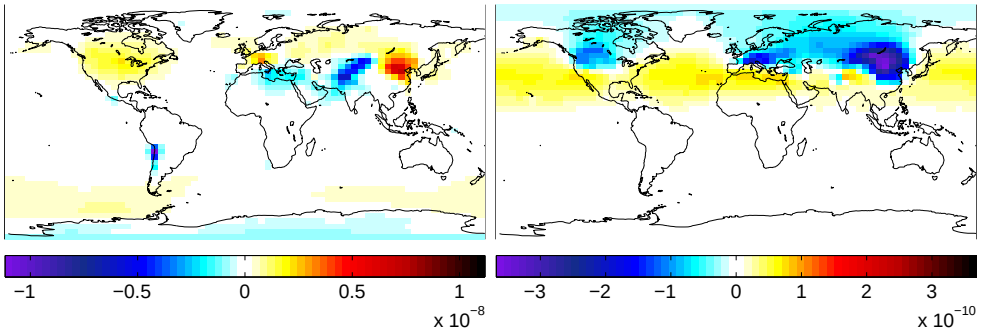

(a) First-order (b) Second-order

Figure C-18: First- and second-order sensitivities of global surface PM concentration with respect to PRPE emissions (in $\mu g\,m^{-3}/kg\,hr^{-1}$)

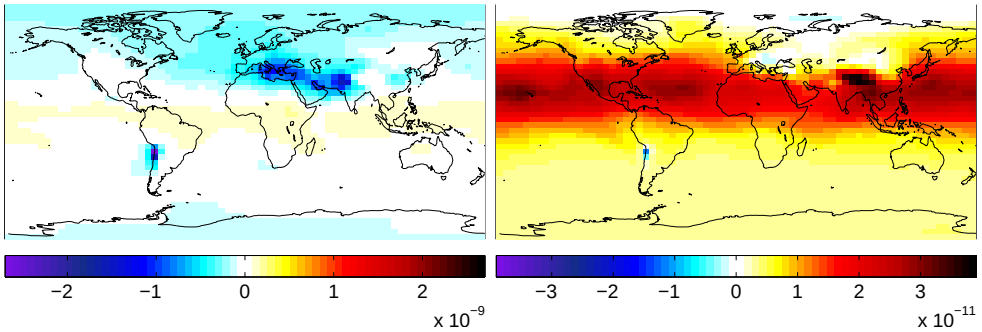

(a) First-order (b) Second-order

Figure C-19: First- and second-order sensitivities of global surface PM concentration with respect to C_3H_8 emissions (in $\mu g\,m^{-3}/kg\,hr^{-1}$)

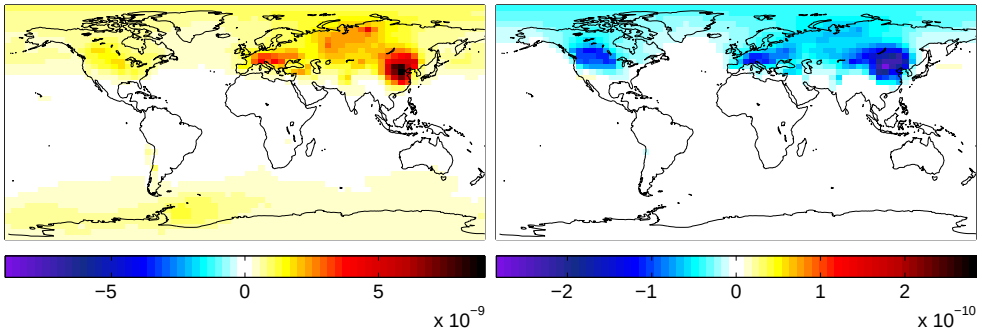

(a) First-order (b) Second-order

Figure C-20: First- and second-order sensitivities of global surface PM concentration with respect to CH_2O emissions (in $\mu g\,m^{-3}/kg\,hr^{-1}$)

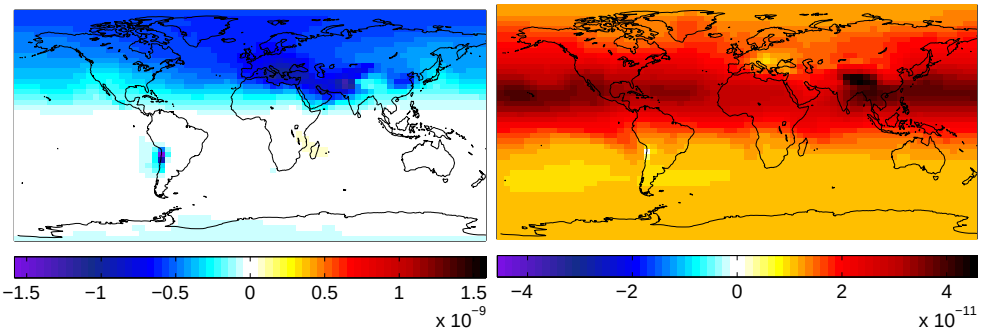

(a) First-order (b) Second-order

Figure C-21: First- and second-order sensitivities of global surface PM concentration with respect to C_2H_6 emissions (in $\mu g\,m^{-3}/kg\,hr^{-1}$)

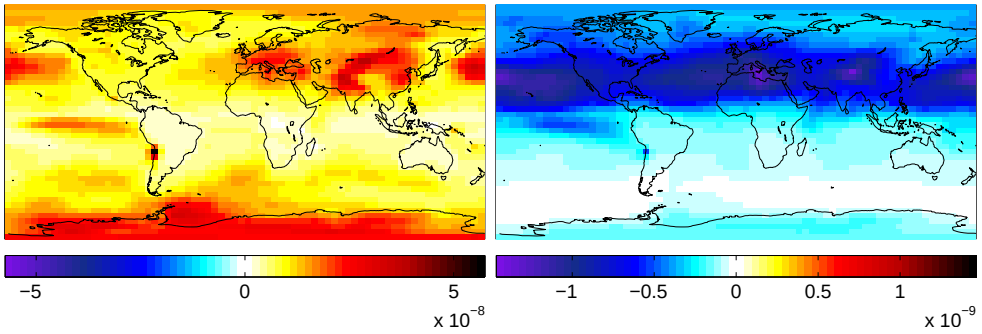

(a) First-order (b) Second-order

Figure C-22: First- and second-order sensitivities of global surface PM concentration with respect to N_2O_5 emissions (in $\mu g\,m^{-3}/kg\,hr^{-1}$)

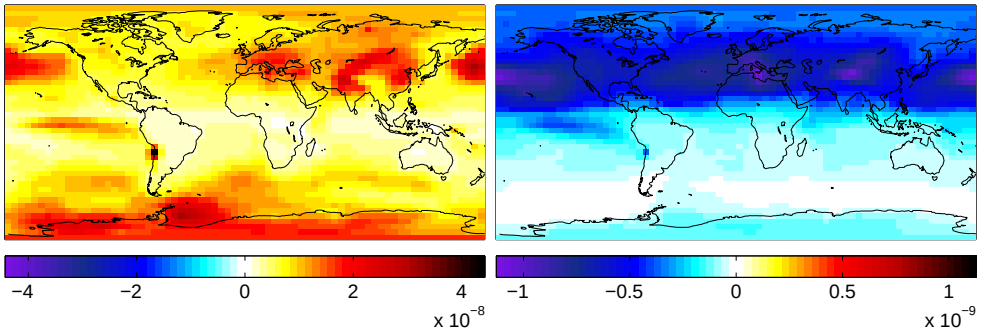

(a) First-order (b) Second-order

Figure C-23: First- and second-order sensitivities of global surface PM concentration with respect to HNO_4 emissions (in $\mu g\,m^{-3}/kg\,hr^{-1}$)

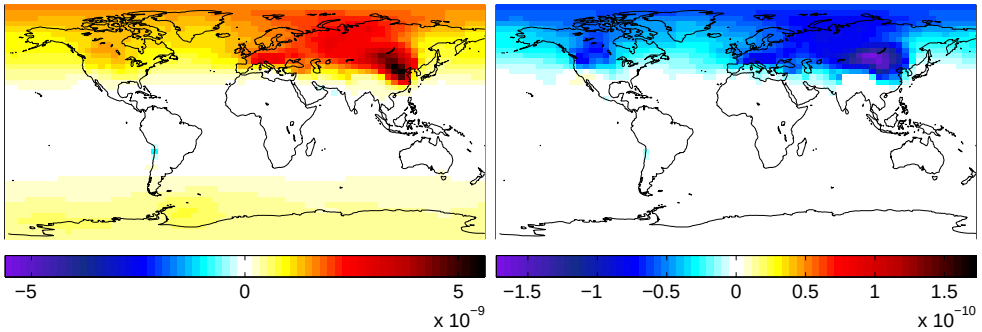

(a) First-order (b) Second-order

Figure C-24: First- and second-order sensitivities of global surface PM concentration with respect to MP emissions (in $\mu g\,m^{-3}/kg\,hr^{-1}$)

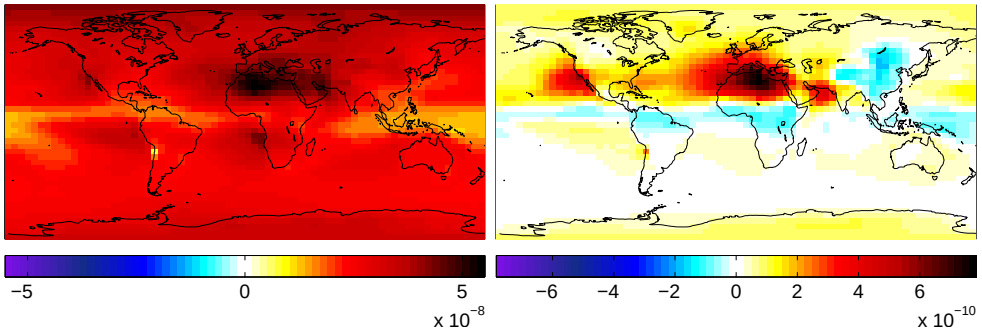

(a) First-order (b) Second-order

Figure C-25: First- and second-order sensitivities of global surface PM concentration with respect to DMS emissions (in $\mu g\,m^{-3}/kg\,hr^{-1}$)

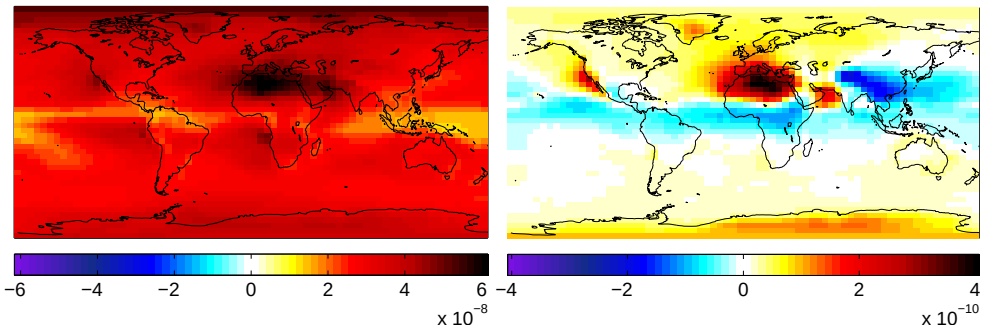

(a) First-order (b) Second-order

Figure C-26: First- and second-order sensitivities of global surface PM concentration with respect to SO_2 emissions (in $\mu g\,m^{-3}/kg\,hr^{-1}$)

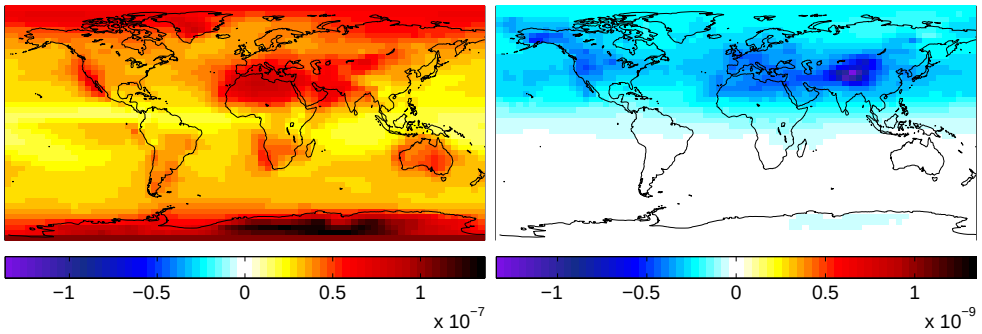

(a) First-order (b) Second-order

Figure C-27: First- and second-order sensitivities of global surface PM concentration with respect to SO_4 emissions (in $\mu g\,m^{-3}/kg\,hr^{-1}$)

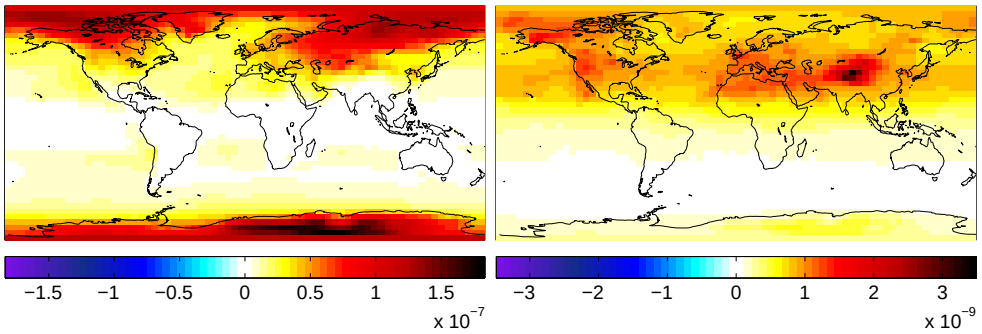

(a) First-order (b) Second-order

Figure C-28: First- and second-order sensitivities of global surface PM concentration with respect to NH_3 emissions (in $\mu g\,m^{-3}/kg\,hr^{-1}$)

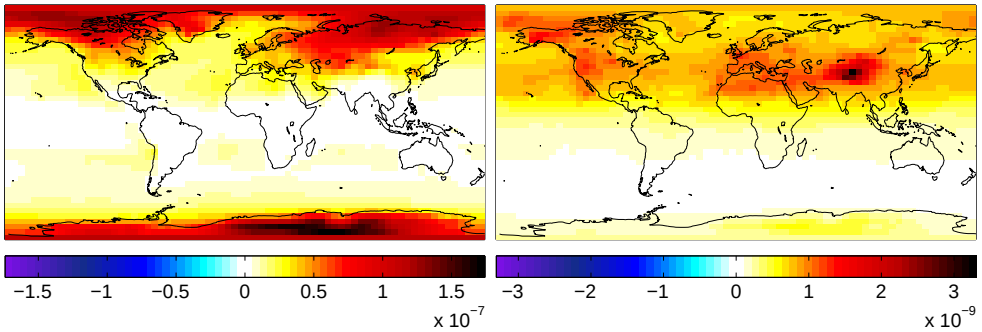

(a) First-order (b) Second-order

Figure C-29: First- and second-order sensitivities of global surface PM concentration with respect to NH_4 emissions (in $\mu g\,m^{-3}/kg\,hr^{-1}$)

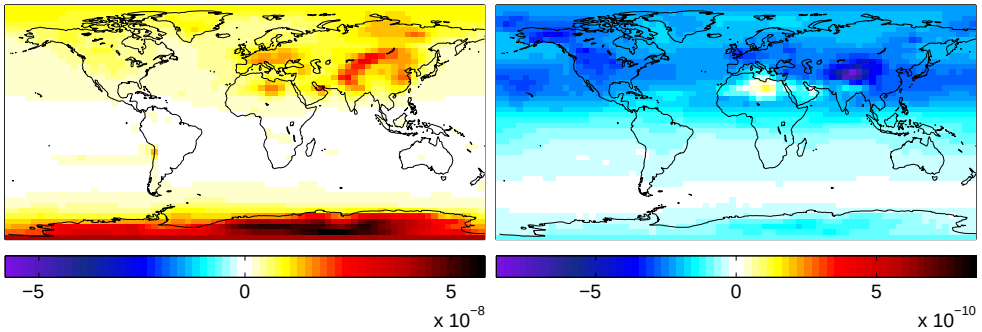

(a) First-order (b) Second-order

Figure C-30: First- and second-order sensitivities of global surface PM concentration with respect to NIT emissions (in $\mu g\,m^{-3}/kg\,hr^{-1}$)

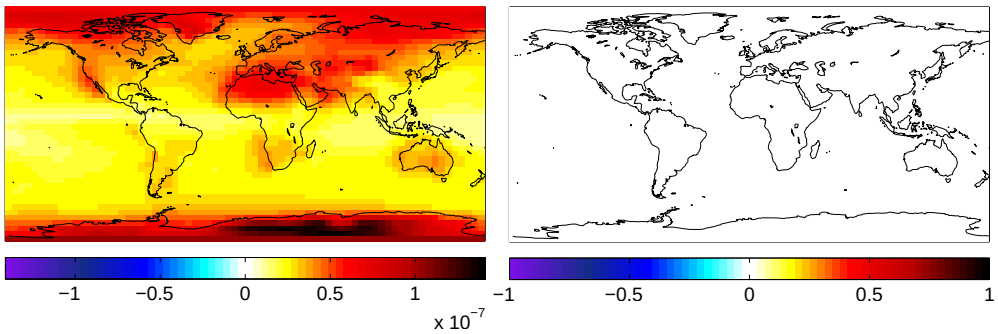

(a) First-order (b) Second-order

Figure C-31: First- and second-order sensitivities of global surface PM concentration with respect to primary PM emissions (in $\mu g\,m^{-3}/kg\,hr^{-1}$)

THIS PAGE INTENTIONALLY LEFT BLANK

Appendix D

GEOS-Chem Tracers

This appendix lists the GEOS-Chem tracers for NO_X-O_X-HC-aerosol simulation.

Table D.1: GEOS-Chem tracers

	Tracer Name	**Description**
1	NOx	NO + NO2+ NO3 + HNO2
2	Ox	O3 + NO2 + 2NO3
3	PAN	Peroxyacetyl Nitrate
4	CO	Carbon Monoxide
5	ALK4	Lumped >= C4 Alkanes
6	ISOP	Isoprene
7	HNO3	Nitric Acid
8	H2O2	Hydrogen Peroxide
9	ACET	Acetone
10	MEK	Methyl Ethyl Ketone
11	ALD2	Acetaldehyde
12	RCHO	Lumped Aldehyde >= C3
13	MVK	Methyl Vinyl Ketone
14	MACR	Methacrolein
15	PMN	Peroxymethacroyl Nitrate
16	PPN	Lumped Peroxypropionyl Nitrate
17	R4N2	Lumped Alkyl Nitrate

	Tracer Name	Description
18	PRPE	Lumped >= C3 Alkenes
19	C3H8	Propane
20	CH2O	Formaldehyde
21	C2H6	Ethane
22	N2O5	Dinitrogen Pentoxide
23	HNO4	Pernitric Acid
24	MP	Methyl Hydro Peroxide
25	DMS	Dimethyl Sulfide
26	SO2	Sulfur Dioxide
27	SO4	Sulfate
28	SO4s	Sulfate on surface of sea-salt aerosol
29	MSA	Methyl Sulfonic Acid
30	NH3	Ammonia
31	NH4	Ammonium
32	NIT	Inorganic Sulfur Nitrates
33	NITs	Inorganic Nitrates on surface of sea-salt aerosol
34	BCPI	Hydrophilic black carbon aerosol
35	OCPI	Hydrophilic organic carbon aerosol
36	BCPO	Hydrophobic black carbon aerosol
37	OCPO	Hydrophobic organic carbon aerosol
38	DST1	Dust aerosol,Reff= 0.7 microns
39	DST2	Dust aerosol, Reff = 1.4 microns
40	DST3	Dust aerosol, Reff = 2.4 microns
41	DST4	Dust aerosol, Reff = 4.5 microns
42	SALA	Accumulation mode sea salt aerosol
		(Reff = 0.1 2.5 microns)
43	SALC	Coarse mode sea salt aerosol
		(Reff = 2.5 4 microns)